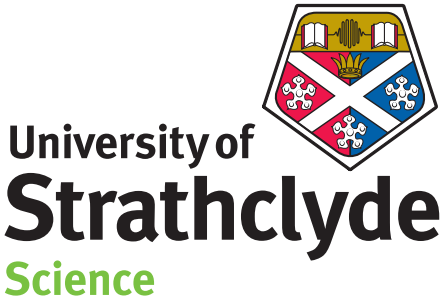

Dispersive and dissipative properties of high order schemes for computational wave propagation

Hafiz Abdul Wajid

Department of Mathematics

University of Strathclyde

Glasgow, UK

September 2009

This thesis is submitted to the University of Strathclyde for the degree of Doctor of Philosophy in the Faculty of Science.

Acknowledgements

First of all I am extremely grateful to my almighty ALLAH for everything HE has blessed me. I would like to thank my parents from the bottom of my heart for their unconditional love and support. My prayers are always for my mum who passed away during my PhD.

It has been an honour for me being a student of Professor Mark Ainsworth and I am grateful to him for all of his help throughout the last three years. His inspirational personality and knowledge will always serve to me as an example.

I also would like to thank all of my family and friends especially Mr. Abdul Majid, Dr. Abid, Dr. Sidra, Dr. Richard Rankin and Mr. Jahanzeb for their support and encouragement. I also would like to thank everybody who is a part of the Department of Mathematics, University of Strathclyde for being so nice.

Special thanks to COMSATS Institute of Information Technology, Pakistan for funding me.

Abstract

We study the dispersive and dissipative behaviour of the spectral element scheme, sometimes called the *Gauss-point mass lumped finite element scheme*, for the wave equation in detail and provide both a qualitative description of the nature of the dispersive and dissipative behaviour of the scheme along with precise quantitative statements of the accuracy in terms of the mesh size, the order of the scheme and the wave number. We then consider a suggestion of Marfurt (1984) whereby one can attempt to provide an optimal blending of finite element and spectral element schemes to obtain a new scheme with superior dispersive and dissipative behaviour. We study the dispersion and dissipation of this scheme obtained by taking a weighted averaging of the consistent (finite element) mass matrix and lumped (spectral element) mass matrix. We show that this optimally blended scheme can be efficiently implemented merely by replacing the usual Gaussian quadrature rule used to assemble the mass and stiffness matrices by novel non-standard quadrature rules which are also derived. We then give analytical expressions for the discrete dispersion relations for the above mentioned schemes for a rectangular grid, and prove that the analytical expressions for the discrete dispersion error in higher dimensions can be obtained using one dimensional discrete dispersion error expressions.

Contents

Chapter 1

Introduction

1.1 Computational wave propagation

Wave propagation phenomena arise in various fields such as acoustics, electromagnetics and geophysics. Examples of some of the problems in these areas include exploration geophysics, nondestructive testing, medical imaging, seismic and radar propagation and security scanning. Ground penetrating radar (GPR) is one of the examples of exploration geophysics that produces a continuous cross-sectional profile of subsurface features by transmitting pulses of high frequency radio waves without drilling or digging. It has applications in civil engineering (detection of buried sewerage of water and gas, and electrical and telecommunication cables) [21] and archaeology (imaging of the buried artifacts such as graves and mortuaries) [20]. Other examples of exploration geophysics include seismic tomography, mineral explorations and many more.

Another example of electromagnetic wave scattering is X-ray Backscattering which is an imaging technique and has applications both in defence and security. Specific applications include the detection of buried landmines [51] and the screen-

ing of people, luggage, vehicles and sea containers [12]. An example of the medical imaging technique is magnetic resonance imaging (MRI) which is widely used in radiology to visualise the internal structure and functions of the human body.

It is clear from the above mentioned problems that the accurate simulation of waves is an important topic. Analytical methods cannot efficiently be used to analyse such phenomena and thus efficient and reliable numerical simulations are required. The finite element method [1, 8, 10, 11, 33, 35, 37, 38, 46, 56, 60] is one of the most appealing computational tools for performing simulations of wave propagation problems involving complex geometries and materials. Other common numerical methods include the finite difference method [49], finite volume method [45], boundary element method [16], spectral method [13] and pseudo-spectral method [24].

The standard computational methods, including those mentioned above, suffer from inherent errors such as *numerical dispersion (phase error or error in wavelength)* and *numerical dissipation (amplitude error)*. This is evidently the result of the discrete nature of these methods. These effects can be avoided completely in one dimension by modifying the numerical scheme and can be reduced by *refining* the discretisation in space in higher dimensions [10]. However, refining the mesh results in a significant increase in the computational cost [37, 38].

To overcome the above limitations requires more accurate and efficient methods. The development of numerical methods which are less dispersive and dissipative and can propagate waves accurately without requiring finer meshes is the focus of this thesis.

1.2 Dispersive and nondispersive waves

Before we delve into the numerical dispersion and dissipation which is the central topic of this text, we first discuss what dispersive and nondispersive waves are. Consider the one dimensional Klein-Gordon equation

$$U_{tt}(x,t) - c^2 U_{xx}(x,t) + bU(x,t) = 0, \quad x \in \mathbb{R},\ t > 0,\ c > 0 \text{ and } b \geq 0 \tag{1.1}$$

where $U_t = \dfrac{\partial U}{\partial t}$ and $U_x = \dfrac{\partial U}{\partial x}$. Inserting a time-harmonic solution of the form $U(x,t) = u(x,t)e^{-i\omega t}$ into above equation where $\omega > 0$ is the angular frequency, we obtain the time-harmonic Klein-Gordon equation

$$c^2 u''(x) - (b - \omega^2)u(x) = 0, \quad x \in \mathbb{R},\ c > 0 \text{ and } b \geq 0. \tag{1.2}$$

The above equation reduces to the Helmholtz equation for $b = 0$. We seek a non-trivial solution of the form

$$u(x) = Ae^{ikx} \tag{1.3}$$

to equation (1.2), where $A \in \mathbb{C}$ is an arbitrary constant and $k \in \mathbb{C}$ is the wavenumber to be determined. Inserting (1.3) into (1.2) and simplifying gives

$$k = \pm\sqrt{\frac{\omega^2 - b}{c^2}}, \tag{1.4}$$

and therefore, (1.2) has a general solution of the form

$$u(x) = A_1 e^{ix\sqrt{(\omega^2-b)/c^2}} + A_2 e^{-ix\sqrt{(\omega^2-b)/c^2}} \tag{1.5}$$

where A_1 and A_2 are arbitrary constants. The corresponding time dependent solution of equation (1.1) is given by

$$U(x,t) = A_1 e^{i(x\sqrt{(\omega^2-b)/c^2}-\omega t)} + A_2 e^{-i(x\sqrt{(\omega^2-b)/c^2}+\omega t)} \tag{1.6}$$

and consists of two waves: one travelling to the left and the other travelling to the right. We note that however in higher dimensions waves travel in all directions. The above relation (1.4) between the wavenumber k and the frequency ω is known as the *continuous dispersion relation*.

The phase velocity of the wave denoted by v^c is defined to be the ratio of the angular frequency ω to the wavenumber k [35] and is given by

$$v^c = \frac{\omega}{k}. \tag{1.7}$$

A wave is defined to be *dispersive* when the speed of the wave depends on either the frequency ω or equally well, the wavenumber k, otherwise the wave is defined to be *nondispersive*. Inserting k from (1.4) into the above equation, we get

$$v^c = \pm\frac{\omega c}{\sqrt{\omega^2 - b}}. \tag{1.8}$$

In this case, the wave speed depends upon the frequency only when b is positive whereas for $b = 0$ expression (1.8) becomes $v^c = \pm c$. Hence, if $b < \omega^2$, then the Klein-Gordon equation is dispersive because waves of different frequencies will travel at different speeds. Moreover, the Helmholtz equation has nondispersive solutions and waves will travel with constant speed c in opposite directions.

1.3 Dissipative and nondissipative waves

We now focus our attention on understanding what dissipative and nondissipative waves are. If the wavenumber k is a complex number i.e. $k = k_r + ik_c \in \mathbb{C}$ where $k_r \in \mathbb{R}$, and k_c is a non zero real number, then the solution is *dissipative*. For $k_c = 0, k \in \mathbb{R}$ and the solution is *nondissipative*. It is clear from (1.4) that $k \in \mathbb{C}$ when $b > \omega^2$ and hence (1.2) is dissipative for $b > \omega^2$. Inserting $\omega^2 - b = -r^2$,

where r is a positive real number into (1.4), we get

$$k = \pm \frac{r}{c} i \tag{1.9}$$

and for these values of k, (1.2) has a general solution of the form

$$u(x) = A_1 e^{rx/c} + A_2 e^{-rx/c}$$

where A_1 and A_2 are arbitrary constants. In contrast to (1.5), this solution is not oscillatory and, for physically relevant solutions, we have decay or dissipation of the solution as $|x| \to \infty$. Further details about dispersive, nondispersive, dissipative and nondissipative waves can be found in [34, 35, 41].

1.4 Numerical dispersion and numerical dissipation

Numerical dispersion and dissipation has been an area of active research for decades. However we have not found a satisfactory definition of these effects in the literature. We start this section by reviewing some of the definitions of numerical dispersion present in the literature.

Two of the most important and widely cited research monographs for wave propagation which cover a wide range of topics on finite element methods for the wave equation are written by Ihlenburg [35] and Cohen [17]. Ihlenburg [35], (1998) comments on the dispersive discrete solutions obtained with linear finite element schemes for the Helmholtz equation (see page 124 of [35]), but no explicit *general* definition of numerical dispersion is given. Cohen [17], p.102, (2002) says that the numerical dispersion of a scheme is measured by the *ratio of the discrete velocity to the continuous velocity and manifests itself by producing parasitic waves.* One can

object to this definition on the grounds that in [1, 5, 35], numerical waves obtained with linear finite element and spectral element schemes are shown to be dispersive but there are no parasitic waves at all in the sense defined in Cohen [17], p.103.

Basabe [22], (2007) defines numerical dispersion as *a numerical noise related to grid spacing which occurs when the actual velocity of high frequency waves in the grid is different from the true velocity.* Our main objection with this definition is that the numerical dispersion is not only related to high frequency waves but is evident for waves of all ranges of frequencies [1, 5, 35].

Oberai and Pinsky [53], (2000) defined numerical dispersion as *errors inherent in the method resulting in numerical waves that propagate with a wavenumber k^h which is different from the continuous wavenumber k.* This definition is more satisfactory but one can question what the authors mean by numerical waves. In fact Oberai and Pinsky state that for simple problems which have exact plane wave solutions e^{ikx}, it can be shown that the numerical solution is of the form $e^{ik^h x}$. However, this definition is rather confusing in that numerical schemes do not admit exact plane wave solutions in general. A very similar definition is given by Kailash [55], (2005) where he defined numerical dispersion as *the change of the wavenumber obtained with the numerical approximations compared to the corresponding wavenumber of the exact solution.* Once again, it is not clear what is meant by the wavenumber obtained with the numerical approximations.

Ainsworth [1], (2004) defined numerical dispersion as *the effect whereby the numerical scheme fails to propagate waves at the correct speed.* The only objection that we have with this definition is that it is not quantitative.

Before giving a general definition of the numerical dispersion, we shall explain first what numerical dispersion is in the case of linear finite elements.

1.4.1 An example of numerical dispersion and dissipation

The objective of this section is to illustrate numerical dispersion and numerical dissipation in the simple case of linear finite element and spectral element schemes for the Helmholtz equation

$$c^2 u''(x) + \omega^2 u(x) = 0, \quad x \in \mathbb{R},\ c > 0 \tag{1.10}$$

obtained by inserting $b = 0$ into (1.2).

We discretise equation (1.10) using piecewise linear finite elements on a uniform mesh of size $h > 0$ and specify the numerical approximation in the form

$$u_h(x) = \sum_{j \in \mathbb{Z}} u^j \theta_j(x)$$

where θ_j is the usual piecewise linear hat function associated with node x_j. We obtain the following equation for the value u^j of the approximation at node $x_j = jh,\ j \in \mathbb{Z}$:

$$u^{j+1} - 2u^j + u^{j-1} + \frac{\omega^2 h^2}{6c^2}(u^{j+1} + 4u^j + u^{j-1}) = 0. \tag{1.11}$$

We have seen that the Helmholtz equation (1.10) admits non-trivial plane wave solutions of the form $u(x) = Ae^{ikx}$ provided that the wavenumber k is related to the frequency ω by the continuous dispersion relation

$$k = \pm \frac{\omega}{c}. \tag{1.12}$$

Obviously, the discrete solution is piecewise linear and (1.11) cannot therefore have a solution of the form Ae^{ikx}. Instead we seek a non-trivial discrete solution specified by values at the nodes $x_j = jh,\ j \in \mathbb{Z}$ of the form $u^j = Ae^{ijk^h h}$ with $k^h \in \mathbb{R}$ denoting the *discrete wavenumber*. Now inserting $u^j = Ae^{ijk^h h}$ into (1.11) and performing ordinary manipulations, we get

$$k^h h = \cos^{-1}\left(\frac{6c^2 - 2\omega^2 h^2}{6c^2 + \omega^2 h^2}\right) \tag{1.13}$$

which is known as the *discrete dispersion relation* relating the discrete wavenumber k^h to the frequency ω. The expression (1.13) is also known as the characteristic equation [14, 60]. Writing the above expression as a series in ωh, we get

$$k^h = \pm\frac{\omega}{c} \mp \frac{h^2}{24}\left(\frac{\omega}{c}\right)^3 + \cdots . \tag{1.14}$$

We now define the discrete phase velocity denoted by v^h as *the ratio of the angular frequency ω to the discrete wavenumber k^h* and is given by

$$v^h = \frac{\omega}{k^h}.$$

Inserting k^h from (1.13) into above equation and expanding as a series in ωh, we get

$$v^h = \pm c \mp \frac{(\omega h)^2}{24c} + \cdots .$$

It is evident that the discrete phase velocity depends upon the frequency ω in contrast to the continuous phase velocity $v^c = \pm c$ which is constant. These velocities are different because continuous phase velocity was obtained by inserting a plane wave solution into (1.10) whereas the discrete phase velocity is obtained by inserting piecewise linear solution into (1.11) and the difference of them measures dispersion i.e.

$$v^c - v^h = \pm\frac{(\omega h)^2}{24c} + \cdots$$

or, in general the difference $v^c - v^h$ is given by

$$v^c - v^h = \frac{\omega}{k} - \frac{\omega}{k^h} = \frac{\omega(k^h - k)}{kk^h}. \tag{1.15}$$

It is clear from (1.12) and (1.14) that continuous wavenumber k is different from the discrete wavenumber k^h as pointed out in the definitions by Oberai and Pinsky and Kailash. However, it is not the change of wavenumbers which measures the numerical dispersion, it is the difference $k^h - k$ which measures numerical dispersion

as it is clear from the above expression. More specifically, for $h > 0$, the difference $k^h h - kh$ gives a measure of the dispersive and dissipative behaviour of a numerical scheme [1–5, 7, 60]. Therefore, in this thesis we will study the difference $k^h h - kh$ for different schemes. Furthermore, it is not the ratio of the velocities which measures numerical dispersion as defined by Cohen, in fact it is the difference of the velocities which measures numerical dispersion. The difference $v^c - v^h$ is different for different numerical schemes and that is why we see a numerical wave either lead or lag compared with the exact wave [5, 7] and the definition given by Ainsworth is much more satisfactory in this regard. Numerical dispersion is sometimes referred as error in phase or error in wavelength and therefore, replacing k and k^h by $k = \dfrac{2\pi}{\lambda}$ and $k = \dfrac{2\pi}{\lambda^h}$ respectively into (1.15), we obtain another equivalent mathematical form of (1.15) given by

$$v^c - v^h = \frac{\omega}{2\pi}(\lambda - \lambda^h)$$

where λ and λ^h are the continuous and discrete wavelengths respectively.

1.4.2 Numerical dispersion

We have analysed numerical dispersion in detail in the case of linear finite elements but this kind of analysis is valid for many numerical schemes. Therefore, for the purpose of the present work, we shall define numerical dispersion as *the difference between the continuous velocity v^c and the discrete velocity v^h*.

The expression (1.14) is markedly different from the actual dispersion relation (1.12) for the Helmholtz equation. Using (1.12) together with (1.14) and rearranging, we get

$$\frac{k^h}{k} - 1 = -\frac{(kh)^2}{24} + \cdots \tag{1.16}$$

or,

$$k^h h - kh = -\frac{(kh)^3}{24} + \cdots .$$

The above expression is well known and has already been obtained in many texts [1, 35, 37, 38, 60].

1.4.3 Implications of numerical dispersion

We shall discuss the implications of (1.16) below. However, before doing so, we shall consider an alternative approach to approximate problem (1.10) using the spectral element method [17, 60]. This results in the following equation for the coefficients $\tilde{u}^j$:

$$\tilde{u}^{j+1} - 2\tilde{u}^j + \tilde{u}^{j-1} + \frac{\omega^2 h^2}{c^2}\tilde{u}^j = 0. \tag{1.17}$$

Again inserting a non-trivial solution of the form $\tilde{u}^j = \tilde{A}e^{ijk^h h}, \tilde{A} \in \mathbb{C}$ into the above equation gives

$$k^h h = \cos^{-1}\left(1 - \frac{\omega^2 h^2}{2c^2}\right)$$

which is the discrete dispersion relation for the spectral element scheme. Again expanding as a series in ωh, we get

$$k^h = \pm\frac{\omega}{c} \pm \frac{h^2}{24}\left(\frac{\omega}{c}\right)^3 + \cdots \tag{1.18}$$

which is also different from the actual dispersion relation (1.12) for the Helmholtz equation. Using (1.12) together with (1.18) and rearranging, we get

$$\frac{k^h}{k} - 1 = \frac{(kh)^2}{24} + \cdots \tag{1.19}$$

or,

$$k^h h - kh = \frac{(kh)^3}{24} + \cdots$$

which is also well known and has already been given in [17, 60]. Now from expressions (1.16) and (1.19), we can make the following observations:

(a) The minus sign in front of the leading term for phase error in the expression (1.16) shows that for the finite element scheme the discrete wavenumber k^h is underestimated i.e. $k^h < k$ and results in *phase lead*. The plus sign in front of the leading term for phase error in the expression (1.19) shows that for the spectral element scheme the discrete wavenumber is overestimated i.e. $k^h > k$ and results in *phase lag*. Moreover, the multiplicative constants in the leading terms for phase error in the discrete dispersion relations (1.16) and (1.19) are both 1/24. This is consistent with numerical solutions obtained with both finite element and spectral element schemes shown in Figure 1.1 where leads and lags of *equal magnitudes* are prominent. Furthermore, with linear elements both schemes are second order accurate i.e.

$$\frac{k^h}{k} - 1 = \mathcal{O}(kh)^2$$

as shown in Figure 1.2.

(b) The mesh size h is also present in the right hand sides of the expressions (1.16) and (1.19). For very small values of kh i.e. when $kh \to 0$ the discrete wavenumber k^h is approximately equal to the exact wavenumber k. Even when we are just analysing the one dimensional discrete dispersion relation, as we are doing here, refining the mesh is computationally very expensive. This is even more problematic when we are simulating a complex problem in higher dimensions [10]. The dispersive effect while solving time-harmonic wave propagation problems in one-dimension can be avoided completely [10] but for problems posed over higher dimensions it can only be reduced [8, 10] by the use of a *finer mesh* or *high order finite elements*. This leads to undesirable computational cost [37, 38], particularly when complex multi-dimensional simulations are performed.

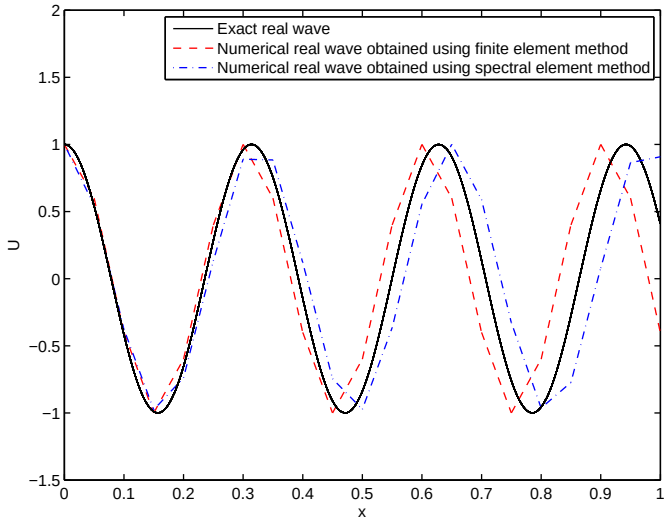

Figure 1.1: Numerical approximations of the solution to problem $u''(x) + \omega^2 u(x) = 0$, for all $x \in (0,1)$ with boundary conditions $u(0) = 1$, $u'(1) - i\omega u(1) = 0$ obtained for $\omega = 20$ with both finite element and spectral element schemes using 20 linear elements. Phase lead and lag of equal magnitudes are evident and correspond to finite element and spectral element schemes.

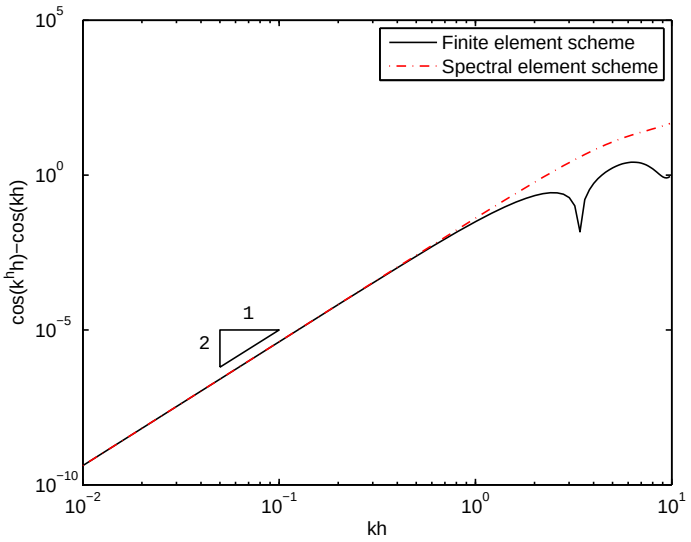

Figure 1.2: Error in the discrete dispersion relations $\cos(k^h h) - \cos(kh)$ versus nondimensional wavenumber kh for linear finite element and spectral element schemes. For linear finite element and spectral element schemes the slope of the lines are two when $kh \to 0$.

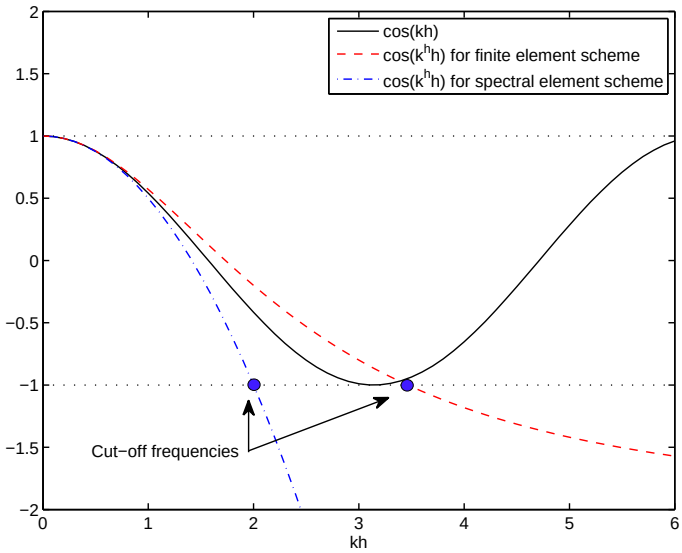

Figure 1.3: Comparison of the exact cosine with discrete cosines of finite element and spectral element schemes for linear order elements. Moreover, Cut-off frequencies are also pointed out both for linear finite and spectral element schemes.

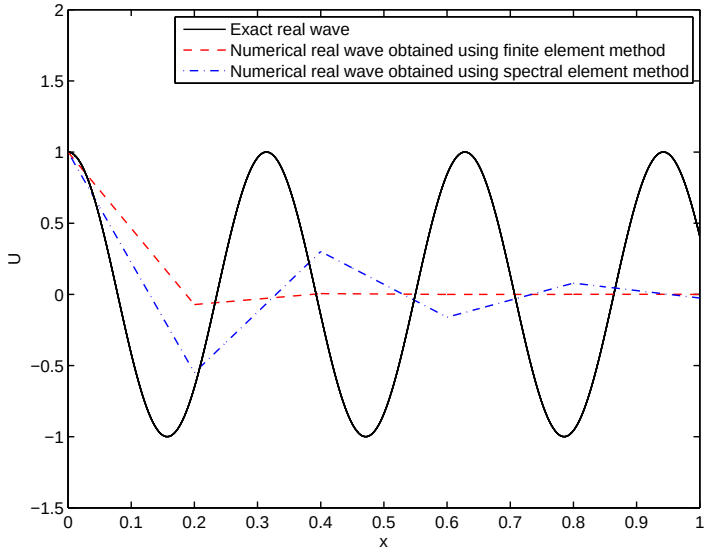

Figure 1.4: Numerical solutions obtained with both linear finite element and spectral element schemes dissipate compared with the exact solution.

1.4.4 Numerical dissipation

We now find the range of values of kh for which we have propagating (real k^h) and evanescent (imaginary k^h) solutions. Solving the inequality

$$\left|\frac{6-2k^2h^2}{6+k^2h^2}\right| \leq 1 \tag{1.20}$$

we find that for $kh < 2\sqrt{3}$, the rational expression $\dfrac{6-2k^2h^2}{6+k^2h^2} \in [-1,1]$ and is shown in Figure 1.3. When $kh > 2\sqrt{3}$, the rational expression $\dfrac{6-2k^2h^2}{6+k^2h^2} < -1$ is shown in Figure 1.3. For $kh < 2\sqrt{3}$, k^h has real values i.e., $k^h \in \mathbb{R}$ and we have propagating solutions whereas for $kh > 2\sqrt{3}$, k^h is a complex number i.e. $k^h \in \mathbb{C}$ and we have evanescent solutions. The value $kh = 2\sqrt{3}$ is known as the *cut-off frequency* of the finite element scheme for $p = 1$. If the discrete wavenumber k^h is a complex number then numerical dissipation is introduced meaning that the amplitude of the numerical solution is different from that of the exact solution. For the spectral element scheme the range of values of kh for propagating and

evanescent solutions are also shown in Figure 1.3. The cut-off frequency for the spectral element scheme is 2. Furthermore, in Figure 1.4 we have shown that for $kh = 4$ both the numerical approximations obtained with linear finite and spectral element schemes dissipate compared to the exact oscillatory solution.

In the following section we review the efforts and partial achievements made by many in the computational wave propagation literature.

1.5 Historical background of discretisation schemes for the wave equation

Finite elements have been extensively used to simulate wave propagation where one of the core issues is the existence of numerical errors like numerical dispersion (phase error) and numerical dissipation (amplitude error). The standard Galerkin finite element methods developed so far are not able to avoid these errors. Realising the importance of minimising dispersion and dissipation, many researchers proposed different methods in this regard.

The first detailed study of the dispersive properties of h and hp-version finite elements for the one dimensional Helmholtz equation was conducted by Ihlenburg and Babuška [36–38]. In these works they analysed dispersion in the asymptotic regime where the non-dimensional wavenumber is very small i.e. $\omega h \rightarrow 0$. Babuška et al. [8] also developed a method for the 2-D Helmholtz equation known as the Generalised Finite Element Method (GFEM). They concluded that dispersive effects are not avoidable for the finite element treatment of the Helmholtz equation but it is possible to design a quasi stabilised finite element method (QS-FEM) having negligible dispersion. Harari and Hughes [32] presented the Galerkin least squares (GLS) finite element method to solve the one dimensional Helmholtz

equation by modifying the variational formulation. Galerkin least squares methods were developed by appending residuals of the Helmholtz equation in least squares form to the Galerkin variational formulation. Furthermore, a local mesh parameter was introduced in order to minimise dispersion error. Both of these methods decreased the number of elements per wavelength required to achieve desired level of accuracy for a given frequency. However, neither of these methods can be used to model transient wave propagation phenomenon because of the dependence of the elemental matrices on the frequencies. This means that parameters introduced in the modification of the variational formulation depend upon the frequency or the wavenumber. Consequently, inverse Fourier transform cannot be used which prohibits the use of these methods for transient wave equation. Later on, Thompson and Pinsky [61] derived optimal GLS mesh parameter for both consistent and lumped mass approximation for two dimensional Helmholtz equation and further reduced the dispersion. However, their method failed to cope with anisotropy. Oberai and Pinsky [53] proposed a new residual based finite element method for Helmholtz equation by appending terms that are proportional to residuals on element interiors and inter-element boundaries. They showed that their scheme is less dispersive and is largely independent of the predominant wave vector direction for regular bilinear quadrilateral finite elements. They also showed with numerical examples that this method retains accuracy both for structured and unstructured meshes.

Several other methods have since been proposed to deal with the issue of numerical dispersion for the Helmholtz equation. Zyserman et al. investigated the dispersive properties of the scalar and elastic wave equations using nonconforming finite elements [63]. High order discontinuous Galerkin finite element methods have also been tried with the aim of efficiently resolving the waves of high fre-

quencies without much dispersion and dissipation [2, 4]. For further details about discontinuous Galerkin methods consult the references given in [2, 4]. Babuška and Melenk [9] proposed the partition of unity method which requires the behaviour of the solution to be known in advance, which for most practical applications is not the case. Cipolla [15] and Oberai and Pinsky [52] introduced the concept of subgrid modelling. Franca et al. [25] developed the method of residual free bubbles while Suleau and Bouillard [58] studied dispersion and pollution of meshless solutions for the Helmholtz equation using the element free Galerkin method.

The first detailed study of the dispersive and dissipative properties of the p-type finite element and spectral element schemes of order up to $p = 5$ was undertaken by Thompson and Pinsky. They presented the idea of *stopping* and *propagating bands* and showed the dispersion curves and conjectured that elements of order p has p stopping and passing bands. They also conjectured that the limit of resolution occurs at πp. They further conjectured that increased phase accuracy while maintaining the Nyquist limit can be achieved only when elements of order $p \geq 4$ are used. Mulder [50] studied the dispersive properties of the acoustic wave equation in one dimension using both finite and spectral element methods and concluded that spectral element methods with Gauss-Lobatto quadrature rules perform better than both the spectral element method with Chebyshev quadrature points and standard finite element methods. Cohen [17] presented the Gauss-point mass lumped finite element scheme and obtained the explicit expressions for the dispersion error for elements of order up to 3 for the transient wave equation. Basabe and Sen [22] studied dispersion in 2D with both finite and spectral elements for both acoustics and elastic wave equations. They provided analytical expressions for the dispersion error and stability conditions for first order elements as well as showing dispersion curves numerically for higher order elements.

1.6 Objectives of the thesis

The objectives of this thesis is to develop more accurate and efficient numerical methods which are less dispersive and dissipative and can be used directly in both the frequency and time domains. It is clear from expressions (1.16) and (1.19) that when the solution is approximated with linear finite elements and spectral elements both the order and the magnitude of the multiplicative constant in the leading term for phase error are the same. This observation prompts the following questions:

1. Do *both* the finite element and spectral element schemes give the same order of accuracy for phase error as the order p is increased?

2. Does the magnitude of the multiplicative constant in the leading term for phase error reduce as the order p is increased?

Answers to these questions are important because a clear understanding of the dispersive and dissipative properties of a scheme is not only valuable theoretically but serves as an initial guess (an a priori error estimate) in practical problems [1, 60]. Thus the development of numerical or computational methods which are less dispersive and dissipative has been and still is an issue for the numerical analysis community [31, 59]. Relatively recently, it is realised [1, 2, 4–7] that a sharp analysis of numerical dispersion and dissipation is possible with the derivation of explicit expressions for discrete dispersion relations. The following two measures are used as a basis for grading a method:

1. the order in ωh of the leading term for the error;

2. the magnitude of the multiplicative constant in the leading term for the error.

The development of methods which either improve the order in ωh or magnitude of the multiplicative constant in the leading term for the error is the focus of this thesis.

The first specific aim of this work is to study the dispersive and dissipative behaviour of the spectral element method. We derive explicit expressions for discrete dispersion relations for the spectral element method broadly adopting a similar approach to that used in [1]. We then study dispersive and dissipative behaviour of the scheme in the cases (a) for fixed order of approximation p, as ωh tends to zero, or (b) for a fixed mesh of size h with $\omega h \gg 1$, as the order of the scheme p is increased. We also compare results obtained using the spectral element scheme in the case of both (a) and (b) to that of the finite element scheme. Moreover, we present numerical results to verify the accuracy of spectral element schemes to that of finite element schemes. The second specific aim of this work is to develop higher order numerical methods following the suggestion of Marfurt to reduce dispersion and dissipation error. More importantly, we establish an equivalence between the optimally blended scheme and non-standard quadrature rules in the case of arbitrary order approximation p as ωh tends to zero. Furthermore, we study dispersive and dissipative properties of this scheme for a fixed mesh of size h with $\omega h \gg 1$, as the order of the scheme p is increased. The final specific aim of this work is to extend the one-dimensional results of the finite element, spectral element and optimally blended schemes to higher dimensions for fixed order of approximation p, as ωh tends to zero on a rectangular grid.

1.7 Organisation of the thesis

In Chapter 2, we describe the spectral element scheme for the scalar wave equation which is sometimes called the *Gauss-point mass lumped finite element scheme*. We study the dispersive behaviour of the scheme in detail and provide a quantitative description of the nature of both the dispersive and dissipative behaviour of the scheme in the case of (a) for fixed order of approximation p, as ωh tends to zero, or (b) for a fixed mesh of size h with $\omega h \gg 1$, as the order of the scheme p is increased. We adopt the same approach used by [1] in the analysis of the conforming finite element method, and derive explicit expressions for discrete dispersion relations for the spectral element method.

In Chapter 3, we study the dispersion and dissipation of the novel numerical scheme obtained by taking a weighted averaging of the consistent (finite element) mass matrix and lumped (spectral element) mass matrix in the case of both (a) and (b). Furthermore, we establish an equivalence between the optimally blended scheme and the novel non-standard quadrature rule.

Chapter 4 is devoted to extending the one-dimensional results of the finite element, spectral element and optimally blended schemes to higher dimensions. In this chapter we show that for a rectangular grid, the analytical expressions for the discrete dispersion error in higher dimensions can be obtained using one dimensional discrete dispersion error expressions.

Chapter 2

Dispersive and dissipative behaviour of the spectral element method

2.1 Introduction

The spectral element method [13] is a spectrally accurate algorithm for solving a wide variety of partial differential equations on unstructured grids. The computational domain is typically broken into quadrilateral elements, within each of which the variables are approximated by high degree polynomials. A set of discrete equations for the coefficients is derived using a weak form of the problem in which the integrals are approximated using a quadrature rule. In particular, if the Gauss-Legendre-Lobatto quadrature rule is chosen in conjunction with a Lagrange basis for the approximation based at the nodes of the Gauss-Legendre-Lobatto rule, then the resulting mass matrix is diagonal in certain cases. For this reason, the same approach is sometimes described the *Gauss-point mass lumped*

finite element scheme [17, 19] in the finite element literature.

The fact that the mass matrix is diagonal means that the method is particularly attractive for the efficient numerical simulation of wave phenomena, if used in conjunction with an explicit time-stepping scheme. The approach has found widespread application in a variety of areas ranging from acoustical waves [46], hydrostatic fluid flow [39], tumour angiogenesis [62], reaction-diffusion problems [48], edge finite element approximation of Maxwell's equations [18] and seismic wave propagation [42–44].

Despite the widespread usage of the spectral element method for computational wave propagation *loc. cit.*, there seems to be no detailed study of the dispersive and dissipative properties of the scheme in the case of (a) for fixed order of approximation p, as ωh tends to zero, or (b) for a fixed mesh of size h with $\omega h \gg 1$, as the order of the scheme p is increased. However, it was only relatively recently [1] that a complete, sharp analysis of the dispersive behaviour of conforming finite element methods was given for finite elements of any order p as the mesh-size h is reduced and, as the order of the method p is increased on a fixed mesh. The analysis of [1] was carried out in the context of the Helmholtz equation but similar results were subsequently obtained for discontinuous Galerkin finite element methods [2, 4] and for edge element approximation of Maxwell's equations [3].

The goal of this chapter is to study dispersive and dissipative properties of the spectral element scheme in detail and to provide both a qualitative description of the nature of the dispersive and dissipative behaviour of the scheme, along with precise quantitative statements of the accuracy, in case of both (a) and (b). For this we adopt a broadly similar approach to one used by [1] in the analysis of the conforming finite element method, where the key step in the analysis was the derivation of an explicit expression for the dispersion relation for the numerical

scheme. Here we derive the corresponding discrete dispersion relation for the spectral element method. However, the discrete dispersion relation for the finite element case obtained in [1] took the form of a rational function expressed in terms of Padé approximants for the tan and cot functions. In contrast, in the case of the spectral element method considered here, the discrete dispersion relation again assumes the form of a rational function but this is no longer related to Padé approximants.

This chapter is organised as follows. We start by developing a uni-dimensional model problem in Section 2.2. In Sections 2.3 and 2.4, discrete dispersion relations are derived for linear and higher order approximating elements for the model problem. Moreover, numerical results obtained with both spectral element and finite element methods are shown. Sections 2.5 and 2.6 contain proofs of the results.

2.2 Model problem and its discretisation

Consider the one-dimensional model problem of wave propagation

$$\frac{\partial^2 u}{\partial t^2} - \frac{\partial^2 u}{\partial x^2} = 0, \quad x \in (0,1),\ t > 0 \tag{2.1}$$

subject to the boundary conditions

$$u(0,t) = e^{-i\omega t} \ \text{ and } \ \frac{\partial u}{\partial x}(1,t) + \frac{\partial u}{\partial t}(1,t) = 0 \ \text{ for } \ t > 0,$$

and initial conditions

$$u(x,0) = u_0(x) \ \text{ and } \ \frac{\partial u}{\partial t}(x,0) = v_0(x), \ \text{ for } \ x \in (0,1)$$

where $\omega > 0$ is the angular frequency. The variational formulation of the above problem is: Find $u(x,t) \in H^1(0,1)$ along with the initial and boundary conditions such that

$$\frac{d^2}{dt^2}(u,v) + (u',v') + \frac{\partial u}{\partial t}(1,t)\overline{v(1)} = 0, \ \ \forall v \in H^1_E(0,1), \ \ t > 0$$

where $(\cdot,\cdot)$ denotes the L^2-inner product on $(0,1)$ and $H^1_E(0,1) = \{v \in H^1(0,1) : v(0) = 0\}$ where $H^1(0,1)$ is the usual Sobolev space. We construct a semi-discretisation in space by introducing a partition $\mathcal{G}_h = \{jh, j = 0,1,\ldots,K\}$ of the interval $(0,1)$ into K subintervals of equal length $h = 1/K$. Let $V_{hp} \subset H^1_E(0,1)$ be the corresponding space of continuous piecewise polynomials of degree $p \in \mathbb{N}$ defined on $\mathcal{G}_h$. We seek an approximate solution $u_{hp} \in V_{hp}$ such that

$$\frac{d^2}{dt^2}(u_{hp}, v_{hp}) + \left(u'_{hp}, v'_{hp}\right) + \frac{\partial u_{hp}}{\partial t}(1,t)\overline{v_{hp}(1)} = 0, \ \forall v_{hp} \in V_{hp}.$$

We can construct a basis for V_{hp} in terms of basis functions $\{\Theta_\ell\}_{\ell=0}^p$ defined on a reference element $(-1,1)$ as follows. Let $-1 = \tilde{\zeta}_0 < \tilde{\zeta}_1 < \ldots < \tilde{\zeta}_p = 1$ be distinct nodes on $[-1,1]$ and define $\Theta_\ell \in \mathbb{P}_p(-1,1)$ by the conditions $\Theta_\ell(\tilde{\zeta}_m) = \delta_{\ell m}$. The corresponding global basis functions for the entire mesh are denoted by $\{\theta_i\}_{i=1}^N$ and satisfy $\theta_i(1) = 0$ for $i = 1,2,\ldots,N-1$, then u_{hp} can be written as

$$u_{hp}(x,t) = \sum_{i=1}^{N} \alpha_i(t)\theta_i(x) \quad x \in (0,1), \ \ t \geq 0$$

where α_i are smooth complex-valued functions satisfying

$$\sum_{i=1}^{N}\left((\theta_i,\theta_j)\frac{d^2\alpha_i}{dt^2}(t) + \alpha_i(t)\left(\theta'_i,\theta'_j\right) + \frac{d\alpha_i}{dt}(t)\delta_{iN}\delta_{jN}|\theta_N(1)|^2\right) = 0 \tag{2.2}$$

for all $j = 1,2,\ldots,N$. By letting $\vec{\alpha}$ denote the vector whose components are $\alpha_i, i = 1,2,\ldots,N$, (2.2) can be written in matrix form as

$$\mathbf{M}\frac{d^2\vec{\alpha}}{dt^2} + \mathbf{C}\frac{d\vec{\alpha}}{dt} + \mathbf{K}\vec{\alpha} = \vec{0}, \tag{2.3}$$

where, for $i,j = 1,2,\ldots,N$

$$\mathbf{K}_{ij} = \left(\theta'_i,\theta'_j\right), \quad \mathbf{M}_{ij} = (\theta_i,\theta_j) \text{ and } \mathbf{C}_{ij} = \delta_{iN}\delta_{jN}|\theta_N(1)|^2. \tag{2.4}$$

We may define a fully-discrete scheme by discretising the temporal derivative using centred differences with step-size $\Delta t > 0$ to give

$$[\mathbf{M} + \frac{\Delta t}{2}\mathbf{C}]\vec{\alpha}_{n+1} = [2\mathbf{M} - (\Delta t)^2\mathbf{K}]\vec{\alpha}_n - [\mathbf{M} - \frac{\Delta t}{2}\mathbf{C}]\vec{\alpha}_{n-1}, \quad n = 1,2,3,\ldots \tag{2.5}$$

where $\vec{\alpha}_n \approx \vec{\alpha}\,(n\Delta t)$. The matrices $\mathbf{K}_{ij}$ and $\mathbf{M}_{ij}$ appearing in (2.4) are the consistent stiffness and mass matrices, which can be assembled in the usual fashion from the corresponding matrices defined on the reference element as follows:

$$\hat{K}_{\ell m} = \frac{2}{h}\int_{-1}^{1} \frac{d\Theta_\ell(s)}{ds}\frac{d\Theta_m(s)}{ds}ds \quad \forall \ell, m \in \{0,1,2,\ldots,p\} \tag{2.6}$$

and

$$\hat{M}_{\ell m} = \frac{h}{2}\int_{-1}^{1} \Theta_\ell(s)\Theta_m(s)ds \quad \forall \ell, m \in \{0,1,2,\ldots,p\}. \tag{2.7}$$

Observe that at each time-step it is necessary to invert the matrix $\mathbf{M} + \dfrac{\Delta t}{2}\mathbf{C}$. In practise the mass matrix $\mathbf{M}$ is often replaced by a lumped mass matrix $\widetilde{\mathbf{M}}$ [40] which means that each time-step involves the inversion of the diagonal matrix $\widetilde{\mathbf{M}} + \dfrac{\Delta t}{2}\mathbf{C}$. The lumped mass matrix is obtained by employing the spectral element method [13].

To derive the spectral element scheme we replace the integrals appearing in (2.6)-(2.7) with a numerical quadrature rule. The $(p+1)$-point Gauss-Lobatto quadrature rule is defined by

$$\int_{-1}^{1} f(s)ds \approx \mathcal{Q}^{(p)}(f) = \sum_{\ell=1}^{p-1} \tilde{w}_\ell f(\tilde{\zeta}_\ell) + \frac{2}{p(p+1)}[f(-1)+f(1)] \tag{2.8}$$

where $\{\tilde{\zeta}_\ell\}_{\ell=1}^{p-1}$ are taken to be the zeros of L_p', and L_p is the p-th order Legendre polynomial [28] with the weights given by ([56], eq.(4.10-26))

$$\tilde{w}_\ell = \frac{2}{p(p+1)[L_p(\tilde{\zeta}_\ell)]^2} \quad \forall \ell \in \{1,2,3,\ldots,p-1\}. \tag{2.9}$$

The quadrature rule is exact for polynomials of degree at most $2p-1$. Now, using (2.8) to approximate the integrals, the elemental stiffness and mass matrices appearing in (2.6)-(2.7) are replaced by the following forms:

$$\hat{K}_{\ell m} \approx \frac{2}{h}\mathcal{Q}^{(p)}(\Theta_\ell'\Theta_m') = \frac{2}{h}\sum_{r=0}^{p} \frac{d\Theta_\ell(\tilde{\zeta}_r)}{ds}\frac{d\Theta_m(\tilde{\zeta}_r)}{ds}\tilde{w}_r \quad \forall \ell, m \in \{0,1,2,\ldots,p\}$$

and

$$\hat{M}_{\ell m} \approx \frac{h}{2}\mathcal{Q}^{(p)}(\Theta_\ell \Theta_m) = \frac{h}{2}\sum_{r=0}^{p} \Theta_\ell(\tilde{\zeta}_r)\Theta_m(\tilde{\zeta}_r)\tilde{w}_r \quad \forall \ell, m \in \{0, 1, 2, \ldots, p\}.$$

As the product $\dfrac{d\Theta_\ell}{ds}\dfrac{d\Theta_m}{ds} \in \mathbb{P}_{2p-2}$, the element stiffness matrix is not affected by the use of the quadrature rule, whereas the mass matrix will be different.

A key idea in the spectral element method is that by choosing the nodes used to construct the basis functions to coincide with the nodes used in the quadrature rule, the elemental mass matrix becomes diagonal:

$$\hat{M}_{\ell m} \approx \frac{h}{2}\mathcal{Q}^{(p)}(\Theta_\ell \Theta_m) = \frac{h}{2}\delta_{\ell m}\tilde{w}_\ell \quad \forall \ell, m \in \{0, 1, 2, \ldots, p\}$$

and consequently the matrix $\widetilde{\mathbf{M}} + \dfrac{\Delta t}{2}\mathbf{C}$ will be diagonal. The corresponding fully-discrete scheme takes the form

$$[\widetilde{\mathbf{M}} + \frac{\Delta t}{2}\mathbf{C}]\vec{\alpha}_{n+1} = [2\widetilde{\mathbf{M}} - (\Delta t)^2\mathbf{K}]\vec{\alpha}_n - [\widetilde{\mathbf{M}} - \frac{\Delta t}{2}\mathbf{C}]\vec{\alpha}_{n-1}, \quad n = 1, 2, 3, \ldots$$

where, thanks to the use of the quadrature rule, it is now only necessary to invert a diagonal matrix at each time step.

2.3 Dispersive and dissipative behaviour in space

In order to focus on the spatial discretisation, we consider a time harmonic solution of the form $u(x,t) = U(x)e^{-i\omega t}$ for $\omega > 0$ fixed where the spatial component U satisfies the equation

$$-U''(x) - \omega^2 U(x) = 0, \quad x \in (0,1) \tag{2.10}$$

with boundary conditions $U(0) = 1$, $U'(1) - i\omega U(1) = 0$. Here, we choose non-homogeneous Dirichlet data.

The analytical solution of the above problem is $U(x) = e^{i\omega x}$, so that both the real and imaginary parts oscillate. In Figure 2.1, we present the numerical approximations obtained using piecewise linear elements with both finite element and spectral element methods. The phase lead and phase lag of the numerical approximations are clearly visible. Furthermore, it is evident that the phase *lead* occurs when the solution is approximated using the finite element method (full integration) whereas phase *lag* corresponds to the approximation obtained with the spectral element method (numerical quadrature). Whilst it is possible to eradicate numerical dispersion and dissipation due to temporal discretisation completely, by using, for example an exponential integrator, this is much more problematic in the case of spatial discretisation. In the one-dimensional case it is possible to modify the scheme to obtain a non-dispersive approximation in space, but this is not possible in higher numbers of spatial dimensions [10].

2.3.1 Dispersion and dissipation of linear elements

Let us study the dispersive and dissipative behaviour of the finite element and spectral element schemes in more detail. Let V_{h1} denote the set of continuous piecewise linear functions with nodes located at the nodes of the grid $\mathcal{G}_h$. We seek an approximation $U_{h1} \in V_{h1}$ of problem (2.10) satisfying $U_{h1}(0) = 1$ such that

$$B(U_{h1}, v_{h1}) = 0, \qquad \forall v_{h1} \in V_{h1} \cap H^1_E(0,1) \tag{2.11}$$

where

$$B(U_{h1}, v_{h1}) = (U'_{h1}, v'_{h1}) - \omega^2 (U_{h1}, v_{h1}) - i\omega U_{h1}(1)\overline{v_{h1}(1)}.$$

We can write U_{h1} in the form

$$U_{h1}(x) = \sum_{i=0}^{N} \alpha_i \theta_i(x)$$

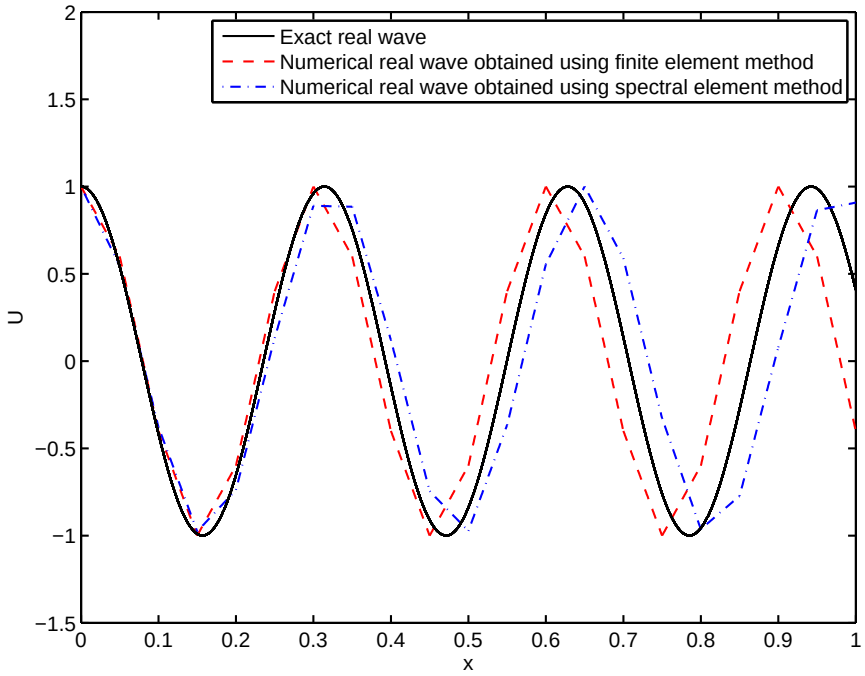
Exact real wave
Numerical real wave obtained using finite element method
Numerical real wave obtained using spectral element method
U
x
2
1.5
1
0.5
0
−0.5
−1
−1.5
0
0.1
0.2
0.3
0.4
0.5
0.6
0.7
0.8
0.9
1

(a)

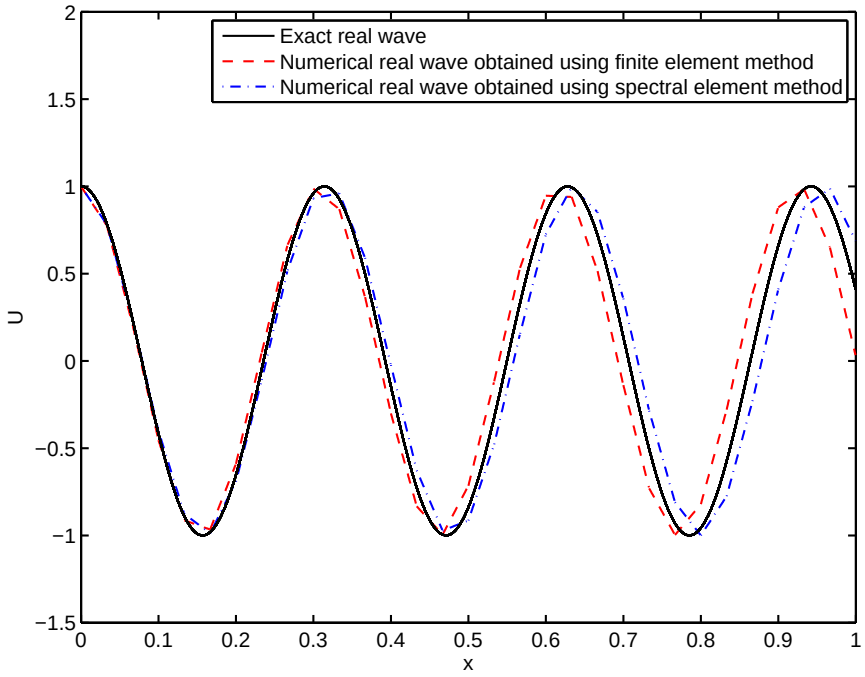
Exact real wave
Numerical real wave obtained using finite element method
Numerical real wave obtained using spectral element method
U
x
2
1.5
1
0.5
0
−0.5
−1
−1.5
0
0.1
0.2
0.3
0.4
0.5
0.6
0.7
0.8
0.9
1

(b)

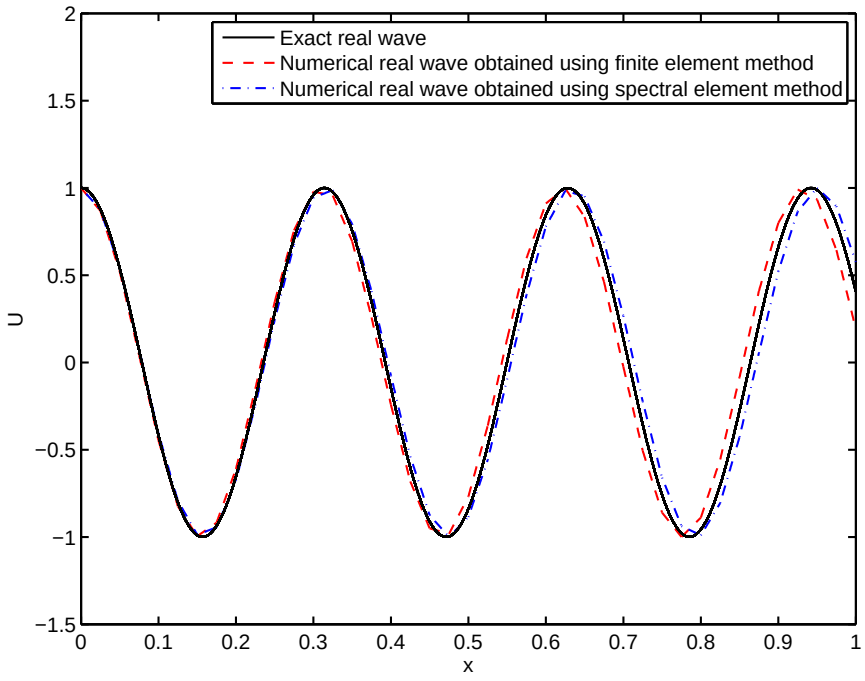

(c)

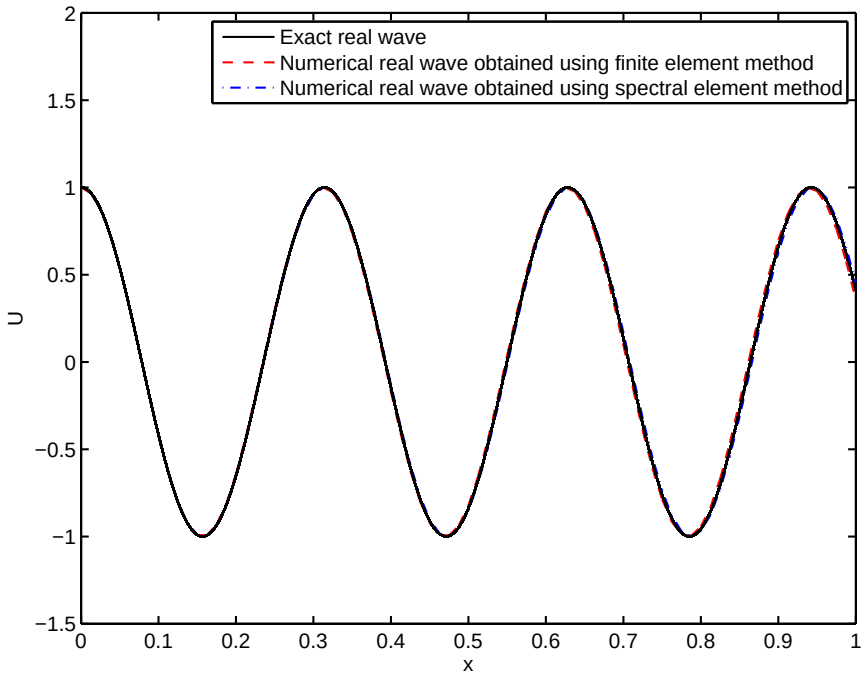

(d)

Figure 2.1: Numerical approximations of the solution to equation (2.10) obtained for $\omega = 20$ with both finite element and spectral element methods using (a) 20, (b) 30, (c) 40 and (d) 80 linear elements.

where $\theta_i(jh) = \delta_{ij}$ for all $i, j = 0, 1, \ldots, N$ are the usual piecewise linear hat functions associated with the nodes in the grid. Substituting U_{h1} into (2.11) and taking $v_{h1} = \theta_j$ for $j \in \{0, 1, \ldots, N\}$, we obtain $\alpha_0 = 1$, and

$$\sum_{i=0}^{N} \alpha_i B\left(\theta_i, \theta_j\right) = 0, \quad j = 1, 2, \ldots, N.$$

Furthermore, since the mesh is uniform, we may express $B(\theta_i, \theta_j)$ in terms of $B(\theta_0, \theta_1)$ and $B(\theta_1, \theta_1)$ to obtain that the above conditions are equivalent to

$$\begin{aligned} \alpha_0 &= 1, \\ \alpha_{j-1} B\left(\theta_0, \theta_1\right) + \alpha_j B\left(\theta_1, \theta_1\right) + \alpha_{j+1} B\left(\theta_0, \theta_1\right) &= 0, \quad j = 1, 2, \ldots, N-1 \\ \alpha_{N-1} B\left(\theta_0, \theta_1\right) + \alpha_N \left[\frac{1}{2} B\left(\theta_1, \theta_1\right) - i\omega\right] &= 0. \end{aligned} \tag{2.12}$$

The system (2.12) is a second order difference equation for which we seek a solution of the form $\alpha_j = c\lambda^j$ where c and λ are constants to be determined. Inserting this form into the equations for $j = 1, 2, \ldots, N-1$ gives

$$\lambda + \frac{1}{\lambda} = -\frac{B\left(\theta_1, \theta_1\right)}{B\left(\theta_0, \theta_1\right)}.$$

It is convenient to express λ in the form $\lambda = e^{\pm i\mu^{(1)}h}$, where $\mu^{(1)} \in \mathbb{C}$ is given by

$$\cos \mu^{(1)} h = -\frac{1}{2} \frac{B\left(\theta_1, \theta_1\right)}{B\left(\theta_0, \theta_1\right)}. \tag{2.13}$$

Hence, using linearity, α_j is given by

$$\alpha_j = b_1 \cos(j\mu^{(1)}h) + b_2 \sin(j\mu^{(1)}h), \ \ \forall j = 0, 1, 2, \ldots, N.$$

Applying the first condition from (2.12) gives

$$1 = \alpha_0 = b_1 \cos(0) + b_2 \sin(0) \Rightarrow b_1 = 1.$$

Similarly, after elementary manipulations the final condition in (2.12) gives

$$b_2 = \frac{[B(\theta_0, \theta_1) \sin(N\mu^{(1)}h) \sin \mu^{(1)}h - i\omega \cos(N\mu^{(1)}h)]}{[B(\theta_0, \theta_1) \cos(N\mu^{(1)}h) \sin \mu^{(1)}h + i\omega \sin(N\mu^{(1)}h)]}, \quad \forall j = 0, 1, 2, \ldots, N.$$

Consequently, the solution of (2.12) is give by

$$\alpha_j = \frac{[B(\theta_0,\theta_1)\cos(N-j)\mu^{(1)}h\sin\mu^{(1)}h + i\omega\sin(N-j)\mu^{(1)}h]}{[B(\theta_0,\theta_1)\cos N\mu^{(1)}h\sin\mu^{(1)}h + i\omega\sin N\mu^{(1)}h]},\ \ \forall j = 0,1,2,\ldots,N.$$

All of the foregoing arguments apply equally well to the spectral element scheme leading to the same expression for the coefficients α_j with the bilinear form $B(\cdot,\cdot)$ replaced by $\tilde{B}(\cdot,\cdot)$, where $\tilde{B}(\cdot,\cdot)$ denotes the bilinear form for the spectral element method obtained using reduced integration. We expect that $\mu^{(1)}h \to \omega h$ as $h \to 0$, corresponding to the fact that the frequency of the discrete approximation approaches the frequency of the true solution as the grid $\mathcal{G}_h$ is refined. For finite $h > 0$, the difference $\mu^{(1)}h - \omega h$ gives a measure of the dispersive and dissipative behaviour of the numerical scheme. We can calculate $\mu^{(1)}h$ explicitly for the above schemes as follows. The first order basis functions on the reference element are given by

$$\Theta_0 = (1-s)/2 \qquad \text{and} \qquad \Theta_1 = (1+s)/2, \quad \forall s \in [-1,1].$$

Hence, by applying a change of variable, we obtain

$$B(\theta_0,\theta_1) = \frac{2}{h}\int_{-1}^{1}(\Theta_0'\Theta_1' - \kappa^2\Theta_0\Theta_1)ds = -\frac{2\kappa^2+3}{3h} \tag{2.14}$$

and

$$B(\theta_1,\theta_1) = \frac{4}{h}\int_{-1}^{1}(\Theta_1'^2 - \kappa^2\Theta_1^2)ds = -\frac{2(4\kappa^2-3)}{3h} \tag{2.15}$$

where $\kappa = \omega h/2$. Similarly,

$$\tilde{B}(\theta_0,\theta_1) = \frac{2}{h}\left[\sum_{\ell=0}^{1}\left(\Theta_0'(\tilde{\zeta}_\ell)\Theta_1'(\tilde{\zeta}_\ell) - \kappa^2\Theta_0(\tilde{\zeta}_\ell)\Theta_1(\tilde{\zeta}_\ell)\right)\tilde{w}_\ell\right] = -\frac{1}{h} \tag{2.16}$$

and

$$\tilde{B}(\theta_1,\theta_1) = \frac{4}{h}\left[\sum_{\ell=0}^{1}\left(\Theta_1'^2(\tilde{\zeta}_\ell) - \kappa^2\Theta_1^2(\tilde{\zeta}_\ell)\right)\tilde{w}_\ell\right] = \frac{2(1-2\kappa^2)}{h} \tag{2.17}$$

with $\tilde{\zeta}_0 = -1, \tilde{\zeta}_1 = 1$ and $\tilde{w}_0 = \tilde{w}_1 = 1$. Consequently, we obtain

$$\mu^{(1)}h = \cos^{-1}\left(\frac{3-4\kappa^2}{3+2\kappa^2}\right) \tag{2.18}$$

for the finite element scheme and

$$\tilde{\mu}^{(1)}h = \cos^{-1}\left(1 - 2\kappa^2\right). \tag{2.19}$$

for the spectral element scheme. If $\kappa = \omega h/2 \ll 1$, then the discrete dispersion relations (2.18) and (2.19) may be expressed as a series in ωh to give the well-known results ([60], eq.(41)):

$$\mu^{(1)}h - \omega h = -\frac{(\omega h)^3}{24} + \cdots$$

and

$$\tilde{\mu}^{(1)}h - \omega h = \frac{(\omega h)^3}{24} + \cdots .$$

Note that the leading term in the phase differences in these expressions are identical in magnitude but have opposite sign. These expressions confirm the behaviour observed in Figure 2.1 where it was observed that the finite element scheme exhibits phase lead whilst the spectral element scheme exhibits phase lag of equal magnitude. Moreover, these expressions were previously derived by a different method in Chapter 1.

2.3.2 Dispersion and dissipation of quadratic elements

In Figure 2.2, we show the effect of raising the order of the approximation from $p = 1$ to $p = 2$ whilst keeping the same number of degrees of freedom. It is clear from Figure 2.2(a) that if we use piecewise quadratic elements instead of piecewise linear elements both the phase lag and phase lead are decreased compared with Figure 2.1(a) where the same number of degrees of freedom are used. Moreover, both the phase errors are reduced as can be seen in Figure 2.2(a). In particular, by employing a similar argument to the one used in the case of first order elements, we obtain the following expressions

$$\mu^{(2)}h - \omega h = -\frac{(\omega h)^5}{1440} + \cdots$$

and

$$\tilde{\mu}^{(2)}h - \omega h = \frac{(\omega h)^5}{2880} + \cdots$$

(see Theorem 2.4.2 which we will prove later). Observe that the order of the error is higher for the quadratic elements as is to be expected. However, we also observe that, as before, the signs of the leading terms in the error are opposite but in this case, the magnitude of the error in the spectral element scheme is one half that of the finite element scheme in the limit $\omega h \to 0$.

2.3.3 Dispersion and dissipation of higher order elements

In Figure 2.3 we present the results obtained by increasing the order of the approximating elements while again keeping the number of degrees of freedom fixed. Comparing the results in Figures 2.1(a) and 2.2(a) with those in Figure 2.3, we observe that the convergence is rather rapid as the order of the method is increased even with a fixed number of degrees of freedom. This suggests that it is more efficient to seek convergence by raising the order of the method rather than refining the mesh in the cases of both finite element and spectral element schemes.

We shall also investigate the nature of the convergence behaviour of the schemes as the order $p \to \infty$ on a fixed mesh. In Figure 2.4, we present the numerical approximations obtained on a fixed mesh of size $h = 1$ with frequency $\omega = 80$ for orders of approximation $p = 37$ to $p = 45$. It is observed that for orders $p \leq 41$, both finite element and spectral element schemes fail to resolve the wave, with the spectral element scheme exhibiting wild over-shoots and under-shoots. However, once the order reaches $p = 42$, there is a dramatic improvement in the resolution of both schemes and for $p \geq 44$, both schemes provide an essentially exact approximation of the wave. We see that the convergence behaviour of the higher order schemes, whereby h is fixed and p is increased, is quite different from

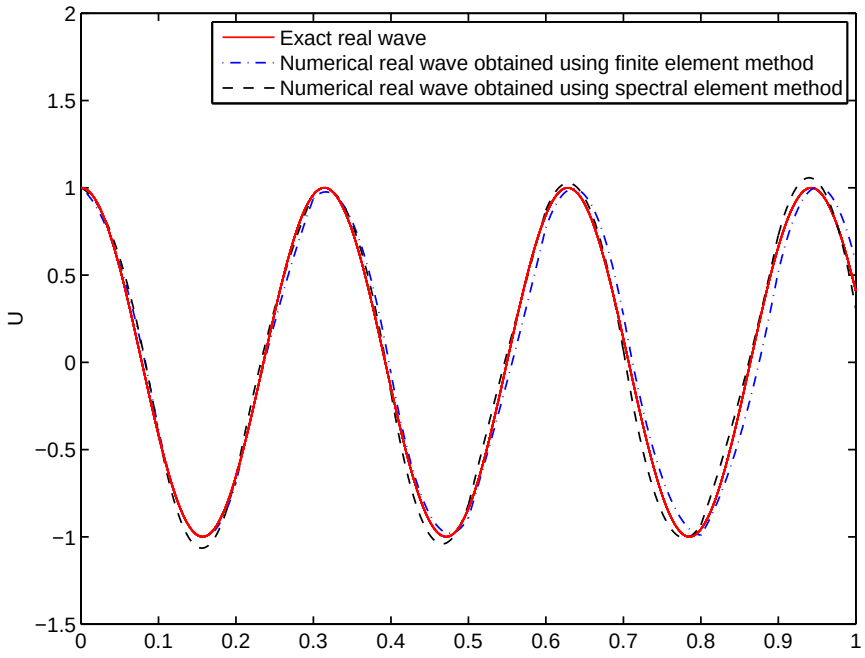

(a)

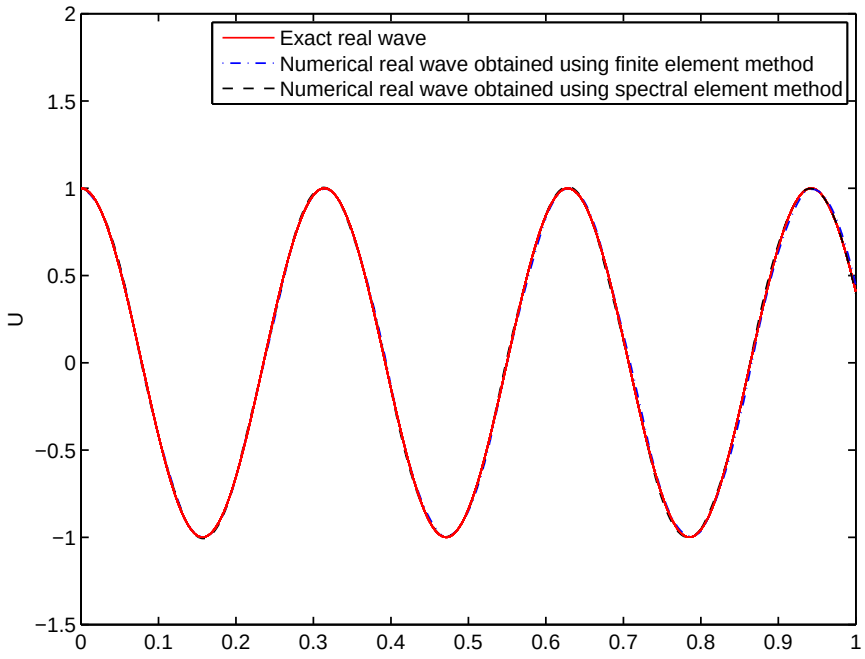

(b)

Figure 2.2: Numerical approximations of the solution to equation (2.10) obtained for $\omega = 20$ with both full and spectral element methods using (a) 10 and (b) 15 quadratic elements.

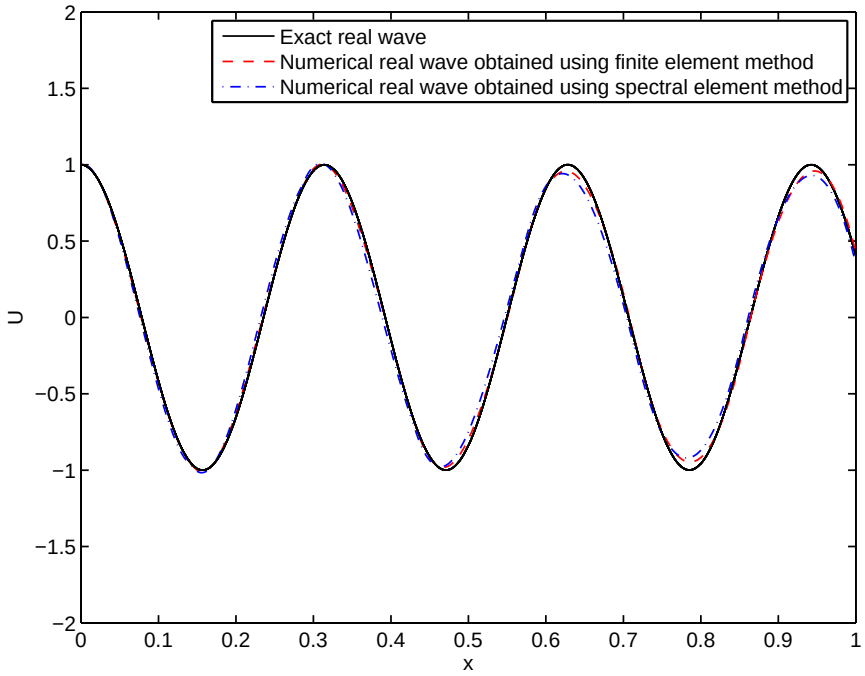
Exact real wave
Numerical real wave obtained using finite element method
Numerical real wave obtained using spectral element method
U
x
2
1.5
1
0.5
0
−0.5
−1
−1.5
−2
0
0.1
0.2
0.3
0.4
0.5
0.6
0.7
0.8
0.9
1

(a) p = 3

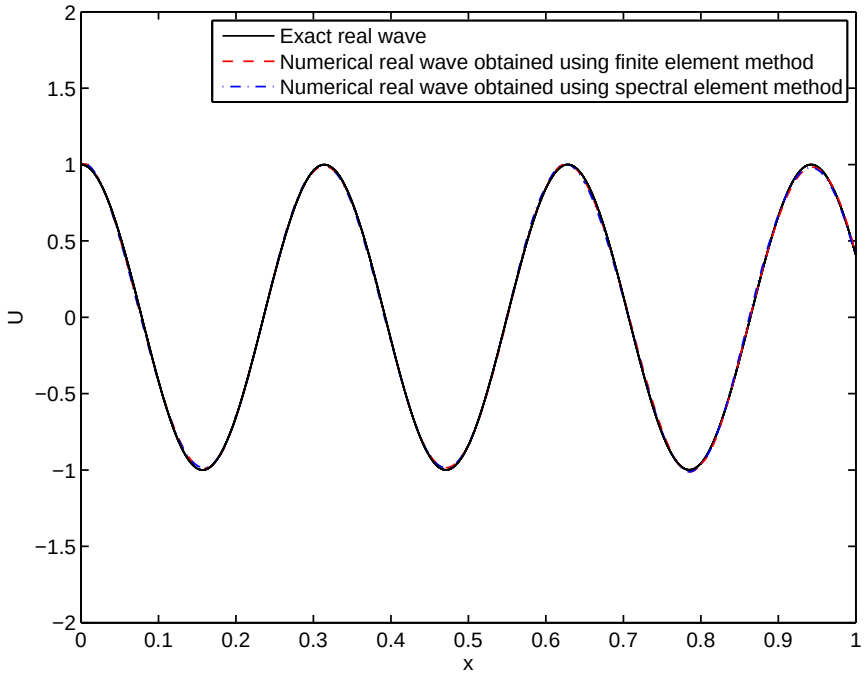
Exact real wave
Numerical real wave obtained using finite element method
Numerical real wave obtained using spectral element method
U
x
2
1.5
1
0.5
0
−0.5
−1
−1.5
−2
0
0.1
0.2
0.3
0.4
0.5
0.6
0.7
0.8
0.9
1

(b) p = 4

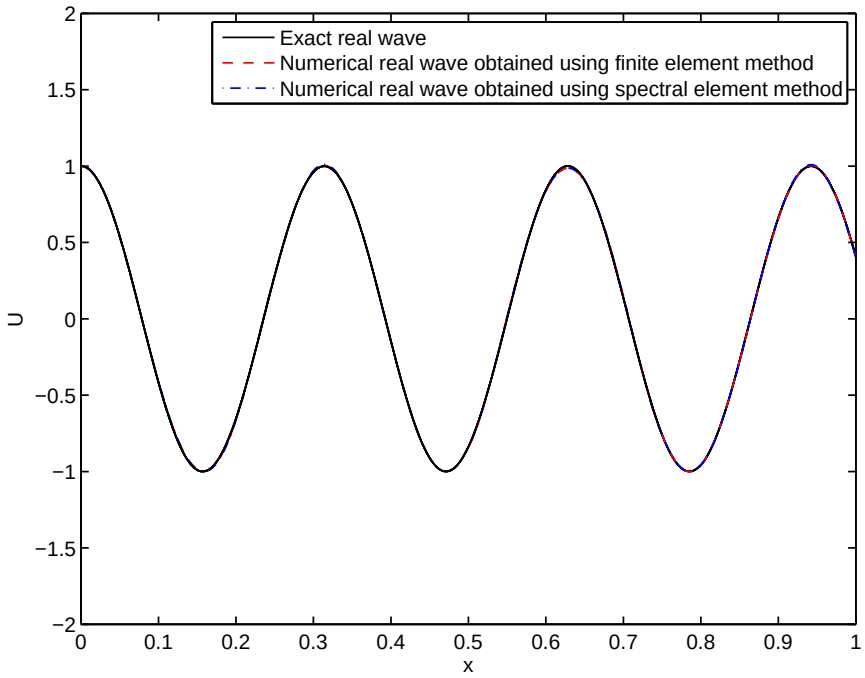

(c) p = 5

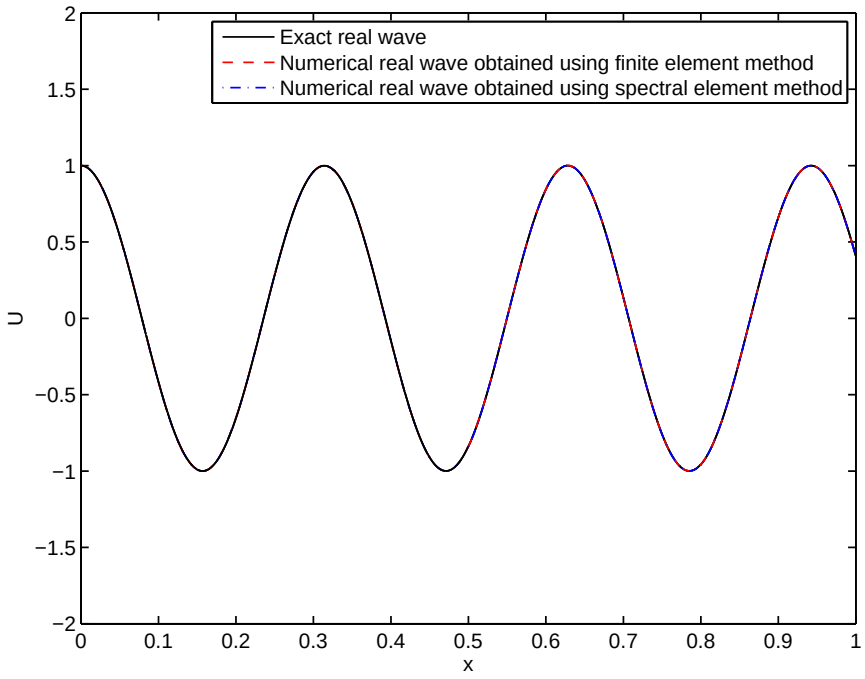

(d) p = 10

Figure 2.3: Numerical approximations of the solution to equation (2.10) obtained for $\omega = 20$ using (a) seven cubic (b) five quartic (c) four 5th order (d) two 10th order elements.

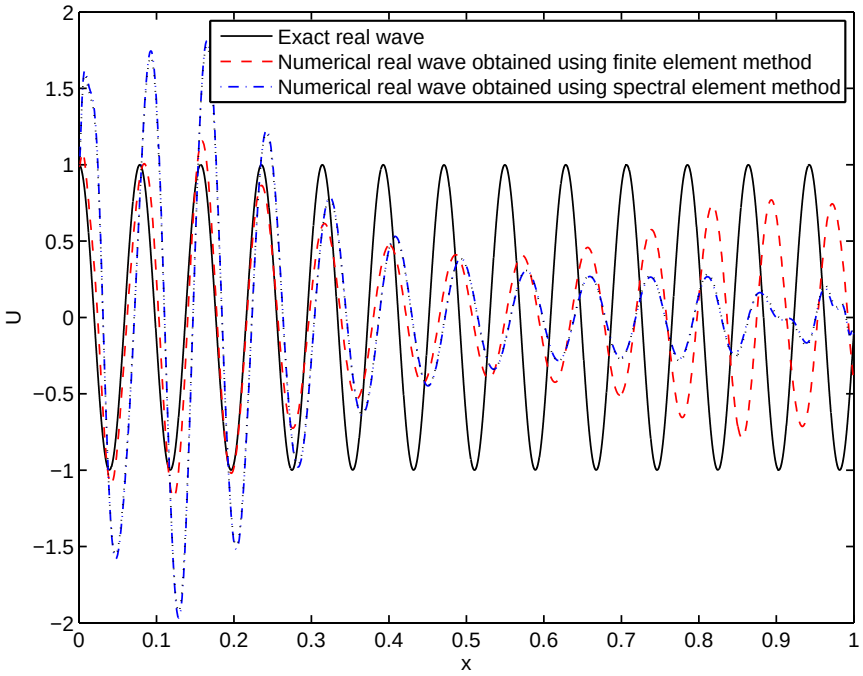
Exact real wave
Numerical real wave obtained using finite element method
Numerical real wave obtained using spectral element method
U
x
2
1.5
1
0.5
0
−0.5
−1
−1.5
−2
0
0.1
0.2
0.3
0.4
0.5
0.6
0.7
0.8
0.9
1

(a) p = 37

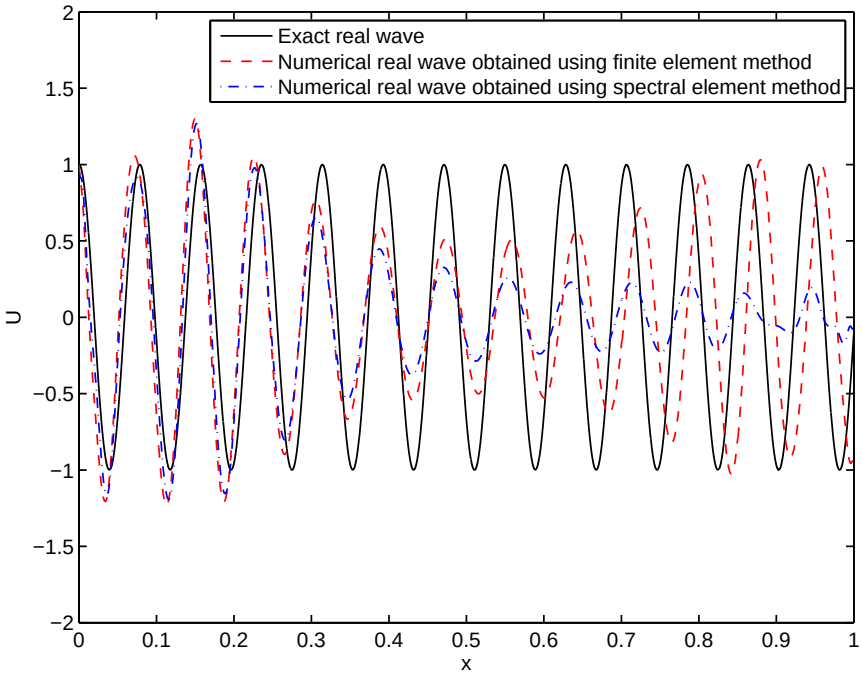
Exact real wave
Numerical real wave obtained using finite element method
Numerical real wave obtained using spectral element method
U
x
2
1.5
1
0.5
0
−0.5
−1
−1.5
−2
0
0.1
0.2
0.3
0.4
0.5
0.6
0.7
0.8
0.9
1

(b) p = 38

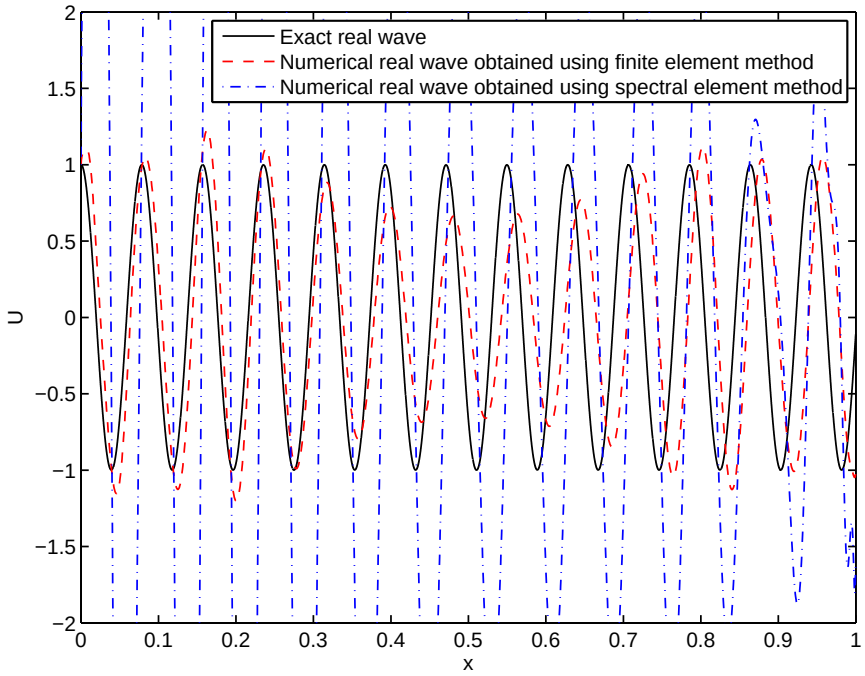
Exact real wave
Numerical real wave obtained using finite element method
Numerical real wave obtained using spectral element method
U
x

(c) p = 39

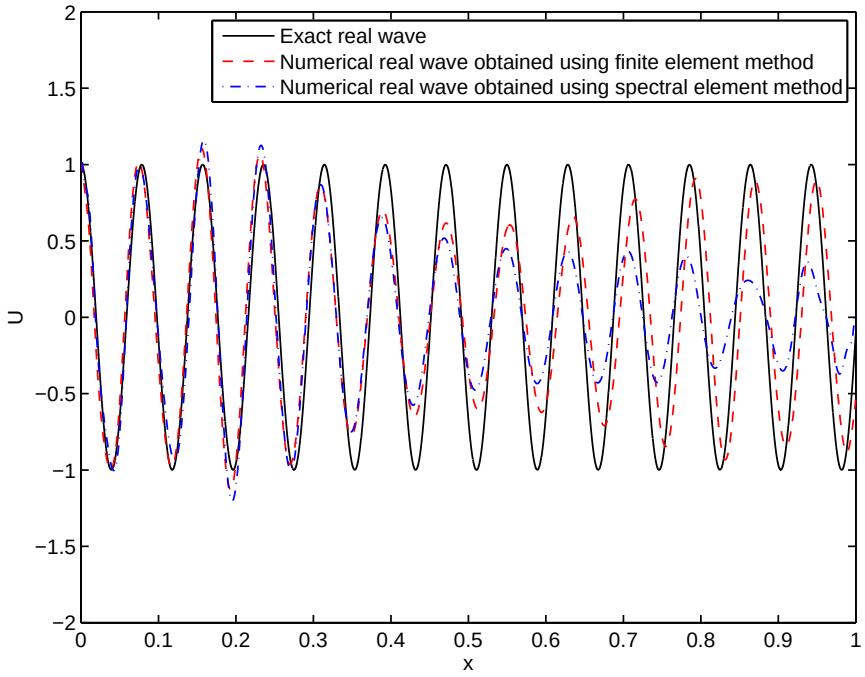
Exact real wave
Numerical real wave obtained using finite element method
Numerical real wave obtained using spectral element method
U
x

(d) p = 40

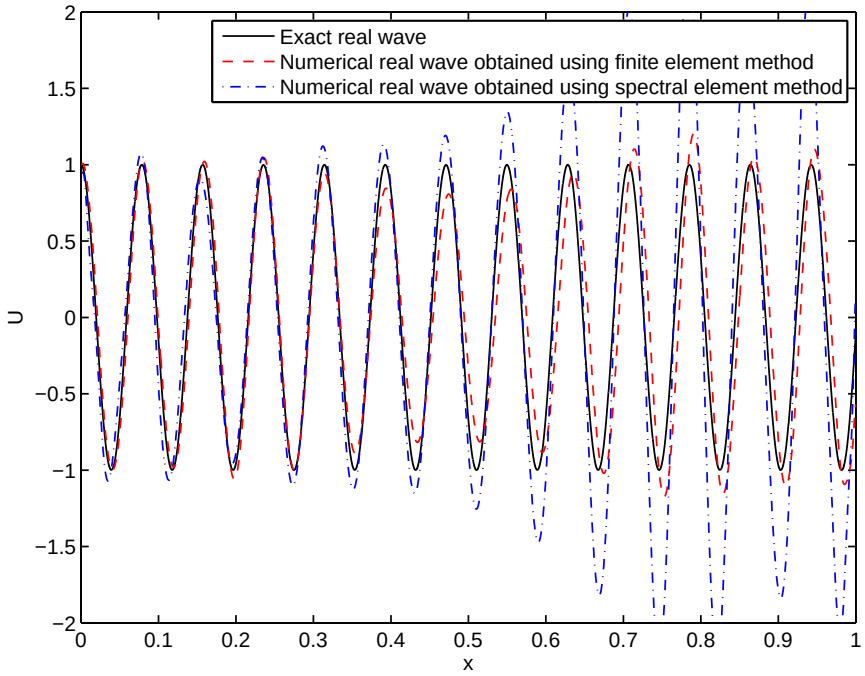
Exact real wave
Numerical real wave obtained using finite element method
Numerical real wave obtained using spectral element method
U
x
2
1.5
1
0.5
0
−0.5
−1
−1.5
−2
0
0.1
0.2
0.3
0.4
0.5
0.6
0.7
0.8
0.9
1

(e) p = 41

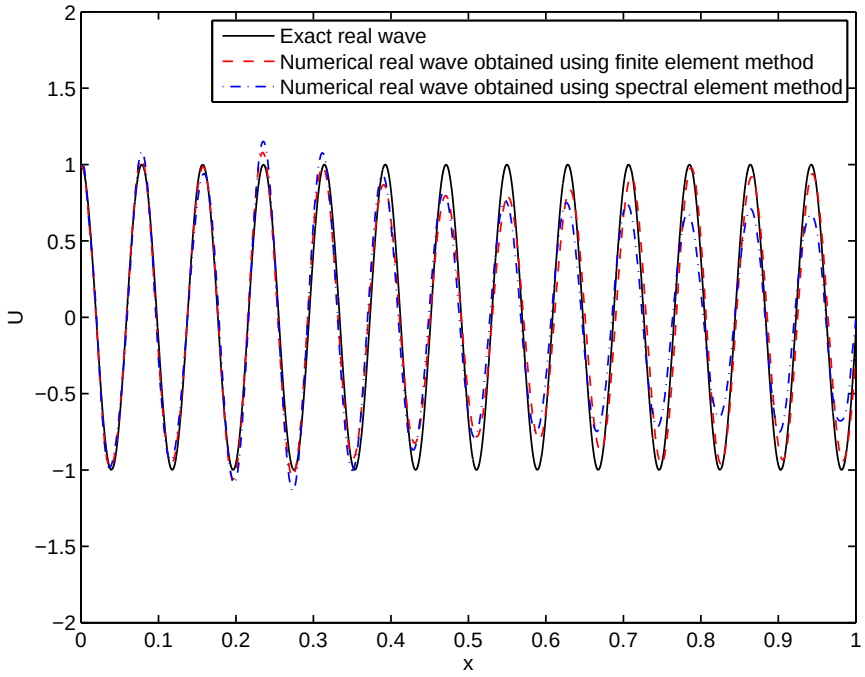
Exact real wave
Numerical real wave obtained using finite element method
Numerical real wave obtained using spectral element method
U
x
2
1.5
1
0.5
0
−0.5
−1
−1.5
−2
0
0.1
0.2
0.3
0.4
0.5
0.6
0.7
0.8
0.9
1

(f) p = 42

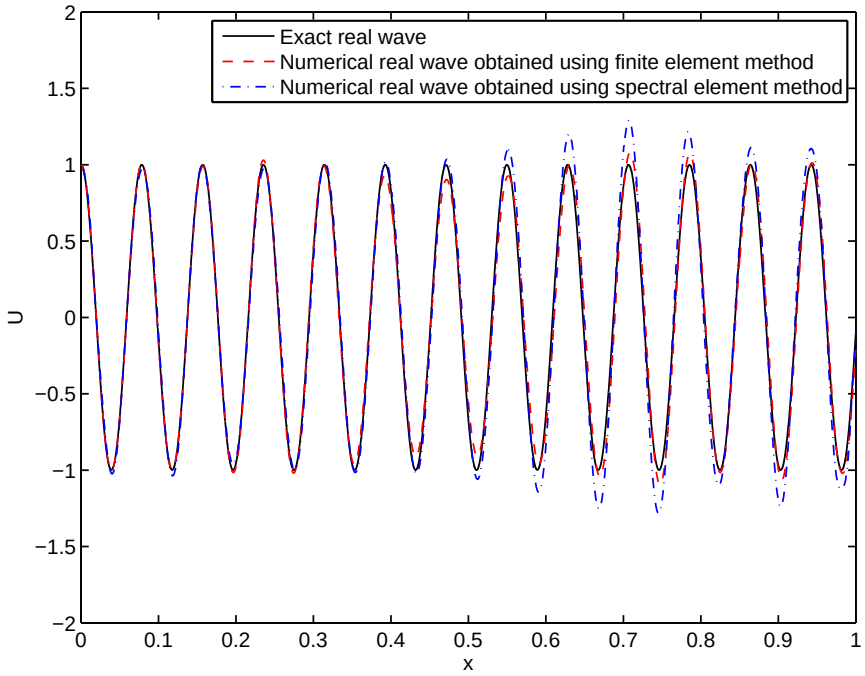
Exact real wave
Numerical real wave obtained using finite element method
Numerical real wave obtained using spectral element method
U
x
2
1.5
1
0.5
0
−0.5
−1
−1.5
−2
0
0.1
0.2
0.3
0.4
0.5
0.6
0.7
0.8
0.9
1

(g) p = 43

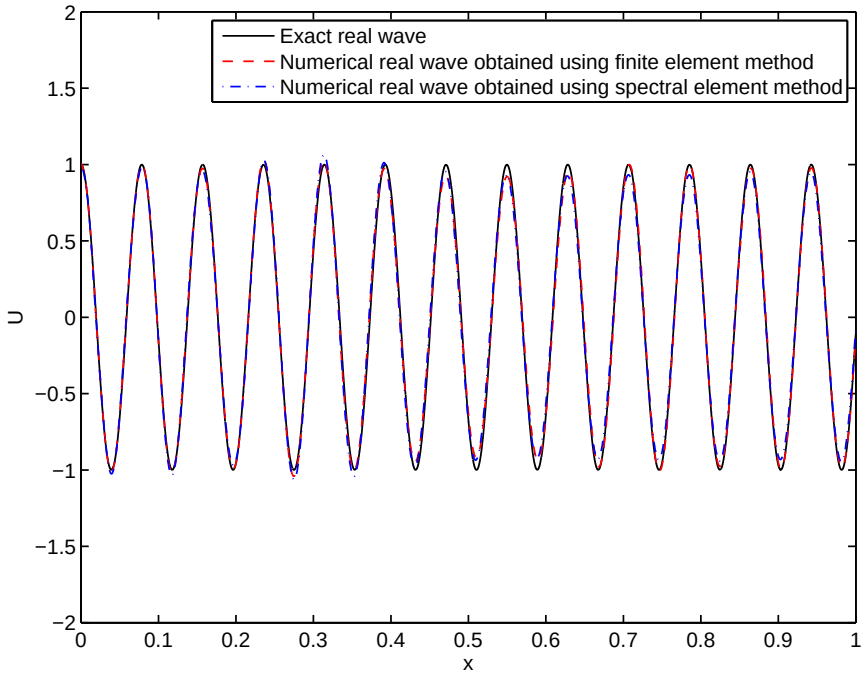
Exact real wave
Numerical real wave obtained using finite element method
Numerical real wave obtained using spectral element method
U
x
2
1.5
1
0.5
0
−0.5
−1
−1.5
−2
0
0.1
0.2
0.3
0.4
0.5
0.6
0.7
0.8
0.9
1

(h) p = 44

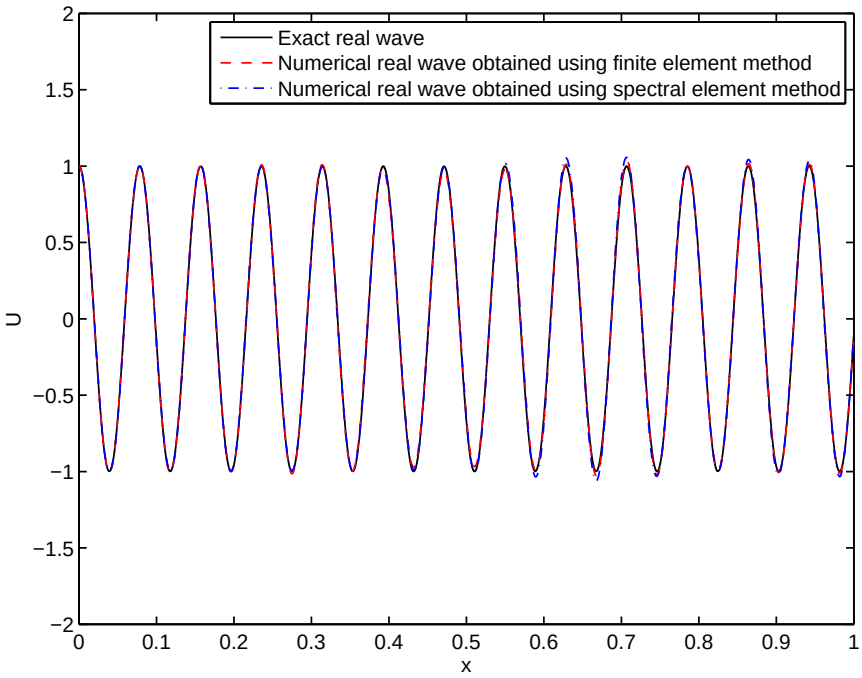

(i) p = 45

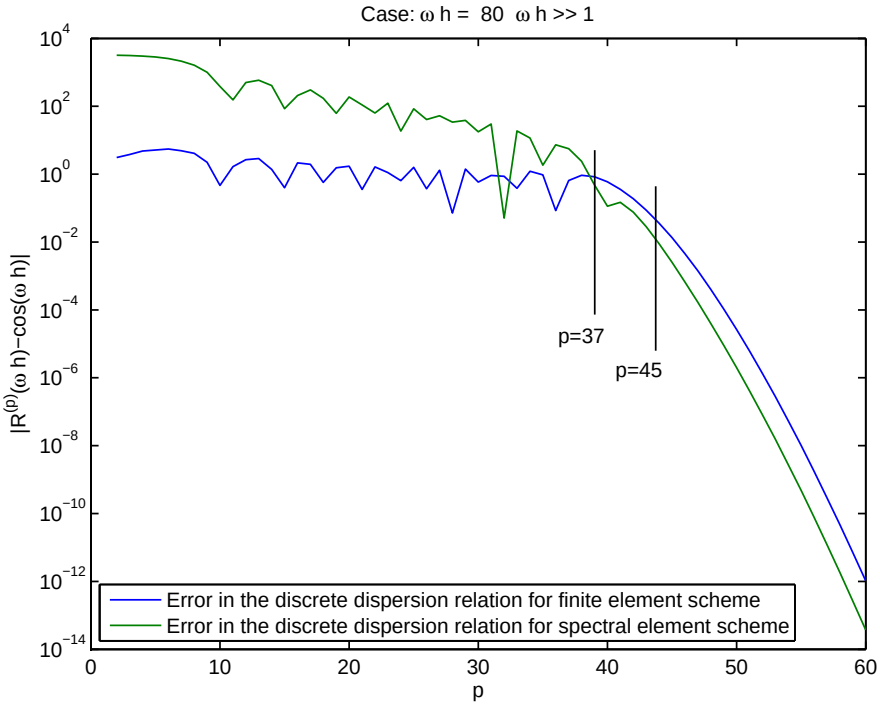

(j) Error Comparison

Figure 2.4: Numerical approximations of the solution to equation (2.10) obtained for $p = 37$ to $p = 45$ with $\omega h = 80$. The error in the discrete dispersion relations of both waves is compared.

that of fixed order approximation. In particular, over a very narrow range of p (in this case from $p = 37$ to $p = 45$), the approximate solution changes from being little more than garbage to providing an essentially exact representation of the true wave. Figure 2.4(j) sheds some light on the nature of this dramatic change in the qualitative behaviour of the schemes over a very narrow range. In particular, we see that $\tilde{\mu}^{(p)}h - \omega h$ mirrors precisely the kind of sharp transition around $p \approx \omega h/2$ seen in the approximate waves. Moreover, for $p \ll \omega h$, it is seen that $\tilde{\mu}^{(p)}h$ for the spectral element scheme is of completely the wrong magnitude (compared with ωh) thereby accounting for the erratic over-shoots and under-shoots in the unresolved regime.

2.4 Higher order discrete dispersion relations

We now derive and study the *exact* discrete dispersion relation for elements of arbitrary order. Our objectives are twofold. Firstly, we wish to compare the phase accuracy of finite element and spectral element schemes of fixed, but arbitrary, order p as the mesh-size becomes small. In particular, we shall show that the superiority of the spectral element scheme observed earlier is maintained for all orders $p \geq 2$. Secondly, we have the more ambitious goal of explaining the dramatic behaviour of the convergence of the schemes as the order is increased on a fixed mesh. The key to both of these analyses will be an explicit expression for the discrete dispersion relation for the spectral element scheme. Such expressions have been obtained (also above) for relatively low orders $p = 1, 2$ whereas our new result will be valid for arbitrary order $p \in \mathbb{N}$. Let V_{hp} denote the set of continuous piecewise polynomials of degree up to $p \geq 2$ on the grid $\mathcal{G}_h$. In order to obtain the discrete dispersion relation for higher order elements, following [1], we introduce

basis functions $\{\tilde{\theta}_i^{(p)}\}_{i=0}^N \in V_{hp}$ satisfying the conditions

$$\tilde{\theta}_i^{(p)}(jh) = \delta_{ij}, \quad jh \in \mathcal{G}_h \tag{2.20}$$

and

$$\tilde{B}(\tilde{\theta}_i^{(p)}, v_{hp}) = 0 \quad \forall v_{hp} \in V_{hp}^\flat \tag{2.21}$$

where

$$V_{hp}^\flat = \{v_{hp} \in V_{hp} : v_{hp}(jh) = 0, x_j \in \mathcal{G}_h\}$$

with $\{\theta_i^{(p)}\}_{i=0}^N$ defined similarly using $B(\cdot,\cdot)$ in place of $\tilde{B}(\cdot,\cdot)$. We seek a solution $U_{hp} \in V_{hp}$ of (2.10) of the form

$$U_{hp}(x) = \sum_{i=0}^{N} \alpha_i \tilde{\theta}_i^{(p)}(x)$$

satisfying $U_{hp}(0) = 1$ such that

$$\tilde{B}(U_{hp}, v_{hp}) = 0, \qquad \forall v_{hp} \in V_{hp} \cap H_E^1(0,1).$$

Now, following the arguments used in (Section 2.2, [1]), we arrive at the expressions for higher order discrete dispersion relations for spectral and finite element schemes

$$\cos\tilde{\mu}^{(p)}h = -\frac{1}{2}\frac{\tilde{B}(\tilde{\theta}_1^{(p)}, \tilde{\theta}_1^{(p)})}{\tilde{B}(\tilde{\theta}_0^{(p)}, \tilde{\theta}_1^{(p)})} \tag{2.22}$$

and

$$\cos\mu^{(p)}h = -\frac{1}{2}\frac{B(\theta_1^{(p)}, \theta_1^{(p)})}{B(\theta_0^{(p)}, \theta_1^{(p)})}. \tag{2.23}$$

Theorem 2.4.1. *Let $\kappa > 0$ be given. Define sequences $\{a_p\}_{p=1}^\infty$ and $\{b_p\}_{p=1}^\infty$ recursively by the rule*

$$\left.\begin{aligned} a_{p+1} &= -\frac{2p+1}{\kappa}b_p + a_{p-1} \\ b_{p+1} &= \quad \frac{2p+1}{\kappa}a_p + b_{p-1} \end{aligned}\right\} \tag{2.24}$$

for $p \in \mathbb{N}$ with $a_0 = 1$, $a_1 = 1$, $b_0 = 0$ and $b_1 = \frac{1}{\kappa}$. Then, the discrete dispersion relation for the spectral element method is given, for $p \in \mathbb{N}$, by $\cos \tilde{\mu}^{(p)} h = R^{(p)}(2\kappa)$ where

$$R^{(p)}(2\kappa) = (-1)^p \left[\frac{a_p \left(\kappa b_{p-1} + p a_p \right) + b_p \left(\kappa a_{p-1} - p b_p \right)}{a_p \left(\kappa b_{p-1} + p a_p \right) - b_p \left(\kappa a_{p-1} - p b_p \right)} \right]. \tag{2.25}$$

The above expression is a rational function of κ since both $\{a_p\}_{p=1}^{\infty}$ and $\{b_p\}_{p=1}^{\infty}$ proved in Lemma 2.5.2 are polynomials in powers of κ^{-1}, whilst the numerators and denominators are polynomials of degrees $2p$ and $2p-2$ in κ respectively. Hence, the degree of $R^{(p)}(2\kappa)$ is $[2p/2p-2]$ for all $p \in \mathbb{N}$. Consider the first order approximation ($p = 1$), then using (2.24) and (2.25), we find that

$$\cos \tilde{\mu}^{(1)} h = R^{(1)}(2\kappa) = 1 - 2\kappa^2$$

in agreement with our expression (2.19). Table 2.1 gives closed form expressions for $R^{(p)}(\omega h)$ for $p = 1, 2, 3, 4$ along with the leading terms in the series expansion for the error when $\omega h \ll 1$.

2.4.1 Accuracy at small wavenumbers

The following theorem (proved in Section 2.5) gives the leading term for the error in the discrete dispersion relation when $\omega h \ll 1$, for arbitrary order $p \in \mathbb{N}$.

Theorem 2.4.2. *Let $p \in \mathbb{N}$. Then, the error in the discrete dispersion relation for the spectral element method is given by*

$$\cos \tilde{\mu}^{(p)} h - \cos \omega h = -\frac{1}{2p} \left[\frac{p!}{(2p)!} \right]^2 \frac{(\omega h)^{2p+2}}{2p+1} + \mathcal{O}\left(\omega h \right)^{2p+4} \tag{2.26}$$

or, if ωh is sufficiently small,

$$\tilde{\mu}^{(p)} h - \omega h = \frac{1}{2p} \left[\frac{p!}{(2p)!} \right]^2 \frac{(\omega h)^{2p+1}}{2p+1} + \mathcal{O}\left(\omega h \right)^{2p+3}. \tag{2.27}$$

Order p	$R^{(p)}(\omega h)$	$\tilde{\mu}^{(p)}h - \omega h$
1	$1 - \frac{(\omega h)^2}{2}$	$\frac{(\omega h)^3}{24}$
2	$\frac{(\omega h)^4 - 22(\omega h)^2 + 48}{2((\omega h)^2 + 24)}$	$\frac{(\omega h)^5}{2880}$
3	$\frac{-(\omega h)^6 + 92(\omega h)^4 - 1680(\omega h)^2 + 3600}{2((\omega h)^4 + 60(\omega h)^2 + 1800)}$	$\frac{(\omega h)^7}{604800}$
4	$\frac{(\omega h)^8 - 260(\omega h)^6 + 16176(\omega h)^4 - 267120(\omega h)^2 + 564480}{2((\omega h)^6 + 108(\omega h)^4 + 7560(\omega h)^2 + 282240)}$	$\frac{(\omega h)^9}{203212800}$

Table 2.1: The discrete dispersion relation $R^{(p)}(\omega h) = \cos \tilde{\mu}^{(p)}h$ for order p approximation given in Theorem 2.4.1. We also indicate the leading term in the series expansion for the error when $\omega h \ll 1$ (see Theorem 2.4.2) .

The leading terms in the series expansion for the error obtained using spectral element method all have positive signs, thereby explaining the phase lag observed in the previous section. This result in the case $p = 1$ agrees with the expression (41) given in Thompson and Pinsky [60]. The case of general order p approximation is not conducted by Thompson and Pinsky, who nevertheless conjectured that the leading term in the expressions should be of order $(\omega h)^{2p+1}$. The correctness of this conjecture is confirmed by Theorem 2.4.2. More interestingly, for higher orders the spectral element scheme provides p-times better accuracy as compared to the discrete dispersion relation obtained with finite element scheme [1], where one finds that the corresponding result for the finite element scheme is:

$$\mu^{(p)}h - \omega h = -\frac{1}{2}\left[\frac{p!}{(2p)!}\right]^2 \frac{(\omega h)^{2p+1}}{2p+1} + \mathcal{O}\left(\omega h\right)^{2p+3}. \tag{2.28}$$

It is evident from expression (2.27) that the error for the spectral element scheme has an additional multiple of $1/p$ for elements of order $p \in \mathbb{N}$ when compared with (2.28), again with a sign change.

2.4.2 Accuracy at large wavenumbers

We now consider the error estimates for high wavenumbers i.e. ωh is large even though h is small. The next theorem gives a full description of the behaviour of the error for large ωh as the order of the approximation p is increased.

Theorem 2.4.3. *Suppose that $\omega h \gg 1$. Then the error $\mathcal{E}^{(p)} = \cos\tilde{\mu}^{(p)}h - \cos\omega h$ in the discrete dispersion relation for the spectral element method passes through four distinct phases as the order $p \in \mathbb{N}$ is increased:*

1. *Constant Magnitude Phase: For $p = \mathcal{O}(1)$, $\mathcal{E}^{(p)} \approx (-1)^p \frac{(\omega h)^2}{2}$.*

2. *Oscillatory Phase: For* $1 \ll 2p+1 < \omega h - o(\omega h)^{1/3}$, $\mathcal{E}^{(p)}$ *oscillates and decays to* $\mathcal{O}(1)$ *as* p *is increased.*

3. *Transition Zone: For* $\omega h - o(\omega h)^{1/3} < 2p+1 < \omega h + o(\omega h)^{1/3}$, *the error* $\mathcal{E}^{(p)}$ *oscillates without further decrease.*

4. *Super-Exponential Decay: For* $2p+1 > \omega h + o(\omega h)^{1/3}$, $\mathcal{E}^{(p)}$ *decreases at a super-exponential rate:*

$$\mathcal{E}^{(p)} \approx \frac{\sin(\omega h)}{2}\left(\frac{\omega h}{4p}\right)^2 f(\sqrt{1-(\omega h/(2p+1))^2})^{p+1/2} \tag{2.29}$$

where $f : w \to (1-w)/(1+w)\exp(2w)$ *so that in the case where* $2p+1 > \omega he/2$

$$\mathcal{E}^{(p)} \approx \frac{\sin(\omega h)}{2}\left(\frac{\omega h}{4p}\right)^2 \left[\frac{\omega he}{2(2p+1)}\right]^{2p+1}. \tag{2.30}$$

Figure 2.5 shows the behaviour of the actual error obtained with the spectral element scheme for different values of ωh with increasing order p. It is seen that the behaviour is consistent with the predictions of Theorem 2.4.3. It is interesting to compare the results in Theorem 2.4.3 with those obtained in [1] for the finite element scheme. Observe that if $\mathcal{E}^p_{FE}$ denotes the corresponding error for the finite element scheme then using the above result and Theorem 3.3 of [1], we have

$$\mathcal{E}^{(p)} \approx \left(\frac{\omega h}{4p}\right)^2 \mathcal{E}^p_{FE}. \tag{2.31}$$

Broadly speaking, this means the performace of the two methods is similar in terms of (a) the fact that there is a sharp transition to super-exponential convergence, and (b) the transition occurs at the same threshold. The most significant difference in the behaviour of the spectral element and finite element schemes occurs in the unresolved regime where $2p+1 < \omega h - o(\omega h)^{1/3}$. For the finite element scheme,

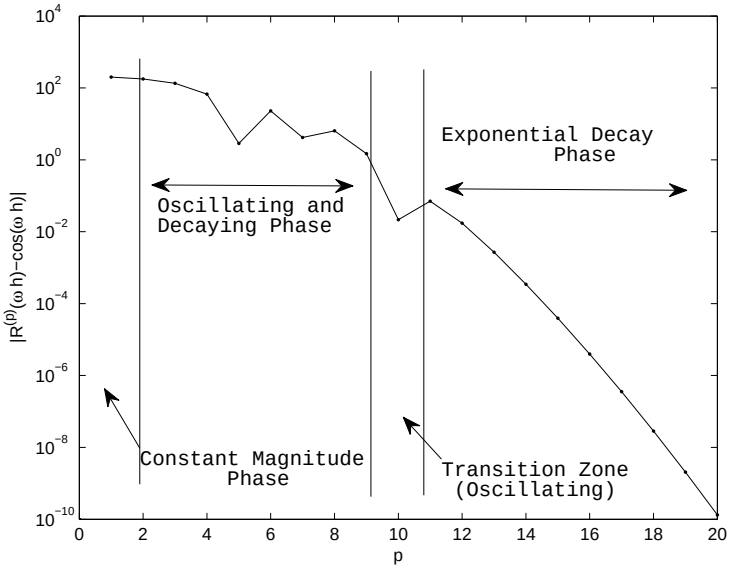

(a) $\omega h = 20$

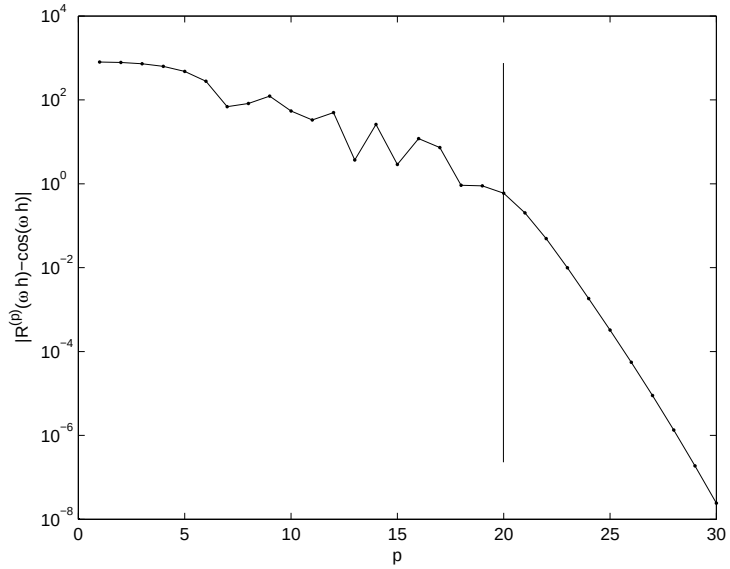

(b) $\omega h = 40$

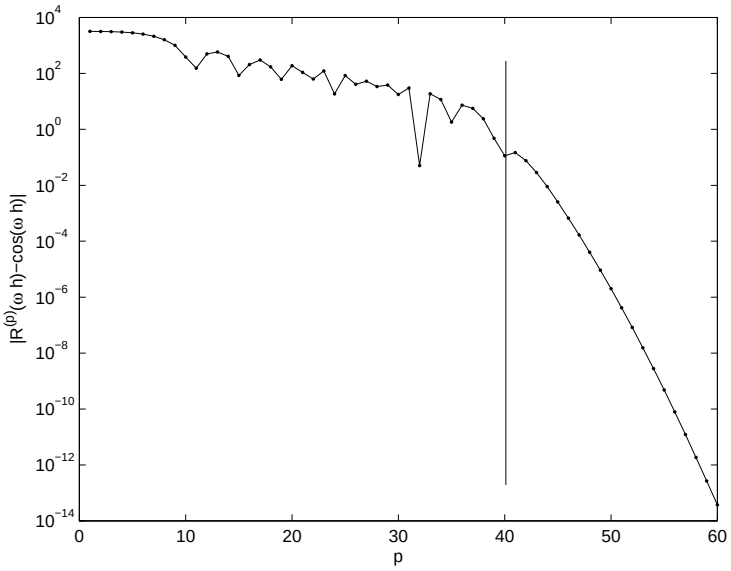

(c) $\omega h = 80$

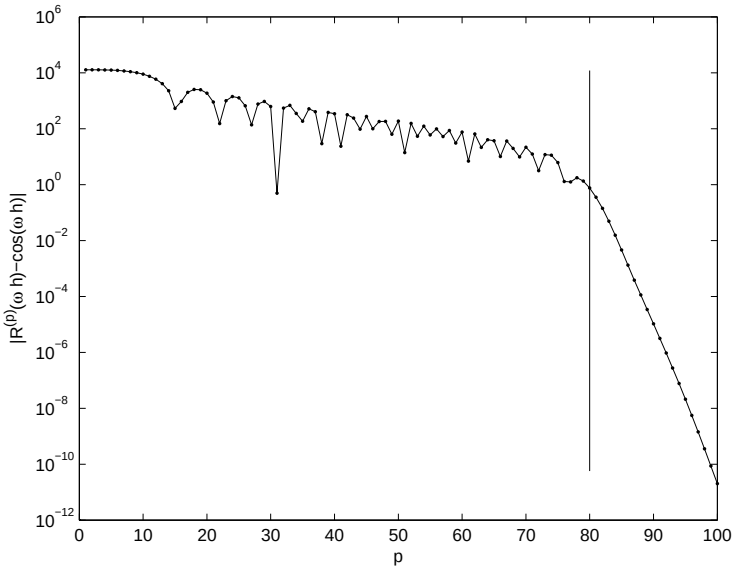

(d) $\omega h = 160$

Figure 2.5: Behaviour of the error in the discrete dispersion relation for spectral element scheme at high wavenumbers $\omega h \gg 1$ as the order p is increased. The transition region between the oscillatory decaying phase and the super-exponential decay of the error is indicated in each case (see Theorem 2.4.3) and occurs when $2p + 1 \approx \omega h$.

the error is of order 1 whereas for the spectral element scheme, the error is of order $\frac{1}{2}(\omega h)^2$. This behaviour was observed in Figure 2.4 where it was found that the spectral element scheme over-shoots and under-shoots erratically in this range. In summary, in agreement with [1], we recommend that the order p and the mesh-size h is chosen so that

$$2p + 1 > \omega h + C(\omega h)^{1/3}, \tag{2.32}$$

where C is a fixed constant and can be taken as unity in practice.

2.5 Proofs of the results

This section provides the proofs of the results for the error in the discrete dispersion relation for the spectral element method.

2.5.1 Basic polynomials

For $u, v \in H^1(-1,1)$, let $\hat{B}(\cdot,\cdot)$ denote the bilinear form

$$\hat{B}(u,v) = \mathcal{Q}^{(p)}(u'v') - \kappa^2 \mathcal{Q}^{(p)}(uv) \tag{2.33}$$

where $\mathcal{Q}^{(p)}$ is the quadrature rule (2.8) and $\kappa > 0$ is a fixed constant. We introduce basic polynomials Φ^p, Ψ^p of degree at most $p \in \mathbb{N}$ satisfying

$$\Phi^p(1) = 1,\ \ \Phi^p(-1) = (-1)^{p+1} :\ \ \hat{B}(\Phi^p, v) = 0 \quad \forall v \in \mathbb{P}_p \cap H_0^1(-1,1) \tag{2.34}$$

and

$$\Psi^p(1) = 1,\ \ \Psi^p(-1) = (-1)^{p} :\ \ \hat{B}(\Psi^p, v) = 0 \quad \forall v \in \mathbb{P}_p \cap H_0^1(-1,1). \tag{2.35}$$

Throughout, it will be assumed that κ does not coincide with an eigenvalue for this problem so that the polynomials are uniquely defined by these conditions.

Thanks to the fact that $\mathbb{P}_p$ is finite dimensional, existence of these polynomials follows directly. Moreover the bilinear form (2.33) is invariant under the change of variable from x to $-x$ meaning that Φ^p and Ψ^p are either even or odd functions. Now if p is odd, then from (2.34), we have $\Phi^p(1) = 1 = \Phi^p(-1)$, which implies Φ^p is not an odd function and therefore Φ^p is an even function. Furthermore, if p is even, then from (2.34), we get $\Phi^p(-1) = -1 = -\Phi^p(1)$, which implies Φ^p is not an even function and therefore Φ^p is an odd function. Similarly, it is now easy to see that Ψ^p is an odd and even function for odd and even integers respectively. These polynomials will play a central role in the derivation of the discrete dispersion relation. The following theorem provides explicit closed forms for the expressions $\hat{B}(\Psi^p, \Psi^p)$ and $\hat{B}(\Phi^p, \Phi^p)$, which we shall need later.

Theorem 2.5.1. *Let $p = 2, 3, 4, \ldots,$ then*

$$\hat{B}(\Phi^p, \Phi^p) = -2\kappa \frac{a_p}{b_p} \tag{2.36}$$

and

$$\hat{B}(\Psi^p, \Psi^p) = -2\kappa \frac{(p+1)a_{p-1} + pa_{p+1}}{(p+1)b_{p-1} + pb_{p+1}}, \tag{2.37}$$

where $\{a_p\}_{p=1}^{\infty}$ and $\{b_p\}_{p=1}^{\infty}$ are defined in Theorem 2.4.1.

Proof. We begin by considering Φ^p. If p is odd, then as explained above Φ^p is an even function which implies $\Phi^p \in \mathbb{P}_{p-1}$. Similarly, in the case when p is even, Φ^p is an odd function which implies $\Phi^p \in \mathbb{P}_{p-1}$. Hence, $\Phi^p \in \mathbb{P}_{p-1}$ for all $p \in \mathbb{N}$. Let $v \in \mathbb{P}_p \cap H_0^1(-1, 1)$, then $v\Phi^p$ and $v'\Phi'^p \in \mathbb{P}_{2p-1}$, so that (2.33) integrates the function exactly when $u = \Phi^p$, and we obtain

$$\hat{B}(\Phi^p, v) = \int_{-1}^{1} \left(\Phi'^p v' - \kappa^2 \Phi^p v \right) dx = 0 \ \ \forall v \in \mathbb{P}_p \cap H_0^1(-1, 1).$$

Hence, we see that $\Phi^p = \Phi_e^p$ or $\Phi^p = \Phi_o^p$, where Φ_e^p and Φ_o^p are polynomials analysed in ([1],(4.1)-(4.2)) and from ([1],(4.13)-(4.14)), again using the fact that

the quadrature rule is exact in this case, we have

$$\hat{B}(\Phi^p, \Phi^p) = \int_{-1}^{1} \left(\Phi'^p \Phi'^p - \kappa^2 \Phi^p \Phi^p\right) dx = -2\kappa \frac{a_p}{b_p} \tag{2.38}$$

which proves the assertion for Φ^p.

We now consider Ψ^p and for the remainder of the proof superscripts will be omitted since no confusion is likely to arise. Since Ψ and $v \in \mathbb{P}_p$ and Ψ' and $v' \in \mathbb{P}_{p-1}$, we can use the fact that the quadrature rule is exact for $\mathbb{P}_{2p-1}$ and integration by parts to obtain

$$\mathcal{Q}^{(p)}(\Psi' v') = \int_{-1}^{1} \Psi' v' dx = [v\Psi']_{-1}^{1} - \mathcal{Q}^{(p)}(\Psi'' v) = -\mathcal{Q}^{(p)}(\Psi'' v) \tag{2.39}$$

since $v(\pm 1) = 0$. Combining this result with (2.35) gives

$$\mathcal{Q}^{(p)}(Fv) = \sum_{\ell=1}^{p-1} \tilde{w}_\ell F(\tilde{\zeta}_\ell) v(\tilde{\zeta}_\ell) = 0 \qquad \forall v \in \mathbb{P}_p \cap H_0^1(-1,1). \tag{2.40}$$

where $F = (\Psi'' + \kappa^2 \Psi) \in \mathbb{P}_p$. Fix $J \in \{1, 2, 3, \ldots, p-1\}$ and let $v \in \mathbb{P}_p \cap H_0^1(-1,1)$ be chosen such that $v(\tilde{\zeta}_\ell) = \delta_{\ell J}$, then (2.40) implies that $F(\tilde{\zeta}_J) = 0$. Hence, $F = 0$ at the zeros of L_p' where L_p is the Legendre polynomial of degree p. Hence, F takes the form

$$F(x) = \Psi''(x) + \kappa^2 \Psi(x) = (\varsigma + \sigma x) L_p'(x) \tag{2.41}$$

for some $\varsigma, \sigma \in \mathbb{R}$. Also, parity considerations imply that $\varsigma = 0$ and σ can never be zero otherwise $\Psi \in \mathbb{P}_{p-2}$ and the bilinear form (2.33) will become exact and we will get back to the case of Φ. Now using the following identity satisfied by Legendre polynomials $xL_p'(x) = \dfrac{1}{2p+1}\left((p+1)L_{p-1}'(x) + pL_{p+1}'(x)\right)$, obtained using equations (13)-(14) given in ([23], Section 10.10), equation (2.41) becomes

$$F(x) = \frac{\sigma}{2p+1}\left(pL_{p+1}'(x) + (p+1)L_{p-1}'(x)\right). \tag{2.42}$$

Define a polynomial $\Upsilon_n \in \mathbb{P}_n$ by the rule

$$\Upsilon_n(x) = \sum_{j=0}^{\lfloor n/2 \rfloor} \left(-\frac{1}{\kappa^2}\right)^{j+1} L_{n+1}^{(2j+1)}(x) \tag{2.43}$$

where $\lfloor\cdot\rfloor$ denotes the integer part. It is elementary to verify that

$$\Upsilon_n''(x) + \kappa^2\Upsilon_n(x) = -L_{n+1}'(x). \tag{2.44}$$

We may write

$$\Psi(x) = \alpha\Upsilon_p(x) + \beta\Upsilon_{p-2}(x) \tag{2.45}$$

for suitable constants α and β, and in addition

$$\begin{aligned}\Psi''(x) + \kappa^2\Psi(x) =& \alpha\left(\Upsilon_p''(x) + \kappa^2\Upsilon_p(x)\right) + \beta\left(\Upsilon_{p-2}''(x) + \kappa^2\Upsilon_{p-2}(x)\right)\\ =& -\left(\alpha L_{p+1}'(x) + \beta L_{p-1}'(x)\right).\end{aligned}$$

Comparing the last equation with (2.42), we are led to the conclusion that $\alpha = -\sigma p/(2p+1)$ and $\beta = -\sigma(p+1)/(2p+1)$, and with these values, (2.45) becomes

$$\Psi(x) = -\frac{\sigma}{2p+1}\left(p\Upsilon_p(x) + (p+1)\Upsilon_{p-2}(x)\right). \tag{2.46}$$

Applying the boundary condition $\Psi(1) = 1$, we obtain $\sigma = -(2p+1)/\eta(1)$, provided that $\eta(1)$ is non-zero, with $\eta(1) = (p+1)\Upsilon_{p-2}(1) + p\Upsilon_p(1)$. Consequently, Ψ is given by

$$\Psi(x) = \frac{\eta(x)}{\eta(1)}. \tag{2.47}$$

We wish to obtain a closed form expression for $\hat{B}(\Psi,\Psi) = \mathcal{Q}^{(p)}(\Psi'^2) - \kappa^2\mathcal{Q}^{(p)}(\Psi^2)$. The function $\Psi'^2 \in P_{2p-2}$, is integrated exactly by the quadrature rule, so that

$$\mathcal{Q}^{(p)}(\Psi'^2) = \int_{-1}^{1}\Psi'^2 dx = [\Psi'\Psi]_{-1}^{1} - \int_{-1}^{1}\Psi\Psi'' dx = 2\Psi'(1) - \mathcal{Q}^{(p)}(\Psi''\Psi)$$

and therefore,

$$\hat{B}(\Psi,\Psi) = 2\Psi'(1) - \mathcal{Q}^{(p)}(\Psi''\Psi) - \kappa^2\mathcal{Q}^{(p)}(\Psi^2) = 2\Psi'(1) - \mathcal{Q}^{(p)}(\Psi(\Psi'' + \kappa^2\Psi)).$$

Equation (2.41) implies that $\mathcal{Q}^{(p)}(\Psi(\Psi'' + \kappa^2\Psi)) = \mathcal{Q}^{(p)}(\sigma x\Psi L_p'(x))$ and therefore,

$$\hat{B}(\Psi,\Psi) = 2\Psi'(1) + \frac{2p+1}{\eta(1)}\mathcal{Q}^{(p)}(x\Psi L_p'(x)). \tag{2.48}$$

Now, using the quadrature rule (2.8), we obtain

$$\mathcal{Q}^{(p)}(x\Psi L_p'(x)) = \sum_{\ell=1}^{p-1} \tilde{w}_\ell \Psi(\tilde{\zeta}_\ell) L_p'(\tilde{\zeta}_\ell) - \frac{2}{p(p+1)}\Psi(-1)L_p'(-1) + \frac{2}{p(p+1)}\Psi(1)L_p'(1),$$

and then, since $\tilde{\zeta}_\ell$ for all $\ell = 1, 2, 3, \ldots, p-1$ are the zeros of L_p', we get

$$\mathcal{Q}^{(p)}(x\Psi L_p'(x)) = \frac{2}{p(p+1)}\left((-1)^{p+1}L_p'(-1) + L_p'(1)\right), \tag{2.49}$$

and then substituting for $L_p'(\pm 1)$ using the expression

$$L_n^{(d)}(\pm 1) = \begin{cases} \dfrac{(n+d)!}{d!(n-d)!}\dfrac{(\pm 1)^{n+d}}{2^d} & \text{for } d = 0, 1, 2, \ldots, n, \\ 0 & \text{otherwise,} \end{cases} \tag{2.50}$$

(see ([1], eq(4.7))), gives $\mathcal{Q}^{(p)}(x\Psi L_p'(x)) = 2$. Substituting this value into equation (2.48), we obtain

$$\hat{B}(\Psi, \Psi) = \frac{2}{\eta(1)}\left(\eta'(1) + 2p + 1\right) \tag{2.51}$$

after straightforward manipulations. Now, as in [1], using (2.43) together with (2.50), the values of Υ and its derivatives at the boundary $x = 1$ are given by $\Upsilon_p'(1) = a_{p+1} - 1, \Upsilon_{p-2}'(1) = a_{p-1} - 1, \Upsilon_p(1) = -b_{p+1}/\kappa$ and $\Upsilon_{p-2}(1) = -b_{p-1}/\kappa$, where a_{p+1}, a_{p-1}, b_{p+1} and b_{p-1} are the expressions obtained from the recurrence relation (2.24). A proof of this will be provided in Lemma 2.5.2 below. Consequently, the values of $\eta(1)$ and $\eta'(1)$ may be written in the form

$$\eta(1) = -\tfrac{1}{\kappa}\left((p+1)b_{p-1} + pb_{p+1}\right)$$

and

$$\eta'(1) + 2p + 1 = (p+1)a_{p-1} + pa_{p+1}.$$

Finally, inserting the above values into (2.51) and simplifying gives

$$\hat{B}(\Psi, \Psi) = -2\kappa\left[\frac{(p+1)a_{p-1} + pa_{p+1}}{(p+1)b_{p-1} + pb_{p+1}}\right]$$

which completes the proof. □

We now give closed form expressions and present some elementary properties of the coefficients a_p and b_p defined in (2.24).

Lemma 2.5.2. *Let $\{a_n\}_{n=0}^{\infty}$ and $\{b_n\}_{n=0}^{\infty}$ be defined as in (2.24). Then $\kappa^n a_n$ is a polynomial of degree n in κ, and*

$$a_n = \sum_{k=0}^{\lfloor n/2 \rfloor} \frac{(-1)^k}{(2k)!} \frac{(n+2k)!}{(n-2k)!} \frac{1}{(2\kappa)^{2k}}, \ n = 0, 1, 2, \ldots \tag{2.52}$$

while $\kappa^n b_n$ is a polynomial of degree $n-1$ in κ, and

$$b_n = \sum_{k=0}^{\lfloor (n-1)/2 \rfloor} \frac{(-1)^k}{(2k+1)!} \frac{(n+2k+1)!}{(n-2k-1)!} \frac{1}{(2\kappa)^{2k+1}}, \ n = 1, 2, 3, \ldots \tag{2.53}$$

with $b_0 = 0$ and $\lfloor . \rfloor$ denoting the integer part. Moreover, these series satisfy

$$\begin{bmatrix} \sin(\kappa - \pi n/2) & \cos(\kappa - \pi n/2) \\ \cos(\kappa - \pi n/2) & -\sin(\kappa - \pi n/2) \end{bmatrix} \begin{bmatrix} a_n \\ b_n \end{bmatrix} = \sqrt{\frac{\pi\kappa}{2}} \begin{bmatrix} J_{n+1/2}(\kappa) \\ -Y_{n+1/2}(\kappa) \end{bmatrix} \tag{2.54}$$

where J and Y are cylindrical Bessel functions of the first and second kind respectively [28].

Proof. It is elementary to prove (2.52) and (2.53) using mathematical induction. The statement regarding $\kappa^n a_n$ and $\kappa^n b_n$ are then simple consequences of (2.52) and (2.53). For $n = 0$, expression (2.52) reads as

$$a_0 = \frac{(-1)^0}{(2\times 0)!} \frac{(2\times 0)!}{(2\times 0)!} \frac{1}{(2\kappa)^{2\times 0}} = 1,$$

while, for $n = 1$, expression (2.52) reads as

$$a_1 = \frac{(-1)^0}{(2\times 0)!} \frac{(1+2\times 0)!}{(1-2\times 0)!} \frac{1}{(2\kappa)^{2\times 0}} = 1.$$

Similarly, expression (2.53) gives

$$b_1 = \frac{(-1)^0}{(2\times 0+1)!} \frac{(2\times 0+2)!}{(1-2\times 0-1)!} \frac{1}{(2\kappa)^{2\times 0+1}} = \frac{1}{\kappa},$$

so the result holds for n up to 1. Now, assume that the series are valid for n up to p. We consider separately the cases where p is odd and even. Firstly, we suppose p is odd so that $p = 2r + 1$ for some $r \in \mathbb{N}$. Then (2.24) gives

$$a_{2r+2} = -\frac{4r+3}{\kappa} b_{2r+1} + a_{2r}.$$

Now, substituting series (2.52) and (2.53) into above equation, we have

$$\begin{aligned}
a_{2r+2} &= -\frac{4r+3}{\kappa}\left(\sum_{k=0}^{r} \frac{(-1)^k}{(2k+1)!}\frac{(2r+2+2k)!}{(2r-2k)!}\frac{1}{(2\kappa)^{2k+1}}\right) \\
&\quad + \sum_{k=0}^{r} \frac{(-1)^k}{(2k)!}\frac{(2r+2k)!}{(2r-2k)!}\frac{1}{(2\kappa)^{2k}} \\
&= 1 - \frac{4r+3}{\kappa}\left(\sum_{k=0}^{r-1} \frac{(-1)^k}{(2k+1)!}\frac{(2r+2+2k)!}{(2r-2k)!}\frac{1}{(2\kappa)^{2k+1}}\right) \\
&\quad + \sum_{k=1}^{r} \frac{(-1)^k}{(2k)!}\frac{(2r+2k)!}{(2r-2k)!}\frac{1}{(2\kappa)^{2k}} + \frac{(-1)^{r+1}}{\kappa}\frac{4r+3}{(2r+1)!}\frac{(4r+2)!}{(2\kappa)^{2r+1}} \\
&= 1 - \frac{4r+3}{\kappa}\left(\sum_{k=1}^{r} \frac{(-1)^{k-1}}{(2k-1)!}\frac{(2r+2k)!}{(2r-2k+2)!}\frac{1}{(2\kappa)^{2k-1}}\right) \\
&\quad + \sum_{k=1}^{r} \frac{(-1)^k}{(2k)!}\frac{(2r+2k)!}{(2r-2k)!}\frac{1}{(2\kappa)^{2k}} + \frac{(-1)^{r+1}}{\kappa}\frac{4r+3}{(2r+1)!}\frac{(4r+2)!}{(2\kappa)^{2r+1}} \\
&= 1 + \sum_{k=1}^{r} \frac{(-1)^k}{(2k)!}\frac{(2r+2k+2)!}{(2r-2k+2)!}\frac{1}{(2\kappa)^{2k}} + \frac{(-1)^{r+1}}{(2r+2)!}\frac{(4r+4)!}{(2\kappa)^{2r+2}} \\
&= \sum_{k=0}^{\lfloor r+1 \rfloor} \frac{(-1)^k}{(2k)!}\frac{(2r+2k+2)!}{(2r-2k+2)!}\frac{1}{(2\kappa)^{2k}}.
\end{aligned}$$

Substituting r in terms of p, we get

$$a_{p+1} = \sum_{k=0}^{\lfloor (p+1)/2 \rfloor} \frac{(-1)^k}{(2k)!}\frac{(p+2k+1)!}{(p-2k+1)!}\frac{1}{(2\kappa)^{2k}}.$$

Hence, the series for a_n is valid for n up to $p+1$. We now consider the series for b_n. Starting with

$$b_{2r+2} = \frac{4r+3}{\kappa} a_{2r+1} + b_{2r}$$

and using (2.52) and (2.53), we have

$$\begin{aligned}
b_{2r+2} &= \frac{4r+3}{\kappa}\left(\sum_{k=0}^{r}\frac{(-1)^k}{(2k)!}\frac{(2r+2k+1)!}{(2r-2k+1)!}\frac{1}{(2\kappa)^{2k}}\right) \\
&\quad+\sum_{k=0}^{r-1}\frac{(-1)^k}{(2k+1)!}\frac{(2r+2k+1)!}{(2r-2k-1)!}\frac{1}{(2\kappa)^{2k+1}} \\
&= \frac{1}{\kappa}\left(\sum_{k=0}^{r-1}\frac{(-1)^k}{(2k)!}\frac{(2r+2k+1)!}{(2r-2k+1)!}\frac{4r+3}{(2\kappa)^{2k}}\right) \\
&\quad+\sum_{k=0}^{r-1}\frac{(-1)^k}{(2k+1)!}\frac{(2r+2k+1)!}{(2r-2k-1)!}\frac{1}{(2\kappa)^{2k+1}}+\frac{(-1)^r}{\kappa}\frac{4r+3}{(2r)!}\frac{(4r+1)!}{(2\kappa)^{2r}} \\
&= \sum_{k=0}^{r-1}\frac{(-1)^k}{(2k+1)!}\frac{(2r+2k+3)!}{(2r-2k+1)!}\frac{1}{(2\kappa)^{2k+1}}+\frac{(-1)^r}{(2r+1)!}\frac{(4r+3)!}{(2\kappa)^{2r+1}} \\
&= \sum_{k=0}^{\lfloor r+1/2\rfloor}\frac{(-1)^k}{(2k+1)!}\frac{(2r+2k+3)!}{(2r-2k+1)!}\frac{1}{(2\kappa)^{2k+1}}.
\end{aligned}$$

Now, replacing r in terms of p, we get

$$b_{p+1}=\sum_{k=0}^{\lfloor p/2\rfloor}\frac{(-1)^k}{(2k+1)!}\frac{(p+2k+2)!}{(p-2k)!}\frac{1}{(2\kappa)^{2k+1}}.$$

Hence, the series b_n is valid for n up to order $p+1$. This concludes the proof in the case when p is odd. We now consider the case when p is even, so that $p=2r$ for some $r\in\mathbb{N}$. For the series a_p, beginning with

$$a_{2r+1}=-\frac{4r+1}{\kappa}b_{2r}+a_{2r-1}$$

and with the aid of series (2.52) and (2.53), we arrive at

$$\begin{aligned}
a_{2r+1} &= -\frac{4r+1}{\kappa}\left(\sum_{k=0}^{r-1}\frac{(-1)^k}{(2k+1)!}\frac{(2r+1+2k)!}{(2r-2k-1)!}\frac{1}{(2\kappa)^{2k+1}}\right) \\
&\quad +\sum_{k=0}^{r-1}\frac{(-1)^k}{(2k)!}\frac{(2r+2k-1)!}{(2r-2k-1)!}\frac{1}{(2\kappa)^{2k}} \\
&= 1-\frac{4r+1}{\kappa}\left(\sum_{k=1}^{r-1}\frac{(-1)^{k-1}}{(2k-1)!}\frac{(2r+2k-1)!}{(2r-2k+1)!}\frac{1}{(2\kappa)^{2k-1}}\right) \\
&\quad +\sum_{k=1}^{r-1}\frac{(-1)^k}{(2k)!}\frac{(2r+2k-1)!}{(2r-2k-1)!}\frac{1}{(2\kappa)^{2k}}+\frac{(-1)^r}{\kappa}\frac{4r+1}{(2r-1)!}\frac{(4r-1)!}{(2\kappa)^{2r-1}} \\
&= 1+\sum_{k=1}^{r-1}\frac{(-1)^k}{(2k)!}\frac{(2r+2k+1)!}{(2r-2k+1)!}\frac{1}{(2\kappa)^{2k}}+\frac{(-1)^r}{(2r)!}\frac{(4r+1)!}{(2\kappa)^{2r}} \\
&= \sum_{k=0}^{\lfloor r+1/2\rfloor}\frac{(-1)^k}{(2k)!}\frac{(2r+2k+1)!}{(2r-2k+1)!}\frac{1}{(2\kappa)^{2k}}.
\end{aligned}$$

Now, writing the above expression in terms of p, we obtain

$$a_{p+1}=\sum_{k=0}^{\lfloor (p+1)/2\rfloor}\frac{(-1)^k}{(2k)!}\frac{(p+2k+1)!}{(p-2k+1)!}\frac{1}{(2\kappa)^{2k}}.$$

Hence, the series a_n is valid for n up to order $p+1$. Now, for b_n starting with

$$b_{2r+1}=\frac{4r+1}{\kappa}a_{2r}+b_{2r-1}$$

and using (2.52) and (2.53), we have

$$\begin{aligned}
b_{2r+1} &= \frac{4r+1}{\kappa}\left(\sum_{k=0}^{r}\frac{(-1)^k}{(2k)!}\frac{(2r+2k)!}{(2r-2k)!}\frac{1}{(2\kappa)^{2k}}\right) \\
&\quad +\sum_{k=0}^{r-1}\frac{(-1)^k}{(2k+1)!}\frac{(2r+2k)!}{(2r-2k-2)!}\frac{1}{(2\kappa)^{2k+1}} \\
&= \sum_{k=0}^{r-1}\frac{(-1)^k}{(2k+1)!}\frac{(2r+2k+2)!}{(2r-2k)!}\frac{1}{(2\kappa)^{2k+1}}+\frac{(-1)^r}{(2r+1)!}\frac{(4r+2)!}{(2\kappa)^{2r+1}} \\
&= \sum_{k=0}^{\lfloor r\rfloor}\frac{(-1)^k}{(2k+1)!}\frac{(2r+2k+2)!}{(2r-2k)!}\frac{1}{(2\kappa)^{2k+1}}.
\end{aligned}$$

Replacing r by p, we finally have

$$b_{p+1} = \sum_{k=0}^{\lfloor p/2 \rfloor} \frac{(-1)^k}{(2k+1)!} \frac{(p+2k+2)!}{(p-2k)!} \frac{1}{(2\kappa)^{2k+1}}.$$

Hence, the series b_n is valid for n up to order $p+1$. Therefore, by induction, we have proved that the series $\{a_n\}$ and $\{b_n\}$ are both valid for all integer $n \geq 0$.

We will now prove the identity (2.54). For this we begin with the following identity which is given in ([28], eq.$(8.461)_1$)

$$J_{n+1/2}(\kappa) = \sqrt{\frac{2}{\pi\kappa}} \Bigg\{ \sin\left(\kappa - \frac{\pi}{2}n\right) \sum_{k=0}^{\lfloor n/2 \rfloor} \frac{(-1)^k}{(2k)!} \frac{(n+2k)!}{(n-2k)!} \frac{1}{(2\kappa)^{2k}} + \cos\left(\kappa - \frac{\pi}{2}n\right) \sum_{k=0}^{\lfloor (n-1)/2 \rfloor} \frac{(-1)^k}{(2k+1)!} \frac{(n+2k+1)!}{(n-2k-1)!} \frac{1}{(2\kappa)^{2k+1}} \Bigg\} \quad (2.55)$$

while combining identities $(8.461)_2$ and (8.465) of [28] gives

$$Y_{n+1/2}(\kappa) = (-1)^{n-1} \sqrt{\frac{2}{\pi\kappa}} \Bigg\{ \cos\left(\kappa + \frac{\pi}{2}n\right) \sum_{k=0}^{\lfloor n/2 \rfloor} \frac{(-1)^k}{(2k)!} \frac{(n+2k)!}{(n-2k)!} \frac{1}{(2\kappa)^{2k}} - \sin\left(\kappa + \frac{\pi}{2}n\right) \sum_{k=0}^{\lfloor (n-1)/2 \rfloor} \frac{(-1)^k}{(2k+1)!} \frac{(n+2k+1)!}{(n-2k-1)!} \frac{1}{(2\kappa)^{2k+1}} \Bigg\} \quad (2.56)$$

where $J_{n+1/2}$ and $Y_{n+1/2}$ are cylindrical Bessel functions of the first and second kind respectively. For non-negative integer n both the series in the first and second terms of the above identities are exactly the same as a_n and b_n given in equations (2.52) and (2.53) respectively. Hence (2.55) and (2.56) result in

$$J_{n+1/2}(\kappa) = \sqrt{\frac{2}{\pi\kappa}} \left(\sin\left(\kappa - \frac{\pi}{2}n\right) a_n + \cos\left(\kappa - \frac{\pi}{2}n\right) b_n \right) \quad (2.57)$$

and

$$Y_{n+1/2}(\kappa) = (-1)^{n-1} \sqrt{\frac{2}{\pi\kappa}} \left(\cos\left(\kappa + \frac{\pi}{2}n\right) a_n - \sin\left(\kappa + \frac{\pi}{2}n\right) b_n \right). \quad (2.58)$$

Now, with the aid of the identities

$$\cos\left(\kappa + \frac{\pi}{2}n\right) = (-1)^n \cos\left(\kappa - \frac{\pi}{2}n\right)$$

and

$$\sin\left(\kappa+\frac{\pi}{2}n\right)=(-1)^n\sin\left(\kappa-\frac{\pi}{2}n\right),$$

equation (2.58) takes the form

$$Y_{n+1/2}(\kappa)=-\sqrt{\frac{2}{\pi\kappa}}\left(\cos\left(\kappa-\frac{\pi}{2}n\right)a_n-\sin\left(\kappa-\frac{\pi}{2}n\right)b_n\right). \tag{2.59}$$

Hence, by writing (2.57) and (2.59) in matrix form, we obtain

$$\begin{bmatrix}\sin(\kappa-\pi n/2) & \cos(\kappa-\pi n/2)\\ \cos(\kappa-\pi n/2) & -\sin(\kappa-\pi n/2)\end{bmatrix}\begin{bmatrix}a_n\\ b_n\end{bmatrix}=\sqrt{\frac{\pi\kappa}{2}}\begin{bmatrix}J_{n+1/2}(\kappa)\\ -Y_{n+1/2}(\kappa)\end{bmatrix},$$

which completes the proof. □

Note that a typographical error in [1] for (2.54) has been rectified here.

Equations (2.36) and (2.37) provide compact representations for the terms $\hat{B}(\Psi^p,\Psi^p)$ and $\hat{B}(\Phi^p,\Phi^p)$ respectively. We first consider $\hat{B}(\Psi^p,\Psi^p)$ for even values of p. Using Lemma 2.5.2, we see that $\kappa^p a_p$ and $\kappa^p b_p$ are polynomials of degrees at most p and $p-1$ in κ respectively, i.e. $\kappa^p a_p\in\mathbb{P}_p$, and $\kappa^p b_p\in\mathbb{P}_{p-1}$. Consequently, it is not difficult to verify that $\kappa^p a_{p+1},\kappa^p a_{p-1}\in\mathbb{P}_p$ and $\kappa^{p+1}b_{p-1},\kappa^{p+1}b_{p+1}\in\mathbb{P}_p$. Hence, $\hat{B}(\Psi^p,\Psi^p)$ is a rational function of degree $[p+2/p]$ in κ for even values of p. Similarly, for odd values of p, $\hat{B}(\Psi^p,\Psi^p)$ is a rational function of degree $[p+1/p-1]$ in κ. Now, as $\Phi^p\in\mathbb{P}_{p-1}$ for all $p\in\mathbb{N}$ i.e. Φ^p is polynomial of degree $p-1$ in κ, the quadrature rule in bilinear form (2.33) is exact for Φ^p. Hence, from Theorem 4.2 in [1], it is clear that $\hat{B}(\Phi^p,\Phi^p)$ is also a rational function of κ for even and odd values of p. As $p=2N$ for even values of p, from Theorem 4.2(2) in [1], $\hat{B}(\Phi^p,\Phi^p)$ is a rational function of degree $[p/p-2]$ in κ. Similarly, for odd values of p, $\hat{B}(\Phi^p,\Phi^p)$ is a rational function of degree $[p+1/p-1]$ in κ when $2N+1$ is replaced by p in Theorem 4.2(1) from [1].

Moreover, in [1] it was shown that $\hat{B}(\Phi^p,\Phi^p)$ could be represented in terms of

Bessel functions as follows:

$$\hat{B}(\Phi^p, \Phi^p) = -2\kappa \frac{J_{p+1/2}(\kappa)\sin\kappa - Y_{p+1/2}(\kappa)\cos\kappa}{J_{p+1/2}(\kappa)\cos\kappa + Y_{p+1/2}(\kappa)\sin\kappa} \quad \text{with } \kappa \neq m\pi$$

and

$$\hat{B}(\Phi^p, \Phi^p) = 2\kappa \frac{J_{p+1/2}(\kappa)\cos\kappa + Y_{p+1/2}(\kappa)\sin\kappa}{J_{p+1/2}(\kappa)\sin\kappa - Y_{p+1/2}(\kappa)\cos\kappa} \quad \text{with } \kappa \neq (m+1/2)\pi.$$

The following result extends these results to $\hat{B}(\Psi^p, \Psi^p)$.

Corollary 2.5.3. *Let $p = 2, 3, \ldots,$ then*

1. if p is even and $\kappa \neq (m+1/2)\pi$ for all $m \in \mathbb{Z}$,

$$\hat{B}(\Psi^p, \Psi^p) = 2\kappa \frac{(p+1)(J_{p-1/2}(\kappa)\cot\kappa + Y_{p-1/2}(\kappa)) - p(J_{p+3/2}(\kappa)\cot\kappa + Y_{p+3/2}(\kappa))}{(p+1)(J_{p-1/2}(\kappa) - Y_{p-1/2}(\kappa)\cot\kappa) - p(J_{p+3/2}(\kappa) - Y_{p+3/2}(\kappa)\cot\kappa)}, \quad (2.60)$$

where J and Y are cylindrical Bessel functions of the first and second kind respectively;

2. if p is odd and $\kappa \neq m\pi$ for all $m \in \mathbb{Z}$,

$$\hat{B}(\Psi^p, \Psi^p) = 2\kappa \frac{(p+1)(Y_{p-1/2}(\kappa)\cot\kappa - J_{p-1/2}(\kappa)) - p(Y_{p+3/2}(\kappa)\cot\kappa - J_{p+3/2}(\kappa))}{(p+1)(J_{p-1/2}(\kappa)\cot\kappa + Y_{p-1/2}(\kappa)) - p(J_{p+3/2}(\kappa)\cot\kappa + Y_{p+3/2}(\kappa))}. \quad (2.61)$$

Proof. This corollary is proved separately for even and odd order polynomials. Consider first the case when p is even. Since, the series $\{a_p\}$ and $\{b_p\}$, for non-negative integers p, satisfy identity (2.54), using (2.54) the values of a_{p-1}, a_{p+1} and b_{p-1}, b_{p+1} are given as follows

$$\left.\begin{aligned} a_{p-1} &= \sqrt{\frac{\pi\kappa}{2}}\left[J_{p-1/2}(\kappa)\cos\kappa + Y_{p-1/2}(\kappa)\sin\kappa\right] \\ a_{p+1} &= \sqrt{\frac{\pi\kappa}{2}}\left[-J_{p+3/2}(\kappa)\cos\kappa - Y_{p+3/2}(\kappa)\sin\kappa\right] \\ b_{p-1} &= \sqrt{\frac{\pi\kappa}{2}}\left[-J_{p-1/2}(\kappa)\sin\kappa + Y_{p-1/2}(\kappa)\cos\kappa\right] \\ b_{p+1} &= \sqrt{\frac{\pi\kappa}{2}}\left[J_{p+3/2}(\kappa)\sin\kappa - Y_{p+3/2}(\kappa)\cos\kappa\right]. \end{aligned}\right\} \quad (2.62)$$

Now, inserting these values into (2.37) and rearranging gives (2.60), which completes the proof in the even case. Now consider the case when p is odd and once again we find the following values of a_{p-1}, a_{p+1} and b_{p-1}, b_{p+1} using (2.54):

$$\left.\begin{aligned} a_{p-1} &= \sqrt{\frac{\pi\kappa}{2}}\left[J_{p-1/2}(\kappa)\sin\kappa - Y_{p-1/2}(\kappa)\cos\kappa\right] \\ a_{p+1} &= \sqrt{\frac{\pi\kappa}{2}}\left[-J_{p+3/2}(\kappa)\sin\kappa + Y_{p+3/2}(\kappa)\cos\kappa\right] \\ b_{p-1} &= \sqrt{\frac{\pi\kappa}{2}}\left[J_{p-1/2}(\kappa)\cos\kappa + Y_{p-1/2}(\kappa)\sin\kappa\right] \\ b_{p+1} &= \sqrt{\frac{\pi\kappa}{2}}\left[-J_{p+3/2}(\kappa)\cos\kappa - Y_{p+3/2}(\kappa)\sin\kappa\right]. \end{aligned}\right\} \tag{2.63}$$

Now, inserting these values into the expression (2.37) and performing straightforward manipulations gives (2.61), which completes the proof. □

In [1], it was shown that $\hat{B}(\Phi^p, \Phi^p)$ was related to certain types of Padé approximant. Here, it is not the case that $\hat{B}(\Psi^p, \Psi^p)$ is a Padé approximant. We have the following results for errors $\hat{B}(\Psi^p, \Psi^p) + 2\kappa\tan\kappa$ and $\hat{B}(\Phi^p, \Phi^p) - 2\kappa\cot\kappa$ denoted by $\mathcal{E}_{\Psi}^{(p)}(\kappa)$ and $\mathcal{E}_{\Phi}^{(p)}(\kappa)$ respectively for even integers and $\hat{B}(\Psi^p, \Psi^p) - 2\kappa\cot\kappa$ and $\hat{B}(\Phi^p, \Phi^p) + 2\kappa\tan\kappa$ denoted by $\mathcal{E}_{\Psi}^{(p)}(\kappa)$ and $\mathcal{E}_{\Phi}^{(p)}(\kappa)$ respectively for odd integers:

Theorem 2.5.4. *Let $p \in \mathbb{N}$ satisfy $p \geq 2$. Then*

1. if p is an even integer, then

1. if $\kappa \neq (m + 1/2)\pi, m \in \mathbb{Z}$,

$$\begin{aligned} \mathcal{E}_{\Psi}^{(p)}(\kappa) &= \hat{B}(\Psi^p, \Psi^p) + 2\kappa\tan\kappa \\ &= -\frac{1}{2}\left(1 + \frac{1}{p}\right)\left[\frac{p!}{(2p)!}\right]^2 \frac{(2\kappa)^{2p+2}}{2p+1} + \mathcal{O}(\kappa^{2p+4}), \end{aligned} \tag{2.64}$$

2. if $\kappa \neq m\pi, m \in \mathbb{Z}$,

$$\mathcal{E}_{\Phi}^{(p)}(\kappa) = \hat{B}(\Phi^p, \Phi^p) - 2\kappa\cot\kappa = 2\left[\frac{p!}{(2p)!}\right]^2 \frac{(2\kappa)^{2p}}{2p+1} + \mathcal{O}(\kappa^{2p+2}); \tag{2.65}$$

2. if p is an odd integer, then

1. if $\kappa \neq m\pi, m \in \mathbb{Z}$,

$$\begin{aligned}\mathcal{E}_{\Psi}^{(p)}(\kappa) &= \hat{B}(\Psi^p, \Psi^p) - 2\kappa\cot\kappa \\ &= -2\left(1+\frac{1}{p}\right)\left[\frac{p!}{(2p)!}\right]^2 \frac{(2\kappa)^{2p}}{2p+1} + \mathcal{O}(\kappa^{2p+2}),\end{aligned} \tag{2.66}$$

2. if $\kappa \neq (m+1/2)\pi, m \in \mathbb{Z}$,

$$\begin{aligned}\mathcal{E}_{\Phi}^{(p)}(\kappa) &= \hat{B}(\Phi^p, \Phi^p) + 2\kappa\tan\kappa \\ &= \frac{1}{2}\left[\frac{p!}{(2p)!}\right]^2 \frac{(2\kappa)^{2p+2}}{2p+1} + \mathcal{O}(\kappa^{2p+4}).\end{aligned} \tag{2.67}$$

Proof. Since the quadrature rule is exact for Φ^p in the bilinear form (2.33). Moreover the estimates (2.65) and (2.67) are the same as equations (4.16) and (4.15) in [1], for $p = 2N$ and $p = 2N+1$ respectively. Therefore, we have

$$\mathcal{E}_{o}^{(p)}(\kappa) = \mathcal{E}_{\Phi}^{(p)}(\kappa) = 2\left[\frac{p!}{(2p)!}\right]^2 \frac{(2\kappa)^{2p}}{2p+1} + \mathcal{O}(\kappa^{2p+2})$$

and

$$\mathcal{E}_{e}^{(p)}(\kappa) = \mathcal{E}_{\Phi}^{(p)}(\kappa) = \frac{1}{2}\left[\frac{p!}{(2p)!}\right]^2 \frac{(2\kappa)^{2p+2}}{2p+1} + \mathcal{O}(\kappa^{2p+4}).$$

Now, to prove estimates (2.64) and (2.66) consider the case when p is even. Straightforward manipulations beginning with equation (2.60) give

$$\hat{B}(\Psi^p, \Psi^p) + 2\kappa\tan\kappa = -\frac{2\kappa}{\cos^2\kappa}\tilde{Q}^{p+3/2}(\kappa)\left(1 - \tilde{Q}^{p+3/2}(\kappa)\tan\kappa\right)^{-1} \tag{2.68}$$

where

$$\tilde{Q}^{p+3/2}(\kappa) = \frac{(p+1)\,J_{p-1/2}(\kappa) - pJ_{p+3/2}(\kappa)}{(p+1)\,Y_{p-1/2}(\kappa) - pY_{p+3/2}(\kappa)}. \tag{2.69}$$

The behaviour of $\tilde{Q}^{p+3/2}(\kappa)$ is studied in Section 2.6, where the following estimate is proved in Lemma 2.6.1 for $\kappa \ll 1$:

$$\tilde{Q}^{p+3/2}(\kappa) = \frac{1}{2}\left(1+\frac{1}{p}\right)\left[\frac{p!}{(2p)!}\right]^2 \frac{(2\kappa)^{2p+1}}{2p+1} + \cdots. \tag{2.70}$$

With the aid of this estimate, we obtain that

$$\hat{B}(\Psi^p, \Psi^p) + 2\kappa \tan \kappa = -\frac{1}{2}\left(1 + \frac{1}{p}\right)\left[\frac{p!}{(2p)!}\right]^2 \frac{(2\kappa)^{2p+2}}{2p+1} + \cdots .$$

The assertions concerning polynomials of odd order are proved starting with (2.61) in a similar fashion, and we have

$$\hat{B}(\Psi^p, \Psi^p) - 2\kappa \cot \kappa = -\frac{2\kappa}{\sin^2 \kappa}\tilde{Q}^{p+3/2}(\kappa)\left(1 + \tilde{Q}^{p+3/2}(\kappa)\cot \kappa\right)^{-1}. \tag{2.71}$$

Finally inserting (2.70) into above equation and performing ordinary manipulations give

$$\hat{B}(\Psi^p, \Psi^p) - 2\kappa \cot \kappa = -2\left(1 + \frac{1}{p}\right)\left[\frac{p!}{(2p)!}\right]^2 \frac{(2\kappa)^{2p}}{2p+1} + \cdots$$

as required. □

2.5.2 Proof of Theorem 2.4.1

The proof of the Theorem 2.4.1 now follows using a virtually identical argument to the proof of Theorem 3.1 in [1]. For the sake of completeness, we give an outline here.

Proof. For $x \in (0, h)$, the functions $\{\tilde{\theta}_i^{(p)}\}_{i=0}^N$ can be written in terms of the basic polynomials Φ and Ψ using $s = 2x/h - 1$:

$$\tilde{\theta}_0^{(p)}(x) = \frac{(-1)^p}{2}[\Psi^p(s) - \Phi^p(s)]$$

and

$$\tilde{\theta}_1^p(x) = \frac{1}{2}[\Psi^p(s) + \Phi^p(s)]$$

where the expressions for $\tilde{\theta}_0^p(x)$ and $\tilde{\theta}_1^p(x)$ take the correct values at the boundary points $x = 0$ and $x = h$. Moreover, we define $V \in \mathbb{P}_p \cap H_0^1(-1, 1)$ by $V(s) =$

$v_{hp}(x)$, where $v_{hp} \in V_{hp}^{\flat}$ is supported on $(0, h)$. Now, using the change of variable $s = 2x/h - 1$, we obtain

$$\tilde{B}(\tilde{\theta}_1^{(p)}, v_{hp}) = h^{-1}\hat{B}(\Psi^p + \Phi^p, V)$$

which vanishes because of the basis polynomials defined in (2.34)-(2.35). Consequently, the orthogonality property is satisfied. Similar arguments hold in the case of $\tilde{\theta}_0^{(p)}$. Since $\omega h = 2\kappa$, the change of variable reveals that

$$\tilde{B}(\tilde{\theta}_1^{(p)}, \tilde{\theta}_1^{(p)}) = h^{-1}\hat{B}(\Psi^p + \Phi^p, \Psi^p + \Phi^p).$$

Furthermore, exploiting the parities of Ψ and Φ, we obtain

$$\tilde{B}(\tilde{\theta}_1^{(p)}, \tilde{\theta}_1^{(p)}) = h^{-1}[\hat{B}(\Psi^p, \Psi^p) + \hat{B}(\Phi^p, \Phi^p)].$$

Similar arguments give

$$\tilde{B}(\tilde{\theta}_0^{(p)}, \tilde{\theta}_1^{(p)}) = (-1)^p(2h)^{-1}[\hat{B}(\Psi^p, \Psi^p) - \hat{B}(\Phi^p, \Phi^p)].$$

Substituting these results into equation (2.22) gives

$$\cos\tilde{\mu}^{(p)}h = (-1)^{p+1}\frac{\hat{B}(\Psi^p, \Psi^p) + \hat{B}(\Phi^p, \Phi^p)}{\hat{B}(\Psi^p, \Psi^p) - \hat{B}(\Phi^p, \Phi^p)} \tag{2.72}$$

and equations (2.36) and (2.37) show that after simplification (2.72) can be written as

$$\cos\tilde{\mu}^{(p)}h = (-1)^p\frac{(p+1)\,(a_pb_{p-1} + b_pa_{p-1}) + p\,(a_pb_{p+1} + b_pa_{p+1})}{(p+1)\,(a_pb_{p-1} - b_pa_{p-1}) + p\,(a_pb_{p+1} - b_pa_{p+1})} \quad \forall p \in \mathbb{N}.$$

Finally, using the recurrence relation defined in (2.24), we have

$$\cos\tilde{\mu}^{(p)}h = (-1)^p\frac{a_p\,(\kappa b_{p-1} + pa_p) + b_p\,(\kappa a_{p-1} - pb_p)}{a_p\,(\kappa b_{p-1} + pa_p) - b_p\,(\kappa a_{p-1} - pb_p)} \quad \forall p \in \mathbb{N}.$$

□

2.5.3 Proof of Theorem 2.4.2

We use Theorem 2.5.4 to prove Theorem 2.4.2 as follows:

Proof. We first consider the case when p is even. We start with equations (2.64)-(2.65) and write $\hat{B}(\Psi^p, \Psi^p)$ and $\hat{B}(\Phi^p, \Phi^p)$ in terms of $\mathcal{E}_\Psi^{(p)}$ and $\mathcal{E}_\Phi^{(p)}$ respectively:

$$\hat{B}(\Psi^p, \Psi^p) = \mathcal{E}_\Psi^{(p)}(\kappa) - 2\kappa \tan \kappa$$

and

$$\hat{B}(\Phi^p, \Phi^p) = \mathcal{E}_\Phi^{(p)}(\kappa) + 2\kappa \cot \kappa.$$

Now, inserting these expression into (2.72), and performing ordinary calculations, we obtain

$$\cos \tilde{\mu}^{(p)} h = \frac{\sin \omega h \left[\mathcal{E}_\Psi^{(p)}(\kappa) + \mathcal{E}_\Phi^{(p)}(\kappa)\right] + 2\omega h \cos \omega h}{\sin \omega h \left[\mathcal{E}_\Psi^{(p)}(\kappa) - \mathcal{E}_\Phi^{(p)}(\kappa)\right] + 2\omega h} \tag{2.73}$$

where $\omega h = 2\kappa$. Subtracting $\cos \omega h$ on both sides of the above equation and simplifying gives the expression for the error in the discrete dispersion relation:

$$\begin{aligned} &\cos \tilde{\mu}^{(p)} h - \cos \omega h \\ &= \frac{\sin \omega h}{\omega h} \left\{ \mathcal{E}_\Phi^{(p)} \sin^2 \left(\frac{\omega h}{2} \right) + \mathcal{E}_\Psi^{(p)} \cos^2 \left(\frac{\omega h}{2} \right) \right\} \left\{ 1 + \frac{\sin \omega h}{2\omega h} \left(\mathcal{E}_\Phi^{(p)} - \mathcal{E}_\Psi^{(p)} \right) \right\}^{-1}. \end{aligned} \tag{2.74}$$

In particular, for small ωh i.e. $\kappa = \omega h/2 \ll 1$, it then follows that

$$\cos \tilde{\mu}^{(p)} h - \cos \omega h = \left(\frac{\omega h}{2} \right)^2 \mathcal{E}_\Phi^{(p)} + \mathcal{E}_\Psi^{(p)} + \cdots \tag{2.75}$$

where

$$\left(\frac{\omega h}{2} \right)^2 \mathcal{E}_\Phi^{(p)} = \frac{1}{2} \left[\frac{p!}{(2p)!} \right]^2 \frac{(\omega h)^{2p+2}}{2p+1} + \cdots$$

and

$$\mathcal{E}_\Psi^{(p)} = -\frac{1}{2} \left(1 + \frac{1}{p} \right) \left[\frac{p!}{(2p)!} \right]^2 \frac{(\omega h)^{2p+2}}{2p+1} + \cdots .$$

Substituting these values into equation (2.75), we get

$$\cos\tilde{\mu}^{(p)}h - \cos\omega h = -\frac{1}{2p}\left[\frac{p!}{(2p)!}\right]^2 \frac{(\omega h)^{2p+2}}{2p+1} + \cdots .$$

We now consider the case when p is odd. In this case, starting with equations (2.66)-(2.67) and following the arguments used for the even order case, we arrive at

$$\begin{aligned}&\cos\tilde{\mu}^{(p)}h - \cos\omega h \\ &= \frac{\sin\omega h}{\omega h}\left\{\mathcal{E}_{\Psi}^{(p)}\sin^2\left(\frac{\omega h}{2}\right) + \mathcal{E}_{\Phi}^{(p)}\cos^2\left(\frac{\omega h}{2}\right)\right\}\left\{1 + \frac{\sin\omega h}{2\omega h}\left(\mathcal{E}_{\Psi}^{(p)} - \mathcal{E}_{\Phi}^{(p)}\right)\right\}^{-1}.\end{aligned} \tag{2.76}$$

For small ωh i.e. $\kappa = \omega h/2 \ll 1$, we have

$$\cos\tilde{\mu}^{(p)}h - \cos\omega h = \left(\frac{\omega h}{2}\right)^2 \mathcal{E}_{\Psi}^{(p)} + \mathcal{E}_{\Phi}^{(p)} + \cdots \tag{2.77}$$

where

$$\left(\frac{\omega h}{2}\right)^2 \mathcal{E}_{\Psi}^{(p)} = -\frac{1}{2}\left(1 + \frac{1}{p}\right)\left[\frac{p!}{(2p)!}\right]^2 \frac{(\omega h)^{2p+2}}{2p+1} + \cdots$$

and

$$\mathcal{E}_{\Phi}^{(p)} = \frac{1}{2}\left[\frac{p!}{(2p)!}\right]^2 \frac{(\omega h)^{2p+2}}{2p+1} + \cdots .$$

Now, substituting these values into (2.77) and simplifying gives

$$\cos\tilde{\mu}^{(p)}h - \cos\omega h = -\frac{1}{2p}\left[\frac{p!}{(2p)!}\right]^2 \frac{(\omega h)^{2p+2}}{2p+1} + \cdots .$$

Hence, it is once again evident that the leading term in the remainder is the same, regardless of the parity of the polynomial order p. It is also worth noting that unlike [1] there are no parity dependent dominating terms in the expressions for the error. Furthermore, for small $\tilde{\mu}^{(p)}h - \omega h$, we obtain the approximation

$$\cos\tilde{\mu}^{(p)}h - \cos\omega h = -(\tilde{\mu}^{(p)}h - \omega h)\sin\omega h + \cdots$$

which for small values of ωh reduces to

$$\cos\tilde{\mu}^{(p)}h - \cos\omega h = -(\tilde{\mu}^{(p)}h - \omega h)\omega h + \cdots.$$

Using above approximation gives estimate (2.27). □

2.5.4 Proof of Theorem 2.4.3

Proof. We begin with the regime where $p \ll \omega h$. The series (2.52)-(2.53) defined in Lemma 2.5.2 give:

$$a_p = 1 - \frac{(p+2)!}{8(p-2)!\kappa^2} + \mathcal{O}(\kappa^{-4})$$

and

$$b_p = \frac{(p+1)!}{2(p-1)!\kappa} - \frac{(p+3)!}{48(p-3)!\kappa^3} + \mathcal{O}(\kappa^{-5}).$$

Now, substituting these values into (2.25) we obtain

$$R^{(p)}(2\kappa) = \cos\tilde{\mu}^{(p)}h \approx \frac{(-1)^{p+1}}{6}\,(2p^4 + 4p^3 + p^2 - p - 12\kappa^2)$$

after elementary calculations. Since $\kappa = \omega h/2 \gg 1$, we can also obtain

$$R^{(p)}(2\kappa) = \cos\tilde{\mu}^{(p)}h \approx (-1)^p\frac{(\omega h)^2}{2}.$$

As $\mathcal{E}^{(p)} = R^{(p)}(2\kappa) - \cos\omega h$, the error in the discrete dispersion relation for $p \ll \omega h$ is given by

$$\mathcal{E}^{(p)} \approx (-1)^p\frac{(\omega h)^2}{2} \qquad \forall p \in \mathbb{N} \text{ such that } p \ll \omega h.$$

Now, for the rest of the proof we make use of the fact that

$$\mathcal{E}_{\Psi}^{(p)}(\kappa)\frac{\cos^2(\omega h/2)}{\omega h} = -\tilde{Q}^{p+3/2}(\kappa)\{1 - \tilde{Q}^{p+3/2}(\kappa)\tan\kappa\}^{-1} \tag{2.78}$$

which can be verified by rewriting equation (2.68), where the quotient $\tilde{Q}^{p+3/2}(\kappa)$ is studied in Theorem 2.6.2 given in the next section. Since the quadrature rule

is exact in bilinear form (2.33) for Φ^p, we can use ([1], eq.(4.22)) with $p = 2N_o$, namely

$$\mathcal{E}_{\Phi}^{(p)}(\kappa)\frac{\sin^2(\omega h/2)}{\omega h} = -Q^{p+1/2}(\kappa)\{1 + Q^{p+1/2}(\kappa)\cot\kappa\}^{-1} \tag{2.79}$$

where the behaviour of the quotient $Q_{p+1/2}(\kappa)$ is studied in the appendix of [1]. First of all, consider the case when p is even with $\kappa = \omega h/2 \gg 1$ fixed. The behaviour of the error $\mathcal{E}^{(p)}$ in different regimes will be determined by the behaviour of either $\tilde{Q}^{p+3/2}(\kappa)$ or $Q^{p+1/2}(\kappa)$.

We consider the preasymptotic regime where $2p + 1 < \omega h - o(\omega h)^{1/3}$ for both $Q^{p+1/2}(\kappa)$ and $\tilde{Q}^{p+3/2}(\kappa)$. For p in this range, it is evident that in the asymptotic regime both $\tilde{Q}^{p+3/2}(\kappa)$ and $Q^{p+1/2}(\kappa)$ oscillate around unity but the error $\mathcal{E}^{(p)}$ does not oscillate around unity because the denominator of (2.74) becomes very small. Therefore, the error $\mathcal{E}^{(p)}$ starts from $(\omega h)^2/2$ and decays by several orders of magnitude to $\mathcal{O}(1)$.

Both $Q^{p+1/2}(\kappa)$ and $\tilde{Q}^{p+3/2}(\kappa)$ have the same bounds for p in the transition region, i.e p in the transition region satisfies $\omega h - o(\omega h)^{1/3} < 2p+1 < \omega h + o(\omega h)^{1/3}$. Moreover, with spectral element method the term appearing in the denominator of (2.74) is oscillating around unity for $\omega h \gg 1$ which was not the case with the finite element method. In addition, from Theorem 2.6.2, the quotient $\tilde{Q}^{p+3/2}$ is also oscillating in this region whilst $Q^{p+1/2}$ decays algebraically at a rate $\mathcal{O}(p^{-1/3})$ which is proved in Theorem $A.2$ of [1]. Hence, $\tilde{Q}^{p+3/2}$ dominates $Q^{p+1/2}$ in the error expression and therefore, the error $\mathcal{E}^{(p)}$ oscillates in the transition region.

In the super-exponential region, where p satisfies $2p + 1 > \omega h + o(\omega h)^{1/3}$, the term appearing in the denominator of (2.74) is of $\mathcal{O}(1)$ for $\omega h \gg 1$. Hence, the error $\mathcal{E}^{(p)}$ is dictated by the behaviour of the sum of $\tilde{Q}^{p+3/2}$ and $Q^{p+1/2}$. Since in this region both $\tilde{Q}^{p+3/2}$ and $Q^{p+1/2}$ decay at a super-exponential rate, the error $\mathcal{E}^{(p)}$ also decays at a super-exponential rate as it is the sum of $\tilde{Q}^{p+3/2}$ and $Q^{p+1/2}$.

Now, consider the case when p is odd. Equation(2.71) implies that

$$\mathcal{E}_{\Psi}^{(p)}(\kappa)\frac{\sin^2(\omega h/2)}{\omega h} = -\tilde{Q}^{p+3/2}(\kappa)\{1+\tilde{Q}^{p+3/2}(\kappa)\cot\kappa\}^{-1}$$

and similarly, for Φ^p, equation (4.21) of [1] with $2N_e+1$ replaced by p gives

$$\mathcal{E}_{\Phi}^{(p)}(\kappa)\frac{\cos^2(\omega h/2)}{\omega h} = -Q^{p+1/2}(\kappa)\{1-Q^{p+1/2}(\kappa)\tan\kappa\}^{-1}.$$

For the odd order case, the proof of the error expression (2.76) follows exactly the same arguments for the oscillatory, transition and super-exponential regions as in the even order case. □

2.6 Analysis of $\tilde{Q}^m(\kappa)$

We now consider the behaviour of the quotient $\tilde{Q}^m(\kappa)$ for both cases, i.e. when $\kappa \ll 1$ and $\kappa \gg 1$. This quotient is defined by

$$\tilde{Q}^m(\kappa) = \frac{\left(m-\frac{1}{2}\right)J_{m-2}(\kappa) - \left(m-\frac{3}{2}\right)J_m(\kappa)}{\left(m-\frac{1}{2}\right)Y_{m-2}(\kappa) - \left(m-\frac{3}{2}\right)Y_m(\kappa)}, \quad m = integer + \frac{1}{2} \tag{2.80}$$

and appeared in equation (2.69) in a form which we shall prove is equivalent to the above in the following lemma for small values of κ.

Lemma 2.6.1. *Let $m = integer + 1/2$ and let $\tilde{Q}^m$ be defined as above. Then, for $\kappa \ll 1$,*

$$\tilde{Q}^m(\kappa) = \frac{1}{2}\frac{(2m-1)}{(2m-3)}\left[\frac{(m-\frac{3}{2})!}{(2m-3)!}\right]^2\frac{(2\kappa)^{2m-2}}{2m-2} + \cdots . \tag{2.81}$$

Proof. Write $m = n+1/2$, where $n \in \mathbb{Z}$. For small κ, identities (8.440) and $(8.399)_2$ of [28] give

$$J_{n+1/2}(\kappa) = \frac{2^{n+1}}{\sqrt{\pi}(2n+1)!!}\left(\frac{\kappa}{2}\right)^{n+1/2} - \frac{2^{n+2}}{\sqrt{\pi}(2n+3)!!}\left(\frac{\kappa}{2}\right)^{n+5/2} + \cdots , \tag{2.82}$$

while combining identities $(8.465)_1$ and $(8.399)_3$ along with identity (8.440) of [28] gives

$$Y_{n+1/2}(\kappa) = -\frac{(2n-1)!!}{2^n\sqrt{\pi}}\left(\frac{\kappa}{2}\right)^{-n-1/2} - \frac{(2n-3)!!}{2^{n-1}\sqrt{\pi}}\left(\frac{\kappa}{2}\right)^{-n+3/2} + \cdots . \tag{2.83}$$

Moreover, replacing n by $n-2$ in the above two identities, we get

$$J_{n-3/2}(\kappa) = \frac{2^{n-1}}{\sqrt{\pi}(2n-3)!!}\left(\frac{\kappa}{2}\right)^{n-3/2} - \frac{2^n}{\sqrt{\pi}(2n-1)!!}\left(\frac{\kappa}{2}\right)^{n+1/2} + \cdots \tag{2.84}$$

and

$$Y_{n-3/2}(\kappa) = -\frac{(2n-5)!!}{2^{n-2}\sqrt{\pi}}\left(\frac{\kappa}{2}\right)^{-n+3/2} - \frac{(2n-7)!!}{2^{n-3}\sqrt{\pi}}\left(\frac{\kappa}{2}\right)^{-n+7/2} + \cdots . \tag{2.85}$$

Now, inserting these identities into (2.80) and simplifying, we arrive at

$$\tilde{Q}^m(\kappa) = \frac{1}{2}\left(\frac{n}{n-1}\right)\left[\frac{(n-1)!}{(2n-2)!}\right]^2 \frac{(2\kappa)^{2n-1}}{2n-1} + \cdots$$

which in terms of m gives the result claimed. □

Lemma 2.6.1 shows that $\tilde{Q}^m(\kappa)$ also decays algebraically as κ becomes small. The behaviour of the ratio $\tilde{Q}^m(\kappa)$ when the order of the Bessel functions and their arguments are both very large is shown in Figure 2.6 for $\kappa = 10$ and $\kappa = 20$. In this case two distinct phases are observed depending on the order m. It is evident from both the graphs of Figure 2.6 that the quotient $\tilde{Q}^m(\kappa)$ initially oscillates around unity. As the order m passes through $\kappa+1$, there is a relatively short-lived transition zone where the ratio first increases and then decays at an algebraic rate as the order m is increased. Therefore, the ratio is still oscillating in the transition zone. Finally, $\tilde{Q}^m(\kappa)$ decays at an exponential rate. The remainder of the section describes the behaviour of the ratio $\tilde{Q}^m$ for high wave numbers i.e. when $\kappa = \omega h/2 \gg 1$.

Theorem 2.6.2. *Let $\tilde{Q}^m(\kappa)$ be defined as above and $m = \text{integer} + \frac{1}{2}$. Then, as m is increased, $\tilde{Q}^m(\kappa)$ passes through two phases:*

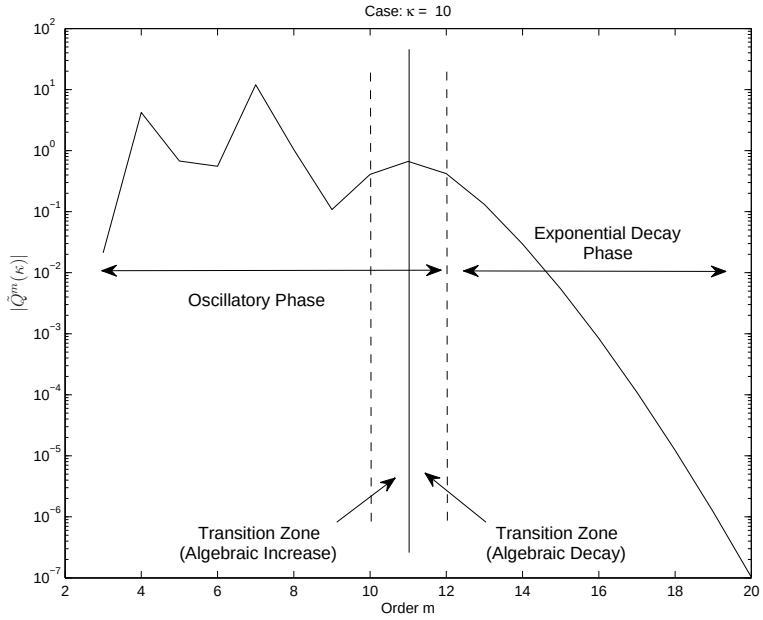

(a)

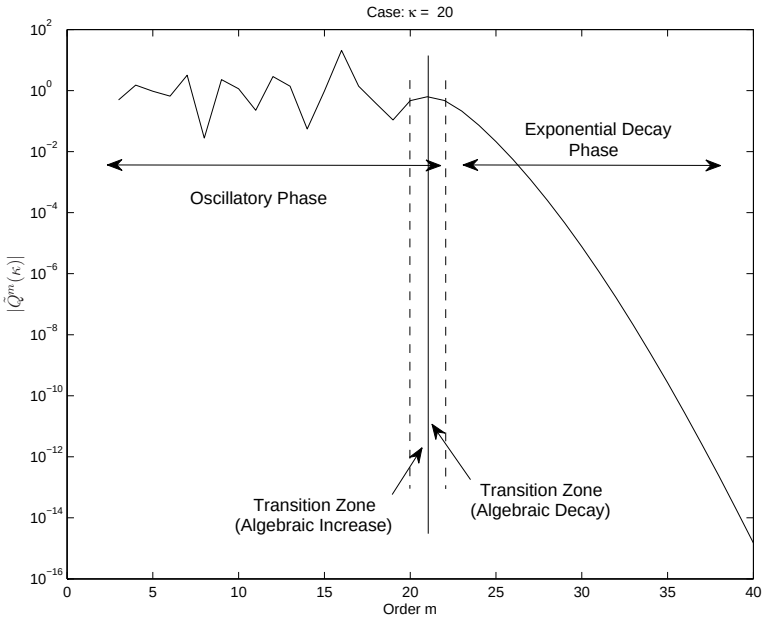

(b)

Figure 2.6: Graphs showing the three phases in the behaviour of $|\tilde{Q}^m(\kappa)|$ for (a) $\kappa = 10$ and (b) $\kappa = 20$ as the order m is increased.

1. *For $m < \kappa + 1 + o(\kappa^{1/3})$, $\tilde{Q}^m(\kappa)$ oscillates around unity but does not decay as m is increased.*

2. *For $m > \kappa + 1 + o(\kappa^{1/3})$, $\tilde{Q}^m(\kappa)$ decays at a super-exponential rate:*

$$\tilde{Q}^m(\kappa) \approx \frac{1}{2}\Bigg\{ \left[\frac{1-\sqrt{1-k^2/(m-2)^2}}{1+\sqrt{1-k^2/(m-2)^2}} e^{2\sqrt{1-k^2/(m-2)^2}}\right]^{\frac{m-2}{2}} \times \left[\frac{1-\sqrt{1-k^2/m^2}}{1+\sqrt{1-k^2/m^2}} e^{2\sqrt{1-k^2/m^2}}\right]^{\frac{m}{2}} \Bigg\} \tag{2.86}$$

so that, for $m \gg \kappa + 1$,

$$\tilde{Q}^m(\kappa) \approx \frac{1}{2}\left[\frac{\kappa e}{2(m-1)}\right]^{2(m-1)}. \tag{2.87}$$

2.6.1 Preasymptotic regime: $m < \kappa + 1$

In the preasymptotic regime we discuss the behaviour of $\tilde{Q}^m(\kappa)$ for uniform asymptotic expansions of Bessel functions with large order and large argument. Moreover, in this case the value of the order m does not exceed the argument $\kappa + 1$ of the Bessel functions. Langer's formulae given in Section 7.13.4 of [23] provide uniform asymptotic expansions for Bessel functions of large order and large argument. Inserting these formulae into (2.80), and performing some manipulations, give

$$\tilde{Q}^m(\kappa) = \frac{J_{1/3}(z_{m-2})\cos(\pi/6) - Y_{1/3}(z_{m-2})\sin(\pi/6) + \mathcal{O}((m-2)^{-4/3})}{J_{1/3}(z_{m-2})\sin(\pi/6) + Y_{1/3}(z_{m-2})\cos(\pi/6) + \mathcal{O}((m-2)^{-4/3})} \times \left\{ \frac{1-\beta\dfrac{J_{1/3}(z_m)\cos(\pi/6) - Y_{1/3}(z_m)\sin(\pi/6) + \mathcal{O}(m^{-4/3})}{J_{1/3}(z_{m-2})\cos(\pi/6) - Y_{1/3}(z_{m-2})\sin(\pi/6) + \mathcal{O}((m-2)^{-4/3})}}{1-\beta\dfrac{J_{1/3}(z_m)\sin(\pi/6) + Y_{1/3}(z_m)\cos(\pi/6) + \mathcal{O}(m^{-4/3})}{J_{1/3}(z_{m-2})\sin(\pi/6) + Y_{1/3}(z_{m-2})\cos(\pi/6) + \mathcal{O}((m-2)^{-4/3})}} \right\} \tag{2.88}$$

where

$$\beta = \left[\frac{(\kappa^2-(m-2)^2)}{(\kappa^2-m^2)}\right]^{1/4} \frac{(2m-3)}{(2m-1)} \left(\frac{z_m}{z_{m-2}}\right)^{1/2} \tag{2.89}$$

with

$$z_m = m(w_m - \tan^{-1} w_m), \qquad w_m = \sqrt{\kappa^2/m^2 - 1},$$

$$z_{m-2} = (m-2)(w_{m-2} - \tan^{-1} w_{m-2}) \quad \textit{and} \quad w_{m-2} = \sqrt{\kappa^2/(m-2)^2 - 1}.$$

2.6.1.1 Oscillatory phase: $m < \kappa + 1 - o(\kappa^{1/3})$

The ratio $\tilde{Q}^m(\kappa)$ oscillates with a magnitude of order unity for m small relative to $\kappa + 1$ in the preasymptotic regime. Since, for small m relative to $\kappa + 1$, the arguments z_m and z_{m-2} of the Bessel functions appearing in (2.88) are large and positive, we can use the asymptotic expansions of Bessel functions with large arguments given in $(8.440)_1$ and $(8.440)_2$ of [28]:

$$J_\nu(z) \sim \left(\frac{\pi z}{2}\right)^{-1/2} \cos\left(z - \frac{1}{2}\nu\pi - \frac{\pi}{4}\right) \tag{2.90}$$

and

$$Y_\nu(z) \sim \left(\frac{\pi z}{2}\right)^{-1/2} \sin\left(z - \frac{1}{2}\nu\pi - \frac{\pi}{4}\right). \tag{2.91}$$

Dropping the higher order terms in (2.88), and with the aid of the above expressions, followed by elementary manipulations, we arrive at

$$\tilde{Q}^m(\kappa) \approx \cot\left(z_{m-2} - \frac{\pi}{4}\right) \left[\frac{1 - \beta' \cos\left(z_m - \frac{\pi}{4}\right) \sec\left(z_{m-2} - \frac{\pi}{4}\right)}{1 - \beta' \sin\left(z_m - \frac{\pi}{4}\right) \operatorname{cosec}\left(z_{m-2} - \frac{\pi}{4}\right)}\right] \tag{2.92}$$

with

$$\beta' = \left[\frac{(\kappa^2 - (m-2)^2)}{(\kappa^2 - m^2)}\right]^{1/4} \frac{(2m-3)}{(2m-1)}.$$

It is evident from Figure 2.7 that the expression (2.92) agrees closely with $\tilde{Q}^m(\kappa)$ and represents qualitatively very accurate behaviour even for modest values of κ in the preasymptotic regime.

2.6.1.2 Transition zone: $\kappa + 1 - o(\kappa^{1/3}) < m < \kappa + 1$

Here we consider the behaviour when m approaches $\kappa+1$ from the left. Since in this region the value of the expression (2.89) used in equation (2.88) is approximately 1, using the series representations for Bessel functions given in equation (8.440) of [28], equation (2.80) becomes

$$\tilde{Q}^m(\kappa) \approx -\frac{1}{\sqrt{3}} + \frac{3}{\pi}\Gamma\left(\frac{2}{3}\right)^2 \left(\frac{z_{m-2}}{2}\right)^{1/3} \left(\frac{z_m}{2}\right)^{1/3} + \cdots . \tag{2.93}$$

Furthermore, $\omega_m \simeq \left[\frac{\kappa - m}{m/2}\right]^{1/2}$ and $\omega_{m-2} \simeq \left[\frac{\kappa - (m-2)}{(m-2)/2}\right]^{1/2}$ where both w_m and w_{m-2} are of order 1. Consequently,

$$z_m \simeq \frac{1}{3} m \omega_m^3 \simeq \frac{2}{3}\left[\frac{\kappa - m}{(m/2)^{1/3}}\right]^{3/2} = o(1) \tag{2.94}$$

and

$$z_{m-2} \simeq \frac{1}{3}(m-2)\omega_{m-2}^3 \simeq \frac{2}{3}\left[\frac{\kappa - (m-2)}{((m-2)/2)^{1/3}}\right]^{3/2} = o(1). \tag{2.95}$$

Substituting the values of z_m and z_{m-2} into (2.93), we finally arrive at

$$\tilde{Q}^m(\kappa) \approx -\frac{1}{\sqrt{3}} + \frac{1}{\pi}\Gamma\left(\frac{2}{3}\right)^2 \sqrt{\kappa - m}\sqrt{\kappa - m + 2}\left(\frac{36}{(m(m-2))}\right)^{1/6} + \cdots$$

which is increasing algebraically at a rate of $\mathcal{O}(m^{1/3})$ as m increases in this region.

2.6.2 Asymptotic regime: $m > \kappa + 1$

In this regime the order m of the Bessel functions exceeds the argument $\kappa + 1$. Again, using Langer's formulae from Section 7.13.4 of [23] together with (2.80)

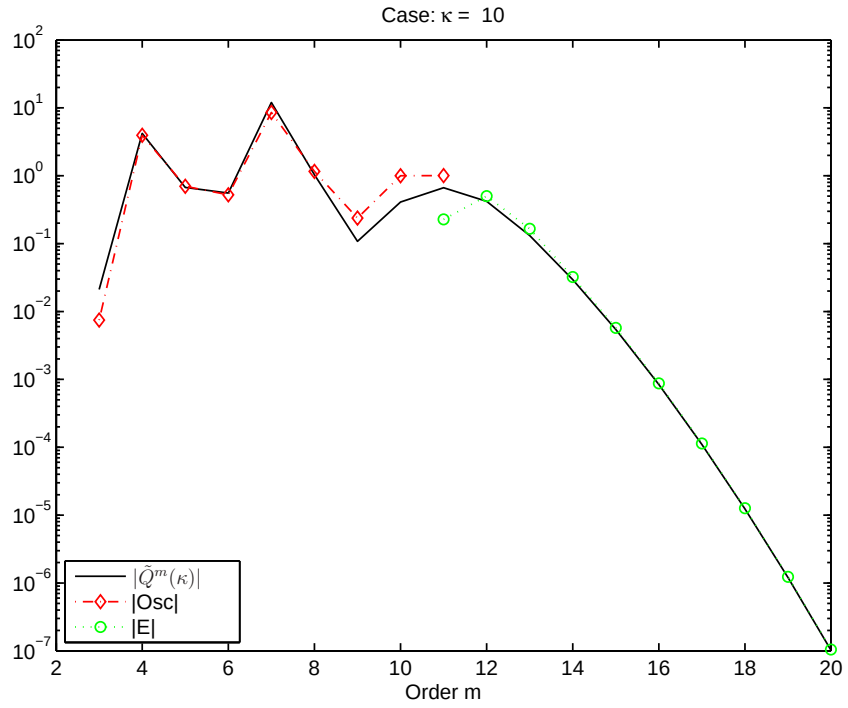
Case: κ = 10
10^{2}
10^{1}
10^{0}
10^{-1}
10^{-2}
10^{-3}
10^{-4}
10^{-5}
10^{-6}
10^{-7}
2 4 6 8 10 12 14 16 18 20
Order m
$|\tilde{Q}^m(\kappa)|$
|Osc|
|E|

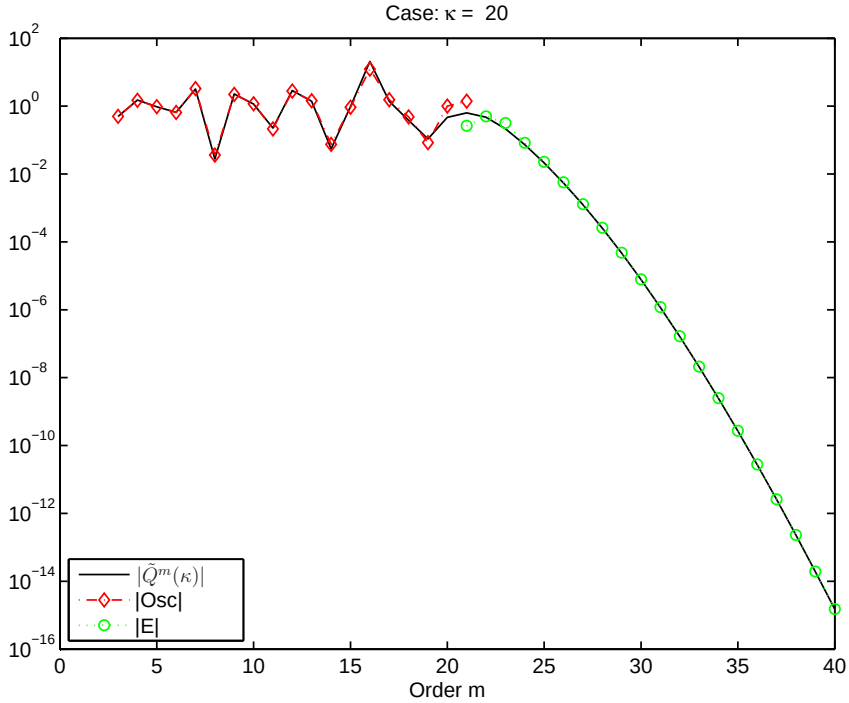
Case: κ = 20
10^{2}
10^{0}
10^{-2}
10^{-4}
10^{-6}
10^{-8}
10^{-10}
10^{-12}
10^{-14}
10^{-16}
0 5 10 15 20 25 30 35 40
Order m
$|\tilde{Q}^m(\kappa)|$
|Osc|
|E|

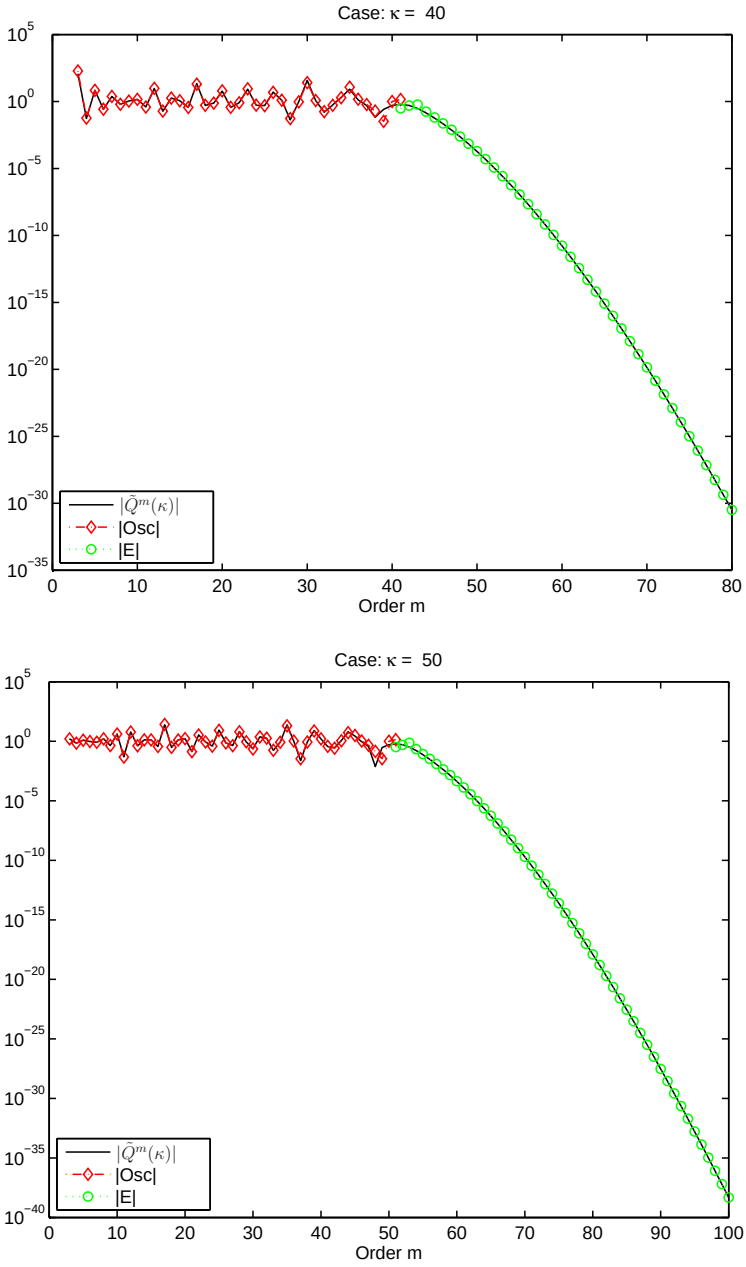

Figure 2.7: Graphs of $|\tilde{Q}^m(\kappa)|$ (given in (2.80)) for $m = 1, ..., 2\kappa$, $|\,\mathrm{Osc}\,|$ (the absolute value of the right hand side of (2.92)) for $m = 1, ..., \kappa + 1$, and $|E|$ (the absolute value of the right hand side of (2.100)) for $m = \kappa + 1, ..., 2\kappa$. Values of $\kappa = 10$, 20, 40 and 50 are shown. Observe the oscillatory behaviour of $|\tilde{Q}^m(\kappa)|$ and the good qualitative agreement provided by the $|\,\mathrm{Osc}\,|$ in the preasymptotic regime $m < \kappa + 1$ for $\omega h \geq 20$. Furthermore, note the quantitative agreement between $|\tilde{Q}^m(\kappa)|$ and $|E|$ in the asymptotic regime $m > \kappa + 1$.

gives

$$\tilde{Q}^m(\kappa) = -\frac{\pi^{-1}K_{1/3}(z_{m-2}) + \mathcal{O}((m-2)^{-4/3})}{I_{1/3}(z_{m-2}) + I_{-1/3}(z_{m-2}) + \mathcal{O}((m-2)^{-4/3})} \times \left\{ \frac{1 - \gamma \dfrac{K_{1/3}(z_m) + \mathcal{O}(m^{-4/3})}{K_{1/3}(z_{m-2}) + \mathcal{O}((m-2)^{-4/3})}}{1 - \gamma \dfrac{I_{1/3}(z_m) + I_{-1/3}(z_m) + \mathcal{O}(m^{-4/3})}{I_{1/3}(z_{m-2}) + I_{-1/3}(z_{m-2}) + \mathcal{O}((m-2)^{-4/3})}} \right\} \quad (2.96)$$

where

$$\gamma = \left[\frac{(m-2)^2 - \kappa^2}{(m^2 - \kappa^2)}\right]^{1/4} \frac{(2m-3)}{(2m-1)} \left(\frac{z_m}{z_{m-2}}\right)^{1/2} \quad (2.97)$$

with

$$z_m = m(\tanh^{-1} w_m - w_m), \qquad w_m = \sqrt{1 - \kappa^2/m^2},$$

$$z_{m-2} = (m-2)(\tanh^{-1} w_{m-2} - w_{m-2}) \quad \textit{and} \quad w_{m-2} = \sqrt{1 - \kappa^2/(m-2)^2}.$$

Now, writing $z = \frac{2}{3}\xi^{3/2}$ and combining this with (11.1.04) and (11.1.12), given in [54], gives

$$\pi^{-1}K_{1/3}(z_m) = \mathrm{Ai}(\xi_m)\left(\frac{\xi_m}{3}\right)^{-1/2}$$

and

$$I_{1/3}(z_m) + I_{-1/3}(z_m) = \mathrm{Bi}(\xi_m)\left(\frac{\xi_m}{3}\right)^{-1/2}$$

where Ai and Bi denote Airy functions of the first and second kinds respectively [28]. Again, using formulae (11.1.07) and (11.1.16) from [54], we get

$$\pi^{-1}K_{1/3}(z_m) \approx \sqrt{\frac{3}{\pi}}\frac{e^{-z_m}}{2}\xi_m^{-3/4} \quad (2.98)$$

and

$$I_{1/3}(z_m) + I_{-1/3}(z_m) \approx -\sqrt{\frac{3}{\pi}}e^{z_m}\xi_m^{-3/4}. \quad (2.99)$$

Replacing m by $m-2$ in the above expressions will give us the rest of the values. Now, inserting these values into (2.96), dropping the higher order terms and simplifying gives

$$\tilde{Q}^m(\kappa) \approx -\frac{e^{-2z_{m-2}}}{2}\left(\frac{1 - \gamma' e^{(z_{m-2} - z_m)}}{1 - \gamma' e^{-(z_{m-2} - z_m)}}\right) \quad (2.100)$$

with

$$\gamma' = \left[\frac{(m-2)^2-\kappa^2}{m^2-\kappa^2}\right]^{1/4} \frac{(2m-3)}{(2m-1)}. \tag{2.101}$$

2.6.2.1 Transition zone: $\kappa+1 < m < \kappa+1+o(\kappa^{1/3})$

In this region, we start with the expression

$$\tilde{Q}^m(\kappa) \approx -\frac{\xi_{m-2}^{1/2}\mathrm{Ai}(\xi_m) - \xi_m^{1/2}\mathrm{Ai}(\xi_{m-2})}{\xi_{m-2}^{1/2}\mathrm{Bi}(\xi_m) - \xi_m^{1/2}\mathrm{Bi}(\xi_{m-2})}$$

which is obtained from (2.96) by using the formulae (11.1.04) and (11.1.12) from [54]. Moreover, using series representations for Airy functions, given in equations (11.1.07) and (11.1.16) of [54], the above expression gives

$$\tilde{Q}^m(\kappa) \approx -\frac{1}{\sqrt{3}} - \frac{3^{1/3}}{\pi}\Gamma\left(\frac{2}{3}\right)^2 \xi_m^{1/2}\xi_{m-2}^{1/2} \tag{2.102}$$

where ξ_m and ξ_{m-2} are related to z_m and z_{m-2} by expressions $\xi_m = (3/2z_m)^{2/3}$ and $\xi_{m-2} = (3/2z_{m-2})^{2/3}$ respectively. Using similar arguments to those used before, we obtain

$$z_m \simeq \frac{1}{3}m\omega_m^3 \simeq \frac{2}{3}\left[\frac{m-\kappa}{(m/2)^{1/3}}\right]^{3/2} = o(1)$$

and

$$z_{m-2} \simeq \frac{1}{3}(m-2)\omega_{m-2}^3 \simeq \frac{2}{3}\left[\frac{m-2-\kappa}{((m-2)/2)^{1/3}}\right]^{3/2} = o(1)$$

or, equally well,

$$\xi_m \simeq \left(\frac{2}{m}\right)^{1/3}(m-\kappa) \text{ and } \xi_{m-2} \simeq \left(\frac{2}{m-2}\right)^{1/3}(m-2-\kappa).$$

Inserting these values into (2.102), we finally obtain

$$\tilde{Q}^m(\kappa) \approx -\frac{1}{\sqrt{3}} - \frac{1}{\pi}\Gamma\left(\frac{2}{3}\right)^2 \sqrt{\kappa-m}\sqrt{\kappa-m+2}\left(\frac{36}{m(m-2)}\right)^{1/6} + \cdots$$

where $\tilde{Q}^m$ is decreasing algebraically at a rate of $\mathcal{O}(m^{-1/3})$ with increasing m. Therefore, $\tilde{Q}^m$ is still oscillating in the transition region. Concluding with spectral element method the ratio $\tilde{Q}^m$ oscillates longer compared with the ratio Q_m obtained with the finite element method given in ([1], A.2).

2.6.2.2 Exponential decay phase: $m > \kappa + 1 + o(\kappa^{1/3})$

When m exceeds $\kappa+1+o(\kappa^{1/3})$ then it is easy to verify that γ', which is defined in (2.101), is approximately equal to 1 and consequently equation (2.100) takes the form

$$\tilde{Q}^m(\kappa) \approx \frac{e^{-(z_{m-2}+z_m)}}{2}. \tag{2.103}$$

Replacing z_{m-2} and z_m by w_{m-2} and w_m in the expressions for $e^{-z_{m-2}}$ and e^{-z_m} respectively, we obtain

$$e^{-z_{m-2}} = \left[\frac{1-w_{m-2}}{1+w_{m-2}}e^{2w_{m-2}}\right]^{\frac{m-2}{2}} \text{ and } e^{-z_m} = \left[\frac{1-w_m}{1+w_m}e^{2w_m}\right]^{\frac{m}{2}}$$

after elementary manipulations. Define a monotonic decreasing function $f : w \to (1-w)/(1+w)e^{2w}$ on $[0,1]$ with values ranging from 1 and 0. In the limiting case we find that

$$f\left(\sqrt{1-k^2/(m-2)^2}\right) \simeq \left[\frac{\kappa e}{2(m-2)}\right]^2 \text{ and } f\left(\sqrt{1-k^2/m^2}\right) \simeq \left[\frac{\kappa e}{2m}\right]^2.$$

So, substituting the values of $e^{-z_{m-2}}$ and e^{-z_m} into (2.103) and simplifying gives

$$\tilde{Q}^m(\kappa) \approx \frac{1}{2}\left[\frac{\kappa e}{2(m-1)}\right]^{2(m-1)}.$$

Hence, we obtain a super-exponential rate of decay when $m-1 > \kappa e/2$.

Chapter 3

Optimally blended spectral-finite element scheme for wave propagation, and non-standard reduced integration

3.1 Introduction

In this chapter we present an optimally blended spectral-finite element scheme and provide a simple means by which optimally blended spectral-finite element scheme can be efficiently implemented.

Even as early as 1984, the possibility of employing a weighted average of the finite element and spectral element schemes has been conjectured as a means by which to obtain the *most promising, cost-effective method* for computational wave propagation (Marfurt, 1984) [47]. Many authors have even commented on the effectiveness of the scheme obtained by forming a simple average of the spectral

and finite element schemes in the case of first order elements, but no systematic treatment or analysis seems to be available.

Challa presented a new scheme in his thesis [14] for the particular cases of linear and quadratic finite elements. He showed that if entries in the mass and stiffness matrices are approximated using a quadrature rule with unknown quadrature points, then in the series expansion of the corresponding discrete dispersion relation one can choose the values of the quadrature points such that two additional orders of accuracy as well as superior phase accuracy is achieved. He extended the scheme to higher dimensions using the tensor product elements on square meshes. In [26, 27], Fried analysed the dispersive properties of the acoustic wave equation. He showed that the finite elements with a lumped mass matrix underestimate the eigenvalues whereas the finite elements with a consistent mass matrix overestimate these eigenvalues. Moreover, in one dimension he formed high order accurate finite elements by blending the consistent and lumped mass matrices for both linear and quadratic elements. He found that the optimal values of the blending parameter for linear and quadratic elements are 1/2 and 2/3 respectively which are exactly the same as the values found in [7]. Interestingly, his scheme also guaranteed two additional orders of accuracy as well as exactly the same phase accuracy being achieved for the optimum value of the blending parameter as obtained in [14] using non-standard quadrature rules. This is consistent with the suggestion of Marfurt [47]. Later on, Guddati and Yue [29, 30] followed a different line of reasoning and obtained the same quadrature points and weights obtained in [14] by Challa in the case of linear finite elements on rectangular meshes. Although the above proposed methods are valuable contributions to the investigation of the dispersion phenomenon, their schemes are valid only for linear and quadratic elements.

Seriani and Oliveira [57] consider the possibility of blending the methods using a criterion whereby the phase error vanishes at a particular, user-specified, value of the normalised wavenumber. However, this approach means that the blending parameter is frequency and mesh dependent and may actually result in an *increase* in the phase error at frequencies that were originally resolved by the pure finite and spectral element approaches. In the present work we adopt a more natural approach to the selection of the blending parameter that is more in the spirit of the design of methods for computational wave propagation, is to maximise the *order* of accuracy in the phase error. We show that the optimal choice of blending parameter for elements of order $p \in \mathbb{N}$ is given by weighting the spectral element method to the finite element method in the ratio $p : 1$. A rigorous proof of this fact is provided along with precise error estimates and orders of accuracy in the phase error.

From an investigation of the literature, we have found that no suitable non-standard quadrature rules exist in the case of elements of arbitrary order $p \in \mathbb{N}$, such that the resulting scheme is identical to the optimally blended spectral-finite element scheme. We show such non-standard quadrature rules exist for all orders, give an explicit construction for the weights and nodes, and study their properties.

The remainder of the chapter is organised as follows. We start with a uni-dimensional model problem in Section 3.2. In Section 3.3, discrete dispersion relations are derived for the optimally blended scheme. The rest of the sections contain proofs of the results.

3.2 Motivation and overview of main ideas and results

In order to motivate the ideas, we begin by presenting the discrete dispersion analysis of the simple 1D model problem.

3.2.1 Piecewise linear approximation in one dimension

Consider the problem

$$u''(x) + \omega^2 u(x) = 0, \quad x \in \mathbb{R} \tag{3.1}$$

where $\omega > 0$ is a given frequency. We note that this problem is just problem (1.10) with $c = 1$. In this case equations (1.11) and (1.17) become

$$u^{j+1} - 2u^j + u^{j-1} + \frac{(\omega h)^2}{6}(u^{j+1} + 4u^j + u^{j-1}) = 0 \tag{3.2}$$

and

$$\tilde{u}^{j+1} - 2\tilde{u}^j + \tilde{u}^{j-1} + (\omega h)^2 \tilde{u}^j = 0 \tag{3.3}$$

for linear finite element and spectral element schemes respectively. In search of a numerical scheme with superior phase accuracy, we follow the suggestion of Marfurt [47] and form a *blended scheme* by taking a linear combination of (3.2) and (3.3):

$$u_\tau^{j+1} - 2u_\tau^j + u_\tau^{j-1} + \frac{(\omega h)^2}{6}\left[(1-\tau)u_\tau^{j+1} + 2(2+\tau)u_\tau^j + (1-\tau)u_\tau^{j-1}\right] = 0 \tag{3.4}$$

where $\tau \in [0, 1]$ is a parameter whose value is to be determined.

Proceeding as before, we discover that the scheme admits non-trivial solutions of the form $u_\tau^j = e^{ij\mu_\tau^{(1)}h}$ where $\mu_\tau^{(1)}$ is the *discrete wavenumber for blended scheme* and depends on ωh, and is given by

$$\mu_\tau^{(1)} h = \cos^{-1}\left(\frac{(\omega h)^2(2+\tau) - 6}{(\omega h)^2(\tau - 1) - 6}\right), \tag{3.5}$$

or, writing the above expression as a series in ωh,

$$\mu_\tau^{(1)} h = \omega h + \frac{(\omega h)^3}{24}(2\tau - 1) + \frac{(\omega h)^5}{1920}(20\tau^2 - 20\tau + 9) + \cdots . \tag{3.6}$$

The above expression reduces to those obtained for the finite element and spectral element schemes in the cases $\tau = 0$ and $\tau = 1$ respectively. However, more interestingly, we observe that by choosing $\tau = 1/2$, *two additional orders of accuracy* in the phase are obtained.

3.2.2 Implementation via non-standard quadrature rules

The practical implementation of the blended scheme may at first sight appears to entail the assembly of the mass matrices for *both* the finite element and spectral element schemes, which would be rather unattractive. We can construct another piecewise linear finite element approximation in which the entries in the mass and stiffness matrices are approximated using the non-standard quadrature rule

$$\int_{-1}^{1} f(x)dx \approx \mathcal{Q}_\tau^{(1)}(f) = f\left(-\zeta^\tau\right) + f\left(\zeta^\tau\right) \tag{3.7}$$

where $\zeta^\tau = \sqrt{\frac{1}{3}(1 + 2\tau)}$ for all $\tau \in (0, 1]$. This rule is exact for linear functions, but not products of linear functions meaning that the entries appearing in the mass matrix are under-integrated. The quadrature rule (3.7) is used to develop a composite quadrature rule $\mathcal{I}_{\tau,h}^{(1)}$ on $\mathbb{R}$ given by

$$\int_{\mathbb{R}} f(x)dx \approx \frac{h}{2} \sum_{j\in\mathbb{Z}} \left\{ f(\zeta_j^{\tau,h}) + f(-\zeta_j^{\tau,h}) \right\} = \mathcal{I}_{\tau,h}^{(1)}(f)$$

where $\pm\zeta_j^{\tau,h} = \left(j + \frac{1}{2}\right) h \pm \frac{h}{2}\zeta^\tau, \forall j \in \mathbb{Z}$.

The new piecewise linear finite element approximation is then defined by seeking a non-trivial function of the form

$$U_\tau^h(\omega; x) = \sum_{j\in\mathbb{Z}} u_\tau^j \theta_j(x), \ x \in \mathbb{R}$$

such that

$$\mathcal{I}^{(1)}_{\tau,h}(\partial_x U^h_\tau \partial_x \theta_p) - \omega^2 \mathcal{I}^{(1)}_{\tau,h}(U^h_\tau \theta_p) = 0 \tag{3.8}$$

for all $p \in \mathbb{Z}$. Interestingly, the resulting scheme gives precisely the same stencil as (3.4) for the coefficients $\{u^j_\tau\}_{j\in\mathbb{Z}}$:

$$u^{j+1}_\tau - 2u^j_\tau + u^{j-1}_\tau + \frac{(\omega h)^2}{6}\left[(1-\tau)u^{j+1}_\tau + 2(2+\tau)u^j_\tau + (1-\tau)u^{j-1}_\tau\right] = 0.$$

In other words, the scheme coincides with the blended scheme in the case of linear elements meaning that the blended scheme can be realised in practice by replacing the standard Gaussian quadrature rule by the non-standard rule (3.7). Similarly, the optimally blended scheme can be obtained by using the quadrature rule (3.7) in conjunction with the choice $\tau = 1/2$.

In summary, the non-standard quadrature rule leads to a scheme which admits a non-trivial solution given by

$$U^h_\tau(\omega; x) = \sum_{j\in\mathbb{Z}} e^{ij\mu^{(1)}_\tau h}\theta_j(x) \tag{3.9}$$

where $\mu^{(1)}_\tau$ is defined in (3.5).

3.2.3 Extension to multiple spatial dimensions

We now turn to the case of higher dimensional problems and investigate whether the blending of spectral and finite element approximation offers similar advantages to those observed in one spatial dimension. Suppose we discretise the equation

$$-\Delta u - \omega^2 u = 0 \ \text{ in } \ \mathbb{R}^3 \tag{3.10}$$

using a tensor product grid $h\mathbb{Z}^3$ on $\mathbb{R}^3$, in conjunction with tri-linear basis functions.

A standard finite element implementation requires the use of a quadrature rule to approximate the integrals over the reference element $\widehat{K} = [-1,1]^3$. Generally, a

tensor product Gauss-Legendre rule would be applied. However, prompted by the earlier observation we propose to instead use a tensor product rule based on the non-standard quadrature rule (3.7):

$$\begin{aligned}\int_{\widehat{K}} f(x,y,z)dxdydz \approx f(\zeta^\tau,\zeta^\tau,\zeta^\tau) + f(\zeta^\tau,\zeta^\tau,-\zeta^\tau) + f(\zeta^\tau,-\zeta^\tau,\zeta^\tau) \\ + f(-\zeta^\tau,\zeta^\tau,\zeta^\tau) + f(-\zeta^\tau,-\zeta^\tau,\zeta^\tau) + f(-\zeta^\tau,\zeta^\tau,-\zeta^\tau) \\ + f(\zeta^\tau,-\zeta^\tau,-\zeta^\tau) + f(-\zeta^\tau,-\zeta^\tau,-\zeta^\tau) \qquad (3.11)\end{aligned}$$

where $\zeta^\tau = \sqrt{\frac{1}{3}(1+2\tau)}$. If we choose $\tau = 0$, then the scheme reduces to the standard finite element approximation whilst the choice $\tau = 1$ gives the spectral element scheme. Consequently, the scheme with a general choice of τ may be considered as a blended approximation. We wish to analyse the dispersive properties of the resulting scheme. Based on our experience in the one dimensional case, we seek a non-trivial solution in the three dimensional case in the form

$$u(x,y,z) = U_\tau^h(\omega_x;x)U_\tau^h(\omega_y;y)U_\tau^h(\omega_z;z)$$

where $\omega_x, \omega_y, \omega_z \in \mathbb{R}$ are constants to be determined and U_τ^h is defined in (3.9).

Inserting this expression into the approximate bilinear form associated with the quadrature rule (3.11) and using a test function $v(x,y,z) = \theta_p(x)\theta_q(y)\theta_r(z)$ leads to:

$$\begin{aligned}&\mathcal{I}^{(1)}_{\tau,h}(\partial_x U_\tau^h(\omega_x;x)\ \partial_x\theta_p)\ \mathcal{I}^{(1)}_{\tau,h}(U_\tau^h(\omega_y;y)\ \theta_q)\ \mathcal{I}^{(1)}_{\tau,h}(U_\tau^h(\omega_z;z)\ \theta_r) + \\ &\mathcal{I}^{(1)}_{\tau,h}(U_\tau^h(\omega_x;x)\ \theta_p)\ \mathcal{I}^{(1)}_{\tau,h}(\partial_y U_\tau^h(\omega_y;y)\ \partial_y\theta_q)\ \mathcal{I}^{(1)}_{\tau,h}(U_\tau^h(\omega_z;z)\ \theta_r) + \\ &\mathcal{I}^{(1)}_{\tau,h}(U_\tau^h(\omega_x;x)\ \theta_p)\ \mathcal{I}^{(1)}_{\tau,h}(U_\tau^h(\omega_y;y)\ \theta_q)\ \mathcal{I}^{(1)}_{\tau,h}(\partial_z U_\tau^h(\omega_z;z)\ \partial_z\theta_r) \\ &= \omega^2\ \mathcal{I}^{(1)}_{\tau,h}(U_\tau^h(\omega_x;x)\ \theta_p)\ \mathcal{I}^{(1)}_{\tau,h}(U_\tau^h(\omega_y;y)\ \theta_q)\ \mathcal{I}^{(1)}_{\tau,h}(U_\tau^h(\omega_z;z)\ \theta_r) \qquad (3.12)\end{aligned}$$

for all $p, q, r \in \mathbb{Z}$. Recalling that U_τ^h satisfies (3.8) leads to the following condition for the parameters ω_x, ω_y and ω_z :

$$(\omega_x^2 + \omega_y^2 + \omega_z^2 - \omega^2)\mathcal{I}^{(1)}_{\tau,h}(U_\tau^h(\omega_x;x)\ \theta_p)\mathcal{I}^{(1)}_{\tau,h}(U_\tau^h(\omega_y;y)\ \theta_r)\mathcal{I}^{(1)}_{\tau,h}(U_\tau^h(\omega_z;z)\ \theta_r) = 0$$

and as a consequence, we deduce that the new scheme admits a non-trivial solution provided that

$$\omega_x^2 + \omega_y^2 + \omega_z^2 = \omega^2.$$

The discrete frequency ω_h of the discrete solution satisfies

$$\omega_h^2 = \left(\mu_\tau^{(1)}(\omega_x; h)\right)^2 + \left(\mu_\tau^{(1)}(\omega_y; h)\right)^2 + \left(\mu_\tau^{(1)}(\omega_z; h)\right)^2$$

and then, thanks to (3.5), we deduce that

$$\omega_h^2 = \omega^2 + \frac{h^2}{12}(2\tau - 1)[(\omega_x)^4 + (\omega_y)^4 + (\omega_z)^4] + \mathcal{O}(\omega^6).$$

We again see that there exists an optimal choice of blending parameter, and moreover, it coincides with the optimal parameter for the one dimensional case. The arguments used above extend to any number of dimensions meaning that the optimal blending parameter is independent of the number of spatial dimensions.

3.2.4 Numerical example

In practice, by making use of the non-standard quadrature rule, the cost of using the optimally blended scheme is virtually the same as that of using the pure finite or spectral element scheme, but can result in markedly superior numerical results. In order to illustrate the potential of such an approach in multi-dimensions, we consider the problem

$$-\nabla^2 u(x, y) - k^2 u(x, y) = 0 \quad \text{in} \quad (0, 1)^2 \tag{3.13}$$

subject to Dirichlet boundary conditions:

$$u = e^{ik_1 x} \quad \text{on} \quad \Gamma_1 = \{x \in (0, 1), y = 0\}$$

$$u = e^{ik_2 y} \quad \text{on} \quad \Gamma_4 = \{y \in (0, 1), x = 0\}$$

where k_1 and k_2 are user-specified constants satisfying $k_1^2 + k_2^2 = k^2$, and non-reflecting boundary conditions:

$$\frac{\partial u}{\partial x} - Gu = 0 \quad \text{on} \quad \Gamma_2 = \{y \in (0,1), x = 1\}$$
$$\frac{\partial u}{\partial y} - Gu = 0 \quad \text{on} \quad \Gamma_3 = \{x \in (0,1), y = 1\}$$

where G is the usual Dirichlet to Neumann map [35]. The Dirichlet boundary conditions are chosen so that the exact solution to the boundary value problem (3.13) is the plane wave solution $u(x, y) = e^{i(k_1 x + k_2 y)}$, with the coefficients chosen to be $k_1 = 20$ and $k_2 = 1$. In Figure 3.1 the accuracy of the real components of the spectral, finite and optimal scheme solutions obtained with 20 linear elements are compared for propagation angles of $\phi = 45^0$ and $\phi = 63.43^0$ relative to the edge Γ_1. The phase lead and lag are evident and correspond to numerical approximations obtained using the finite element and spectral element schemes respectively. Moreover, the phase accuracy of the numerical approximation obtained using the optimal scheme is noticeably better than that of finite element and spectral element schemes. In Figure 3.2, we show the effect of increasing the number of elements in each direction with the same propagation angles as used in Figure 3.1. It is clear that with 30 linear elements the numerical approximations obtained using the finite element and spectral element schemes converge to the exact solution but phase lead and phase lag are still prominent whilst the numerical approximation corresponding to the optimal scheme is virtually completely resolved.

3.2.5 Extension to quadratic elements

Using similar arguments to those used for first order elements, we obtain the following expression for the discrete wavenumber of the blended scheme for quadratic

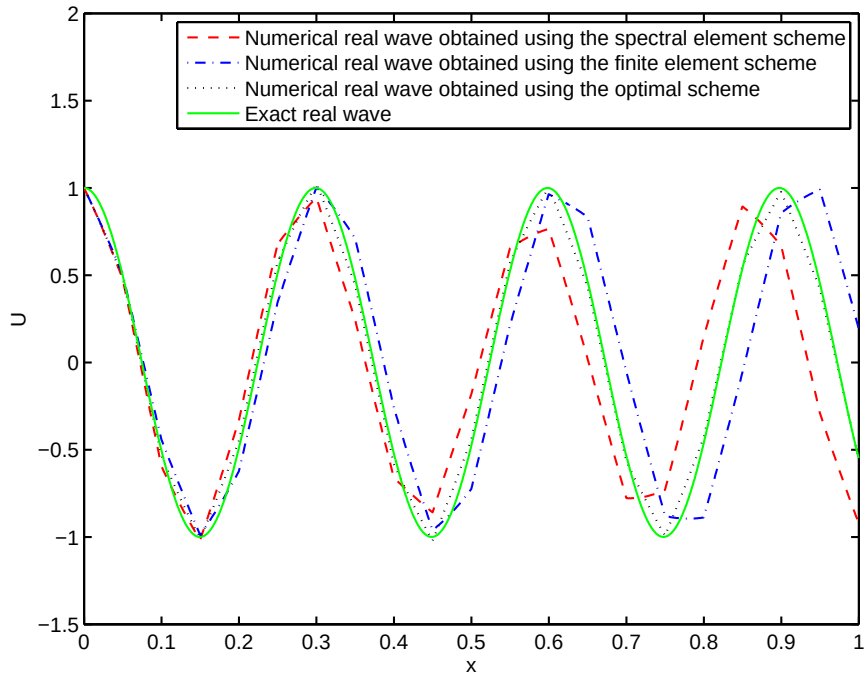

(a) $\phi = 45^o$

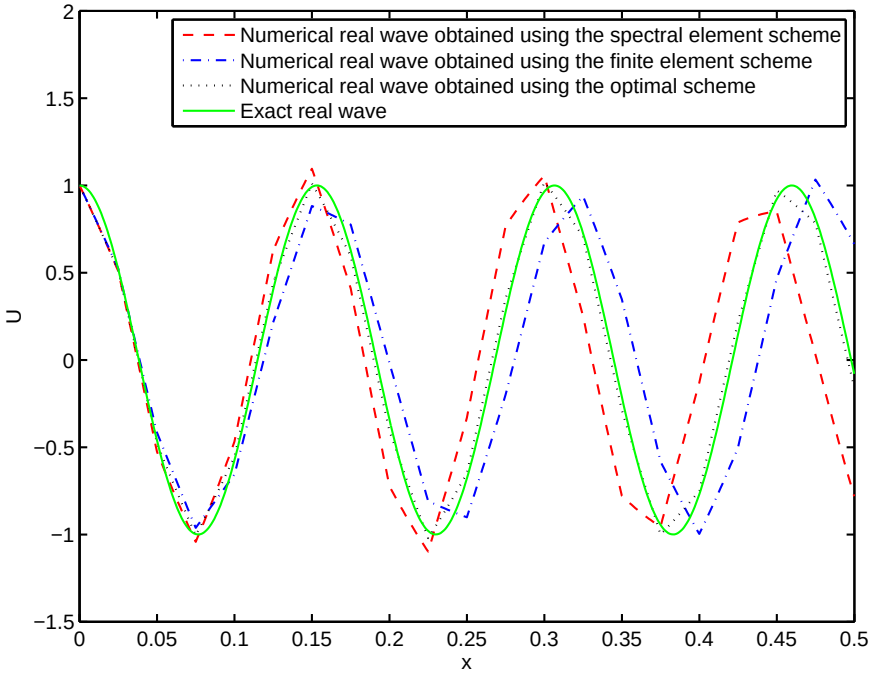

(b) $\phi = 63^o$

Figure 3.1: Numerical approximations of the solution with linear spectral, finite and optimal schemes to equation (3.13) using $kh = 1$ along the directions ϕ relative to the x-axis.

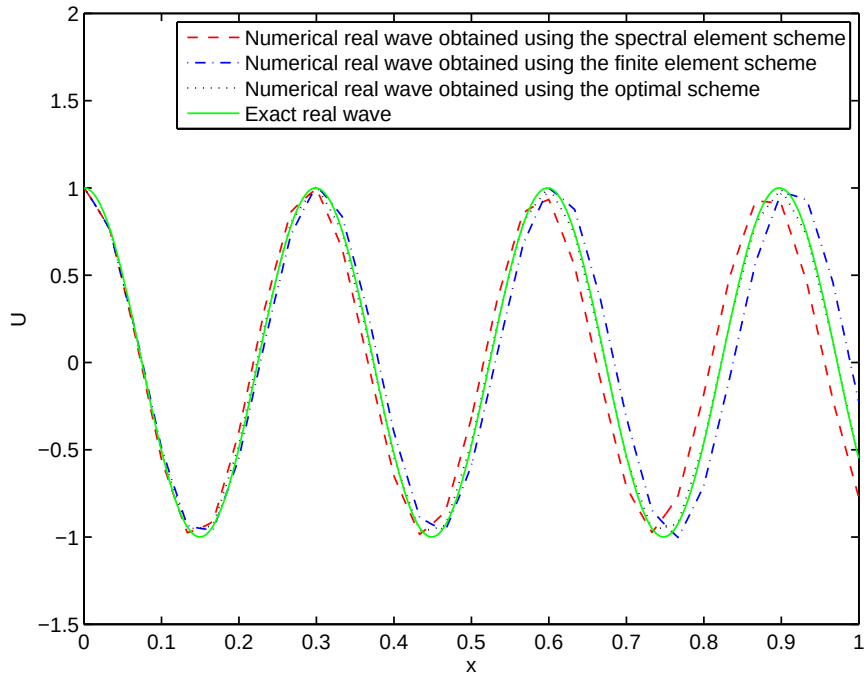

(a) $\phi = 45^o$

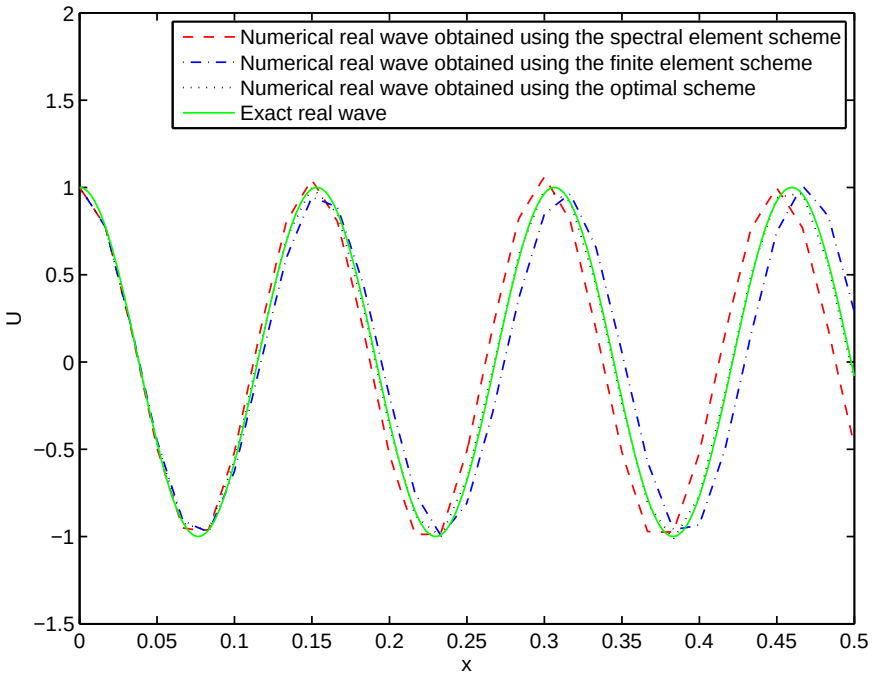

(b) $\phi = 63^o$

Figure 3.2: Numerical approximations of the solution with linear spectral, finite and optimal schemes to equation (3.13) using $kh = 0.67$ along the directions ϕ relative to the x-axis.

elements

$$\mu_\tau^{(2)} h = \omega h + \frac{3\tau - 2}{2880}(\omega h)^5 + \frac{63\tau^2 - 126\tau + 88}{2419200}(\omega h)^7 + \cdots .$$

For $\tau = 0$ and $\tau = 1$, the above expression reduces to the ones obtained for finite element [1] and spectral element [5] schemes. The choice $\tau = 2/3$ means the first term of the above expression vanishes and gives two additional orders of accuracy in the phase compared with the standard schemes. Furthermore, the absolute value of the coefficient of the leading term with the optimum value of τ is decreased by factors of 50 and 25 compared to the leading coefficient obtained with the finite element and spectral element schemes respectively.

We can extend the scheme to higher numbers of spatial dimensions in precisely the same way as we described earlier for linear elements, provided that a suitable non-standard quadrature rule can be identified. One obtains the optimally blended scheme in the case of quadratic elements if the following quadrature rule:

$$\int_{-1}^{1} f(x)dx \approx \frac{1}{3(3+2\tau)}\left\{5f\left(-\sqrt{\frac{1}{5}(3+2\tau)}\right)+4(2+3\tau)f(0)+5f\left(\sqrt{\frac{1}{5}(3+2\tau)}\right)\right\} \tag{3.14}$$

is used to approximate the entries in the mass and stiffness matrices. Moreover, for the optimum value of $\tau = 2/3$, (3.14) reduces to the quadrature rule given in [14]. In Figure 3.3, we show the effect of using piecewise quadratic elements instead of piecewise linear elements with the same propagation angles relative to the bottom edge Γ_1. As expected, the numerical approximations corresponding to the finite element and spectral element schemes are respectively leading and lagging even with quadratic elements but again the optimal scheme performs much better even when kh is relatively large. The results obtained by reducing the size of the elements are given in Figure 3.4.

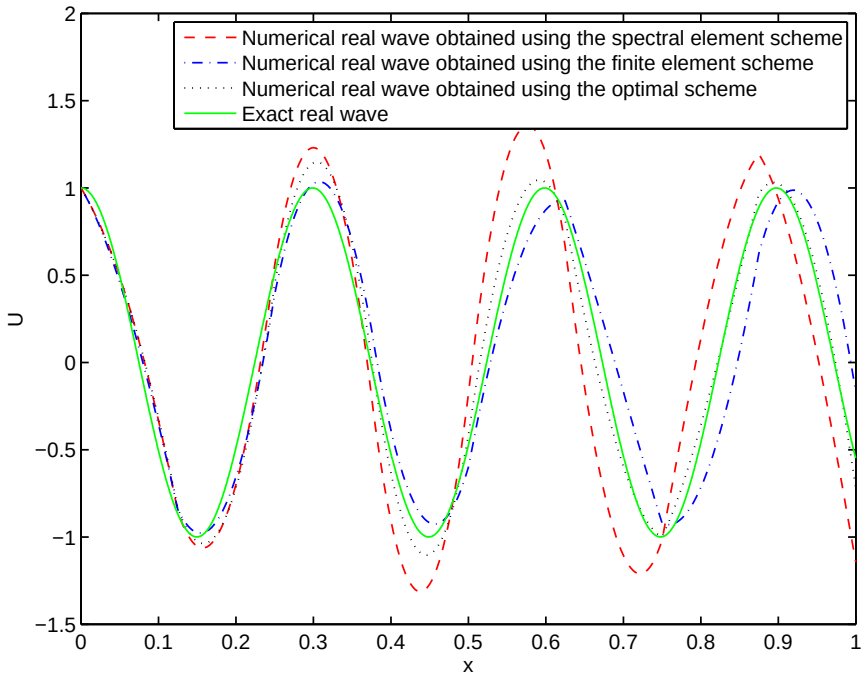

(a) $\phi = 45^o$

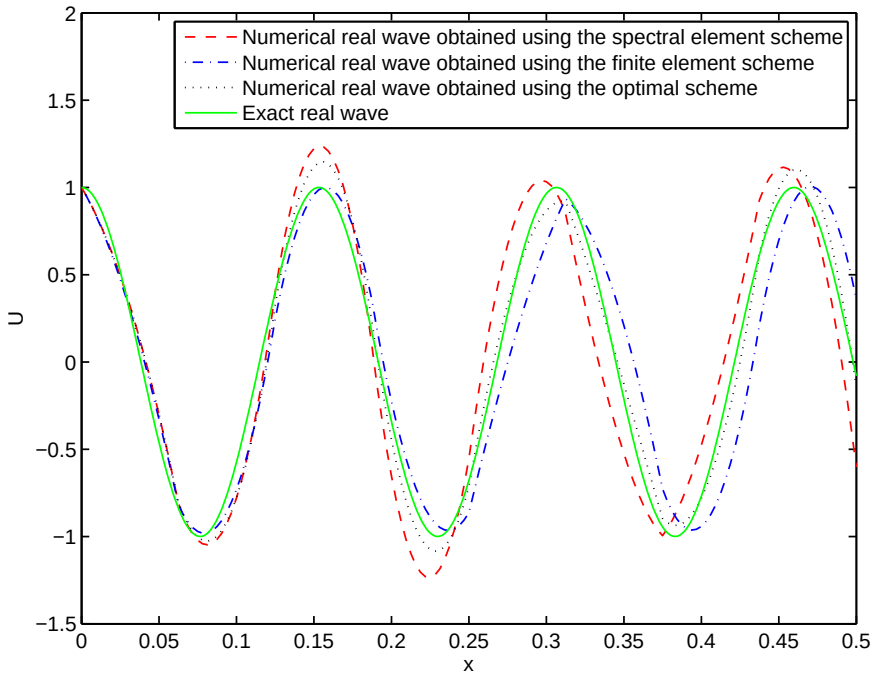

(b) $\phi = 63^o$

Figure 3.3: Numerical approximations of the solution with quadratic spectral, finite and optimal schemes to equation (3.13) using $kh = 2.5$ along the directions ϕ relative to the x-axis.

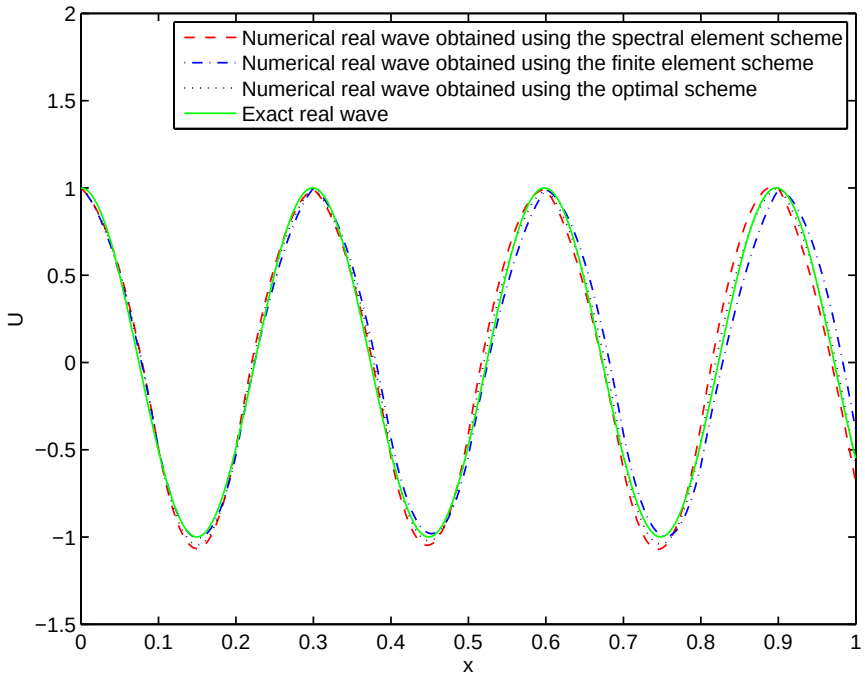

(a) $\phi = 45^o$

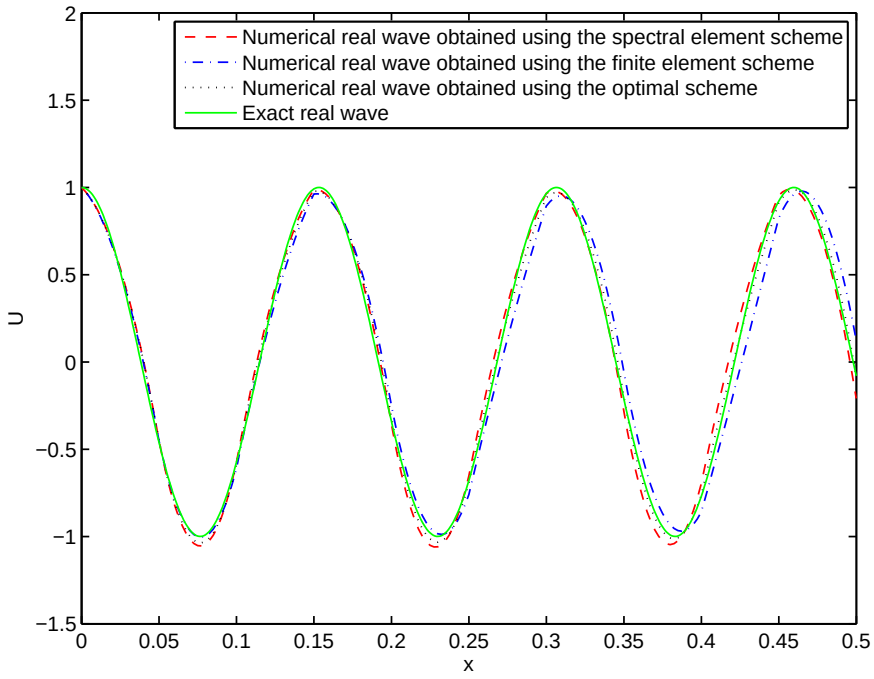

(b) $\phi = 63^o$

Figure 3.4: Numerical approximations of the solution with quadratic spectral, finite and optimal schemes to equation (3.13) using $kh = 2$ along the directions relative to the x-axis.

3.2.6 Extension to cubic elements

Turning to the case of cubic elements, we have the following expression for the discrete wavenumber for the blended scheme

$$\mu_\tau^{(3)} h = \omega h + \frac{4\tau - 3}{604800}(\omega h)^7 + \frac{4\tau^2 - 15\tau + 11}{63504000}(\omega h)^9 + \cdots$$

where the first term vanishes corresponding to the optimum value of the blending parameter $\tau = 3/4$ and we again observe that two additional orders of accuracy are achieved.

Once again, we can extend the scheme to arbitrary order elements provided a suitable quadrature rule is available. For cubic (and higher order) elements, no such rule seems to be known in the literature. However, we may use the following new quadrature rule (which is a special case of Theorem 3.2.1)

$$\int_{-1}^{1} f(x)dx \approx \frac{7840}{\sqrt{681}} \left\{ \frac{(f(-\zeta_+^\tau) + f(\zeta_+^\tau))}{(39 + \sqrt{681})(\sqrt{681} - 3)} + \frac{(f(-\zeta_-^\tau) + f(\zeta_-^\tau))}{(39 - \sqrt{681})(3 + \sqrt{681})} \right\} \quad (3.15)$$

where $\zeta_\pm^\tau = \sqrt{2730 \pm 70\sqrt{681}}/70$, to approximate entries in the stiffness and mass matrices which gives us the optimally blended scheme in the case of cubic elements. The numerical approximations obtained with piecewise cubic elements are shown in Figures 3.5 and 3.6 for four and five cubic elements in each direction and once again the optimal scheme performs noticeably better compared to the finite element and spectral element schemes.

3.2.7 Extension to arbitrary order elements

The question naturally arises of how the above results extend to elements of arbitrary order. In Theorem 3.3.2, we show that for elements of order $p \in \mathbb{N}$, the

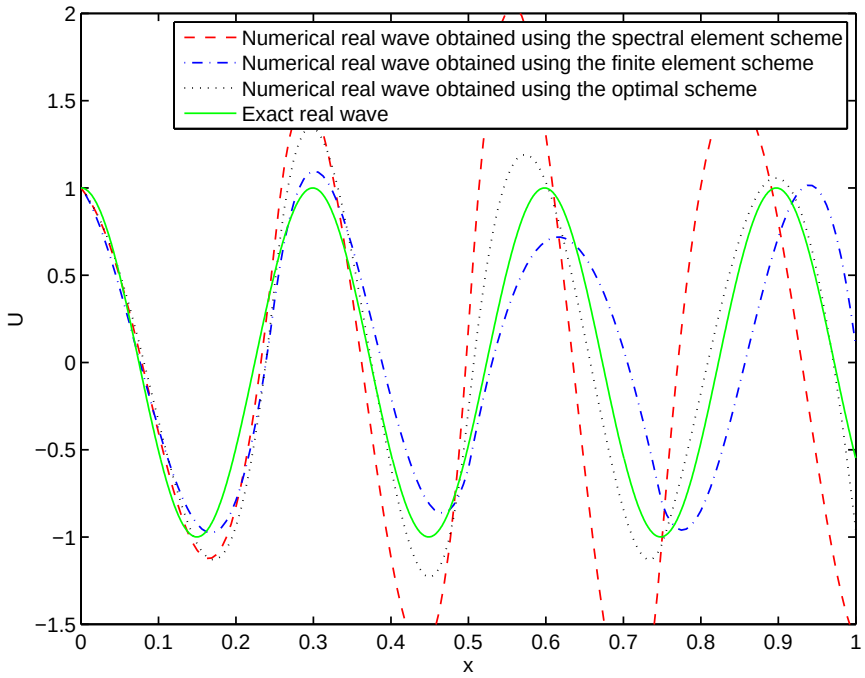

(a) $\phi = 45^o$

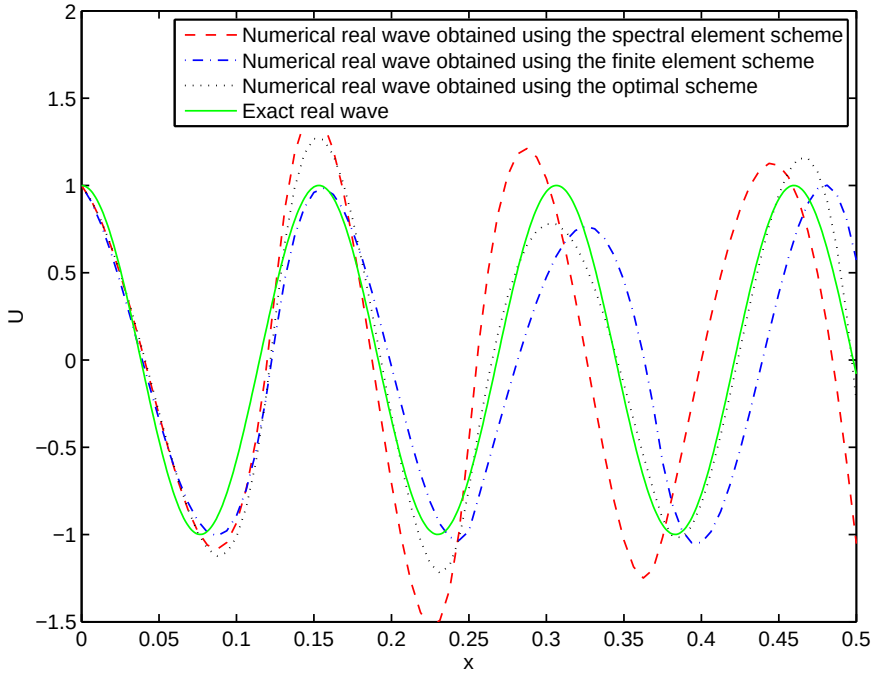

(b) $\phi = 63^o$

Figure 3.5: Numerical approximations of the solution with cubic spectral, finite and optimal schemes to equation (3.13) using $kh = 5$ along the directions ϕ relative to the x-axis.

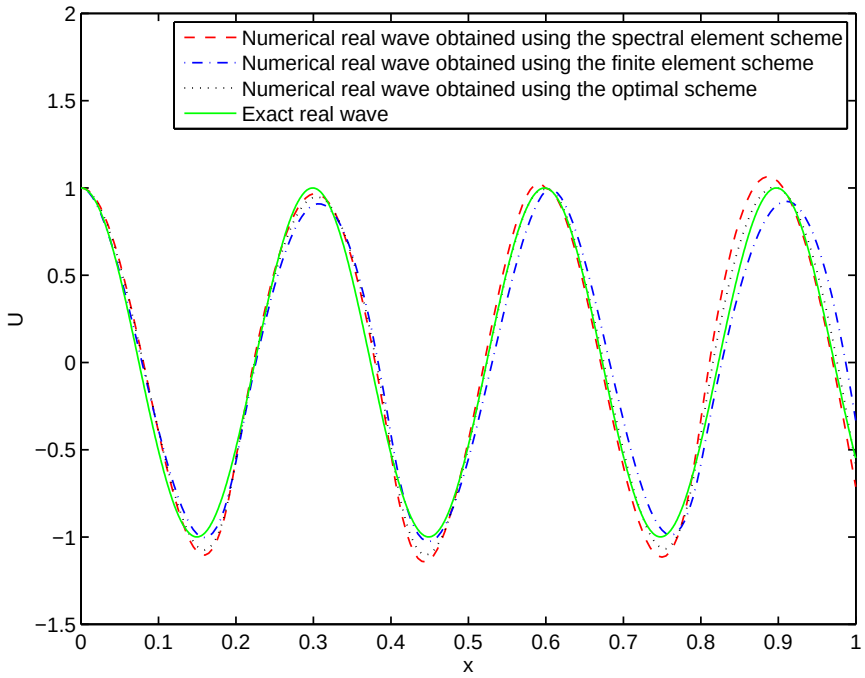

(a) $\phi = 45^o$

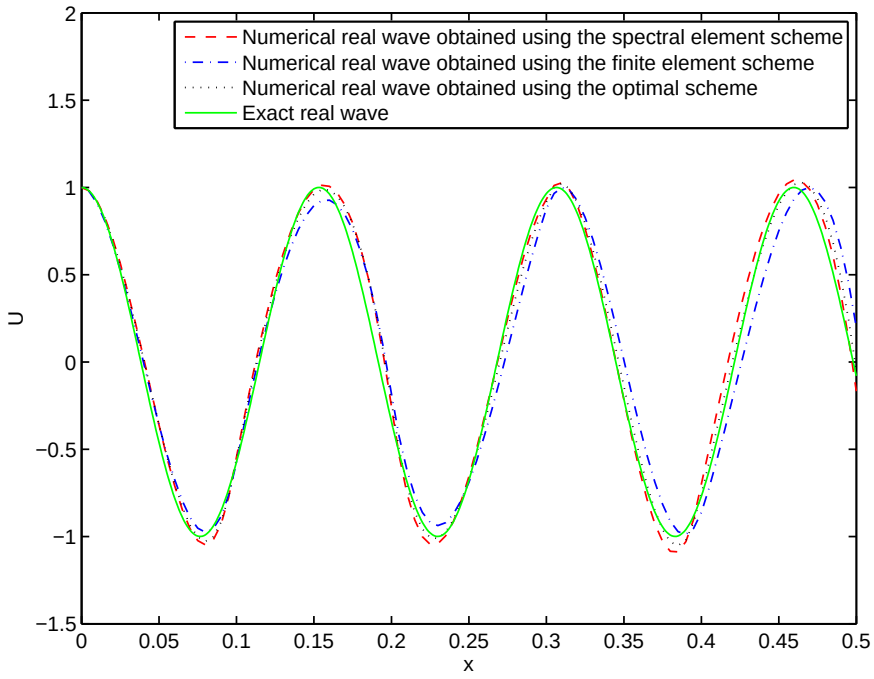

(b) $\phi = 63^o$

Figure 3.6: Numerical approximations of the solution with cubic spectral, finite and optimal schemes to equation (3.13) using $kh = 4$ along the directions ϕ relative to the x-axis.

discrete wavenumber for the blended scheme is given by

$$\mu_\tau^{(p)} h = \omega h + \frac{1}{2}\left[\frac{p!}{(2p)!}\right]^2 \left[\tau\left(1+\frac{1}{p}\right)-1\right]\frac{(\omega h)^{2p+1}}{2p+1} + \frac{1}{2}\left[\frac{(p+1)!}{(2p+2)!}\right]^2 \frac{(\omega h)^{2p+3}}{2p+3} C_\tau^{(p)} + \mathcal{O}(\omega h)^{2p+5}$$

where $C_\tau^{(p)}$ is defined in Theorem 3.3.2. In the case $\tau = 0$, this result agrees with Theorem 3.2 in [1] whilst in the case $\tau = 1$, we obtain the result given in Theorem 2.4.2 of the previous chapter. One immediate consequence of this new result is that the optimal blending parameter is given by $\tau = \dfrac{p}{p+1}$. With this choice, we obtain

$$\mu_\tau^{(p)} h = \omega h + \frac{1}{2}\left[\frac{(p+1)!}{(2p+2)!}\right]^2 \frac{(\omega h)^{2p+3}}{2p+3} C_\tau^{(p)} + \mathcal{O}(\omega h)^{2p+5}$$

showing that in general we obtain two additional orders of accuracy with the optimal choice of blending parameter τ. Moreover, in Corollary 3.3.3, we show that the absolute value of the leading coefficient in the error $\mu_\tau^{(p)} h - \omega h$ is considerably reduced by the use of blending. The proof of these statements forms the topic of the Section 3.4.

3.2.8 Non-standard quadrature rule for elements of arbitrary order

The use of such non-standard quadrature rules in the *implementation* of the optimally blended scheme is rather attractive in practice and provides a simple way to extend the blended schemes to higher number of spatial dimensions. More specifically it means that *an existing, standard finite element code can be adapted to implement the optimally blended scheme merely by replacing the usual Gaussian quadrature rule by the non-standard quadrature rule.* Unfortunately, the existence of suitable non-standard quadrature rules for general *p-th* order elements does not seem to be available in the existing literature.

If we denote the bilinear form for the finite element and spectral element schemes by $B(\cdot,\cdot)$ and $\widetilde{B}(\cdot,\cdot)$ respectively, then the bilinear form for the blended scheme is given by

$$B_\tau(u,v) = (1-\tau)B(u,v) + \tau\widetilde{B}(u,v) \tag{3.16}$$

for piecewise polynomials u and v. The difference between the bilinear forms for the finite element and spectral element schemes lies in the fact that the spectral element scheme uses the Gauss-Lobatto quadrature rule which we denote by $\mathcal{Q}^{(p)}$ to evaluate the integrals, whilst the finite element scheme evaluates (via Gauss-Legendre quadrature) the integrals exactly. Consequently, the bilinear form for the blended scheme (3.16) should be based on a quadrature rule $\mathcal{Q}_\tau^{(p)}$ for which

$$\mathcal{Q}_\tau^{(p)}(f) = (1-\tau)\int_{-1}^{1} f(x)dx + \tau\mathcal{Q}^{(p)}(f) \quad \forall f \in \mathbb{P}_{2p+1}.$$

The following result constitutes the extension of the non-standard quadrature rules to elements of arbitrary order:

Theorem 3.2.1. *Let $\tau \in [0,1)$ be fixed, and let $\mathcal{Q}_\tau^{(p)}$ be a $(p+1)$-point quadrature rule with nodes $\{\zeta_i^\tau\}_{i=0}^p$ chosen as the zeros of $L_{p+1} - \tau L_{p-1}$, where L_{p+1} and L_{p-1} are the Legendre polynomials of degrees $p+1$ and $p-1$ respectively, with weights given by*

$$w_\ell^\tau = \frac{2[p(1+\tau)+\tau]}{p(p+1)L_p(\zeta_\ell^\tau)[L'_{p+1}(\zeta_\ell^\tau) - \tau L'_{p-1}(\zeta_\ell^\tau)]}, \ \forall \ell = 0,1,\ldots,p. \tag{3.17}$$

Then, the weights are positive, and the nodes are distinct and contained in $(-1,1)$. Furthermore, $\mathcal{Q}_\tau^{(p)}$ satisfies the following identity

$$\mathcal{Q}_\tau^{(p)}(f) = (1-\tau)\int_{-1}^{1} f(x)dx + \tau\mathcal{Q}^{(p)}(f) \quad \forall f \in \mathbb{P}_{2p+1} \tag{3.18}$$

where $\mathcal{Q}^{(p)}$ is the $(p+1)$-point Gauss-Legendre-Lobatto quadrature rule defined in (Chapter 2, eq.(2.8)). Consequently, $\mathcal{Q}_\tau^{(p)}$ is exact for all $f \in \mathbb{P}_{2p-1}$.

The proof of this result is given in Section 3.4. Observe that for $\tau = 0$ and $\tau = 1$, $\mathcal{Q}_\tau^{(p)}$ reduces to the standard Gauss-Legendre and Gauss-Legendre-Lobatto rules respectively.

In Table 3.1, zeros and corresponding weights of the optimal quadrature rule $\mathcal{Q}_\tau^{(p)}$ are given for the optimum value of the blending parameter $\tau = p/(p+1)$. It is a simple matter to compute the higher order rules using the expressions given in Theorem 3.2.1.

Order p	Abscissas ζ_ℓ^τ	Weights w_ℓ^τ
1	± 0.8164965809	1
2	0	1.2307692308
	± 0.9309493363	0.3846153846
3	± 0.9643352759	0.1998260144
	± 0.4293520583	0.8001739855
4	0	0.6937669377
	± 0.9783156780	0.1217872771
	± 0.6387313983	0.5313292541

Table 3.1: Nodes and corresponding weights of the optimal quadrature rule $\mathcal{Q}_\tau^{(p)}$ for $\tau = p/(p+1)$, and orders $p = 1, \ldots, 4$.

The quadrature rule $\mathcal{Q}_\tau^{(p)}$ can then be used to extend the one dimensional scheme to higher dimensions for elements of arbitrary order as described in Section 3.2 for first order elements. Using the same arguments used there leads to the conclusion that the discrete frequency ω_{hp} for the resulting scheme satisfies

$$\omega_{hp}^2 = \left(\mu_\tau^{(p)}(\omega_x; h)\right)^2 + \left(\mu_\tau^{(p)}(\omega_y; h)\right)^2 + \left(\mu_\tau^{(p)}(\omega_z; h)\right)^2$$

where $\omega_x^2 + \omega_y^2 + \omega_z^2 = \omega^2$. Thanks to (3.20) given in Theorem 3.3.1, we obtain

$$\omega_{hp}^2 = \omega^2 + \left[\frac{p!}{(2p)!}\right]^2 \left[\tau\left(1 + \frac{1}{p}\right) - 1\right] \frac{h^{2p}}{2p+1}[\omega_x^{2p+2} + \omega_y^{2p+2} + \omega_z^{2p+2}] + \mathcal{O}(\omega^{2p+4})$$

which is valid for general τ and for all $p \geq 2$. For the optimal choice of $\tau = p/(p+1)$, using Corollary 3.3.3, we have

$$\omega_{hp}^2 = \omega^2 + \frac{8}{(2p-1)} \left[\frac{(p+1)!}{(2p+2)!}\right]^2 \frac{h^{2p+2}}{2p+3}[\omega_x^{2p+4} + \omega_y^{2p+4} + \omega_z^{2p+4}] + \mathcal{O}(\omega^{2p+6}).$$

3.3 Analysis of dispersion for elements of arbitrary order

Our first result gives the discrete dispersion relation for blending of spectral-finite element approximation for elements of arbitrary order $p \in \mathbb{N}$, with blending parameter $\tau \in [0, 1]$; and generalises the particular cases given in Section 3.2. The following theorems are proved in Section 3.4:

Theorem 3.3.1. *Let $\kappa > 0$ and consider the sequences $\{a_p\}_{p=1}^\infty$ and $\{b_p\}_{p=1}^\infty$ defined by the recursion relations*

$$\left.\begin{aligned} a_{p+1} &= -\frac{2p+1}{\kappa} b_p + a_{p-1} \\ b_{p+1} &= \frac{2p+1}{\kappa} a_p + b_{p-1} \end{aligned}\right\} \tag{3.19}$$

for $p \in \mathbb{N}$ with $a_0 = 1$, $a_1 = 1$, $b_0 = 0$ and $b_1 = 1/\kappa$. Then, the discrete dispersion relation for the optimal scheme of order $p \in \mathbb{N}$ is given by

$$\cos \mu_\tau^{(p)} h = R_\tau^{(p)}(\omega h) = (-1)^p \frac{\Lambda_1^{(p)}(\kappa) + \Lambda_2^{(p)}(\kappa)}{\Lambda_1^{(p)}(\kappa) - \Lambda_2^{(p)}(\kappa)} \tag{3.20}$$

where $\kappa = \dfrac{\omega h}{2}$ *and*

$$\Lambda_1^{(p)}(\kappa) = a_p \left(\kappa b_{p-1}(\tau(p+1)+p) + p(2p+1)a_p\right)$$

and

$$\Lambda_2^{(p)}(\kappa) = b_p \left(\kappa a_{p-1}(\tau(p+1)+p) - p(2p+1)b_p\right).$$

The sequences $\{a_p\}_{p=1}^{\infty}$ and $\{b_p\}_{p=1}^{\infty}$ originally appeared in Theorem 2.4.1, and are proved in Lemma 2.5.2 of Chapter 2 in the analysis of the pure spectral element scheme. For $\tau = 1$ the above expression (3.20) reduces to the discrete dispersion relation (2.25) obtained in Chapter 2 for spectral element schemes, whilst in the case $\tau = 0$ expression (3.20) gives an alternative form of the discrete dispersion relation (3.2) obtained in [1] for finite element schemes. As pointed out in [1], $R_\tau^{(p)}(\omega h)$ is a rational function of degree $[2p/2p]$ in κ for all $p \in \mathbb{N}$ which, in the case of the pure finite element method ($\tau = 0$), corresponds to certain types of Padé approximants.

The following theorem proved in Section 3.4 gives the leading term for the error in the discrete dispersion relation for the blended scheme with parameter $\tau \in [0, 1]$:

Theorem 3.3.2. *Let $p \geq 2$ and $\tau \in [0, 1]$. Then, the error in the discrete dispersion relation* (3.20) *is given by*

$$\begin{aligned}\cos \mu_\tau^{(p)} h - \cos \omega h = {} & \frac{1}{2}\left[\frac{p!}{(2p)!}\right]^2 \left[1 - \tau\left(1 + \frac{1}{p}\right)\right] \frac{(\omega h)^{2p+2}}{2p+1} \\ & - \frac{1}{2}\left[\frac{(p+1)!}{(2p+2)!}\right]^2 \frac{(\omega h)^{2p+4}}{2p+3} C_\tau^{(p)} + \mathcal{O}(\omega h)^{2p+6}\end{aligned}$$

or, if ωh is sufficiently small,

$$\mu_\tau^{(p)} h - \omega h = \frac{1}{2}\left[\frac{p!}{(2p)!}\right]^2 \left[\tau\left(1+\frac{1}{p}\right)-1\right]\frac{(\omega h)^{2p+1}}{2p+1} + \frac{1}{2}\left[\frac{(p+1)!}{(2p+2)!}\right]^2 \frac{(\omega h)^{2p+3}}{2p+3} C_\tau^{(p)} + \mathcal{O}(\omega h)^{2p+5} \tag{3.21}$$

where

$$C_\tau^{(p)} = \tau^2 \frac{(2p+3)}{(2p-1)}\left(1+\frac{1}{p}\right)^2 - \tau(2p+3)\left(1+\frac{1}{p}\right) + 2\frac{2p^2+p+1}{2p-1}.$$

As expected, when $\tau = 0$ or $\tau = 1$ the above result reduces to spectral and finite element schemes respectively. More interestingly, (3.21) indicates that the blending term in the error can be eliminated by choosing $\tau = p/(p+1)$ resulting in an additional two orders of accuracy in the discrete dispersion relation:

Corollary 3.3.3. *Let $p \geq 2$. For $\tau = p/(p+1)$, the error in the discrete dispersion relation* (3.20) *is given by*

$$\mu_\tau^{(p)} h - \omega h = \frac{4}{(2p-1)}\left[\frac{(p+1)!}{(2p+2)!}\right]^2 \frac{(\omega h)^{2p+3}}{2p+3} + \mathcal{O}\left(\omega h\right)^{2p+5}. \tag{3.22}$$

Proof. Substitute $\tau = p/(p+1)$ in (3.21) and applying straightforward manipulations, we obtain (3.22) as required. □

In Table 3.2 we give closed form expressions for the rational function $R_\tau^{(p)}(\omega h)$ obtained from Theorem 3.3.1 along with the leading terms in the error for $\omega h \ll 1$ obtained from Theorem 3.3.2 for orders p from 1 up to 3 and $\tau \in [0,1]$. Moreover, the error in the leading term for the optimum value of τ i.e. $\tau = p/(p+1)$ obtained from Corollary 3.3.3 is given for small wavenumber limit.

We make the following observations regarding the optimally blended scheme:

1. The leading term is two orders more accurate compared with the standard spectral and finite element schemes, see [1, 5, 35, 60] where the leading term in the expressions was accurate to order $\mathcal{O}(\omega h)^{2p}$. This is illustrated in Figure 3.7 where

Order p	$R_\tau^{(p)}(\omega h)$
1	$\dfrac{(\omega h)^2(\tau+2)-6}{(\omega h)^2(\tau-1)-6}$
2	$\dfrac{(\omega h)^4(2\tau+3)-2(\omega h)^2(3\tau+52)+240}{(\omega h)^4(1-\tau)-2(\omega h)^2(3\tau-8)+240}$
3	$\dfrac{(\omega h)^6(3\tau+4)-4(\omega h)^4(26\tau+135)+240(\omega h)^2(\tau+48)-25200}{(\omega h)^6(\tau-1)+2(\omega h)^4(8\tau-15)+120(\omega h)^2(2\tau-9)-25200}$

Order p	$\mu_\tau^{(p)}h-\omega h$	$\mu_\tau^{(p)}h, \tau=p/(p+1)$
1	$\dfrac{(\omega h)^3(2\tau-1)}{24}+\dfrac{(\omega h)^5(20\tau^2-20\tau+9)}{1920}$	$\dfrac{(\omega h)^5}{480}$
2	$\dfrac{(\omega h)^5(3\tau-2)}{2880}+\dfrac{(\omega h)^7(63\tau^2-126\tau+88)}{2419200}$	$\dfrac{(\omega h)^7}{75600}$
3	$\dfrac{(\omega h)^7(4\tau-3)}{604800}+\dfrac{(\omega h)^9(4\tau^2-15\tau+11)}{63504000}$	$\dfrac{(\omega h)^9}{31752000}$

Table 3.2: The discrete dispersion relation $R_\tau^{(p)}(\omega h)=\cos\mu_\tau^{(p)}h$ for order p approximation given in Theorem 3.3.1. We also indicate the leading term in the series expansion for the error when $\omega h \ll 1$ for both general $\tau\in[0,1]$ (see Theorem 3.3.2) and $\tau=p/(p+1)$ (see Corollary 3.3.3) for $p\geq 2$.

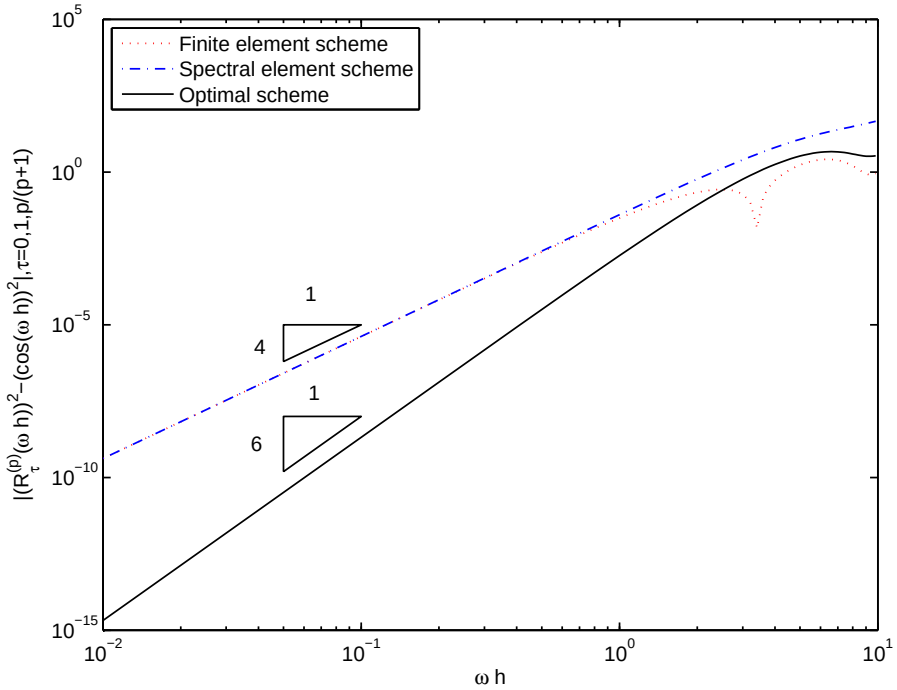
Finite element scheme
Spectral element scheme
Optimal scheme
1
4
1
6
ω h
$|(R_\tau^{(p)}(\omega h))^2-(\cos(\omega h))^2|, \tau=0.1, p/(p+1)$

(a) p = 1

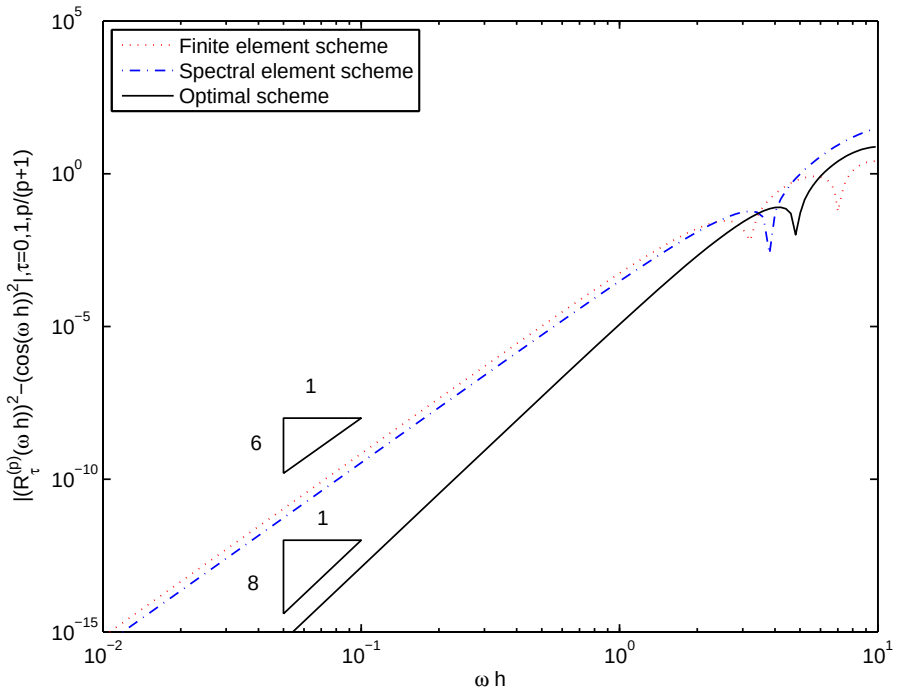
Finite element scheme
Spectral element scheme
Optimal scheme
1
6
1
8
ω h
$|(R_\tau^{(p)}(\omega h))^2-(\cos(\omega h))^2|, \tau=0.1, p/(p+1)$

(b) p = 2

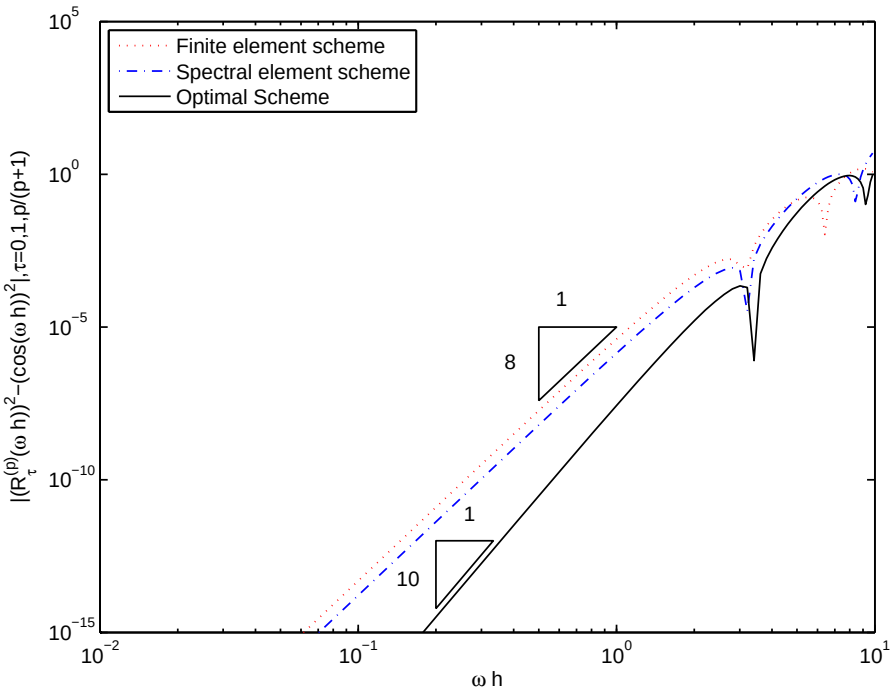

(c) p = 3

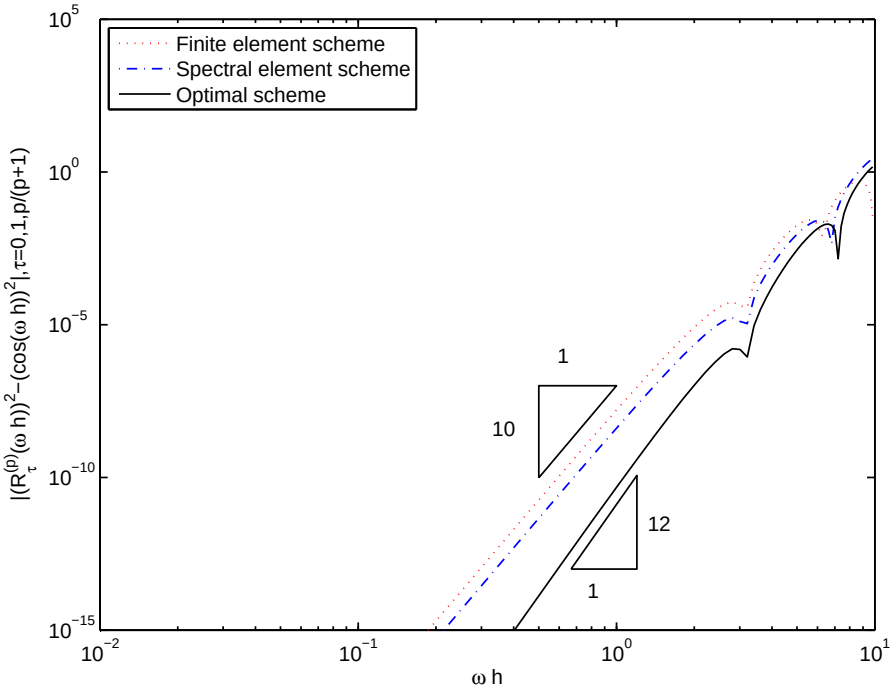

(d) p = 4

Figure 3.7: Error in discrete dispersion relations of orders $p = 1$ to 4 versus wavenumber for finite element, spectral element and optimally blended schemes. For p-th order finite element and spectral element schemes the slope of the lines is $2p + 2$ where as for optimal scheme the slope of the line is $2p + 4$.

it is observed that for a p-th order scheme the slope of the lines with spectral element and finite element schemes is $2p+2$ whereas with the optimal scheme the slope is $2p+4$.

2. The coefficient of the leading term in the error obtained with the blended scheme for the optimum value of τ is $-2/(4p^2-1)(2p+3)$ and $2p/(4p^2-1)(2p+3)$ times better compared with the leading terms in the error obtained with finite [1] and spectral [5] element schemes respectively. This is also illustrated in Figure 3.7 where it is observed that the absolute value of the error for the optimal scheme is superior to that of the standard schemes even for modest values of ωh.

3. Figure 3.8 shows the *frequency spectra* of the finite element, spectral element and optimally blended scheme for elements of order $p = 1, \ldots, 4$. In particular, one can see the so-called *cut-off frequencies* of the schemes corresponding to the values of ωh at which the magnitude of the rational function $R_\tau^{(p)}(\omega h)$ becomes greater than unity. For such frequencies, the discrete wavenumber $\mu_\tau^{(p)}$ is imaginary and the discrete waves cease to propagate. These frequencies can be computed explicitly for the first order elements $p = 1$ by considering when the inequality $|R_\tau^{(p)}(\omega h)| > 1$ is satisfied. Inserting the expression for $R_\tau^{(p)}(\omega h)$ from Table 3.2 reveals that the inequality holds for ωh greater than

$$\omega h = \sqrt{\frac{12}{1+2\tau}}. \tag{3.23}$$

For the finite element scheme ($\tau = 0$) and spectral element scheme ($\tau = 1$) we obtain cut-off frequencies of $2\sqrt{3}$ and 2 respectively, in agreement with the results presented in [60]. For the optimally blended scheme, the cut-off frequency is given by $\sqrt{6}$. These frequencies are indicated in Figure 3.8(a). All of the schemes corresponding to $p = 1$ elements fail to admit propagating waves for higher frequencies and thus have single *stopping band* extending to infinity. In general, the schemes based on elements of order p have p stopping bands, as shown in Figure 3.8 (b)-(d).

The so-called *spatial resolution limit* [60] is defined to be number of elements per wavelength corresponding to the cut-off frequency. The spatial resolution limit for $p = 1$ elements is obtained by inserting (3.23) into (3.5) to obtain

$$\cos \mu_\tau^{(1)} h = R_\tau^{(1)} \left(\sqrt{\frac{12}{1+2\tau}} \right) = -1$$

or

$$\mu_\tau^{(1)} h = \pi$$

giving a spatial resolution limit for the $p = 1$ elements of

$$\frac{\lambda}{h} = \frac{2\pi}{\mu_\tau^{(1)} h} = \frac{2\pi}{\pi} = 2.$$

Examination of Figure 3.8 (b)-(d) reveals that for a p-th order scheme, the spatial resolution limit is given by $2/p$ elements per wavelength in agreement with the observation of [60].

3.4 Proofs of the results

This section provides the proofs of general results for the error in the discrete dispersion relation for the blended scheme.

3.4.1 Basic polynomials

Let $p \in \mathbb{N}$ be given and $\tau \in [0, 1]$ be a parameter to be determined. Define the bilinear form

$$\hat{B}_\tau(v, w) = (1 - \tau) \int_{-1}^{1} (v'w' - \kappa^2 vw) dx + \tau \mathcal{Q}^{(p)}(v'w' - \kappa^2 vw) \tag{3.24}$$

where $\mathcal{Q}^{(p)}$ is the $(p + 1)$ point Gauss-Lobatto quadrature rule and $\kappa > 0$ is a constant. If $v, w \in \mathbb{P}_p$ then $v'w' \in \mathbb{P}_{2p-2}$ and the quadrature rule $\mathcal{Q}^{(p)}$ integrates

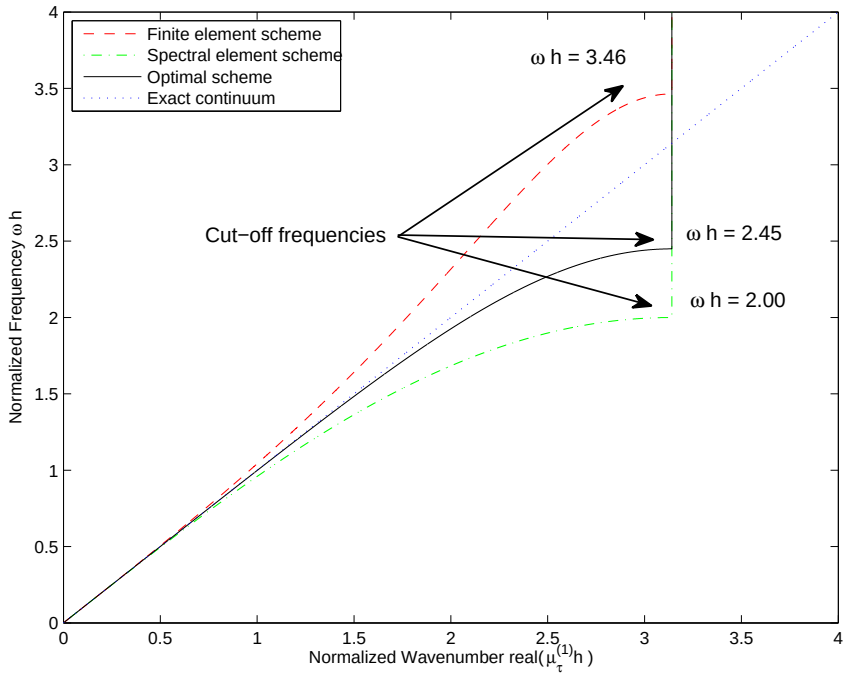
Finite element scheme
Spectral element scheme
Optimal scheme
Exact continuum
ω h = 3.46
Cut−off frequencies
ω h = 2.45
ω h = 2.00
Normalized Frequencey ω h
Normalized Wavenumber real(μ(1)τ h)

(a) p=1

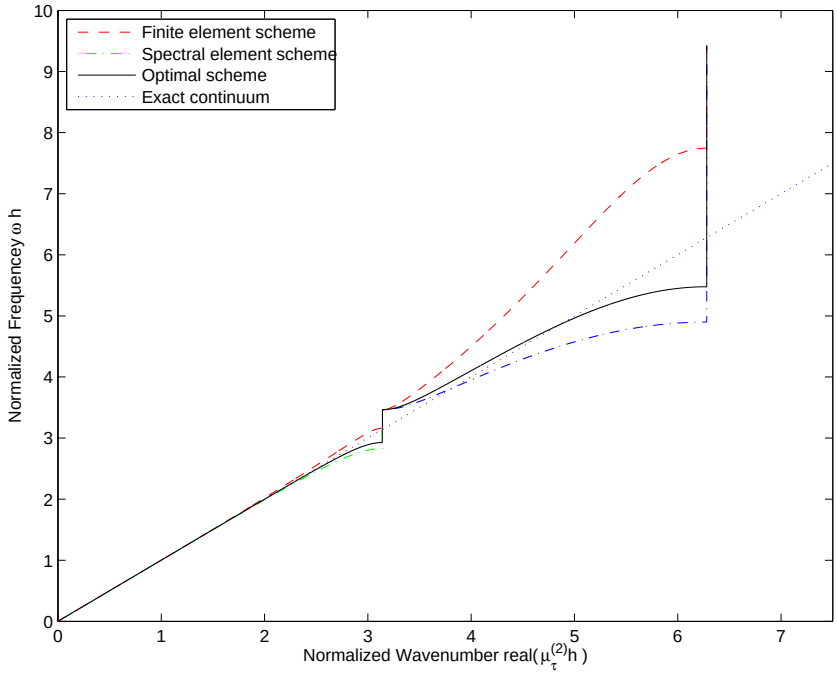
Finite element scheme
Spectral element scheme
Optimal scheme
Exact continuum
Normalized Frequencey ω h
Normalized Wavenumber real(μ(2)τ h)

(b) p=2

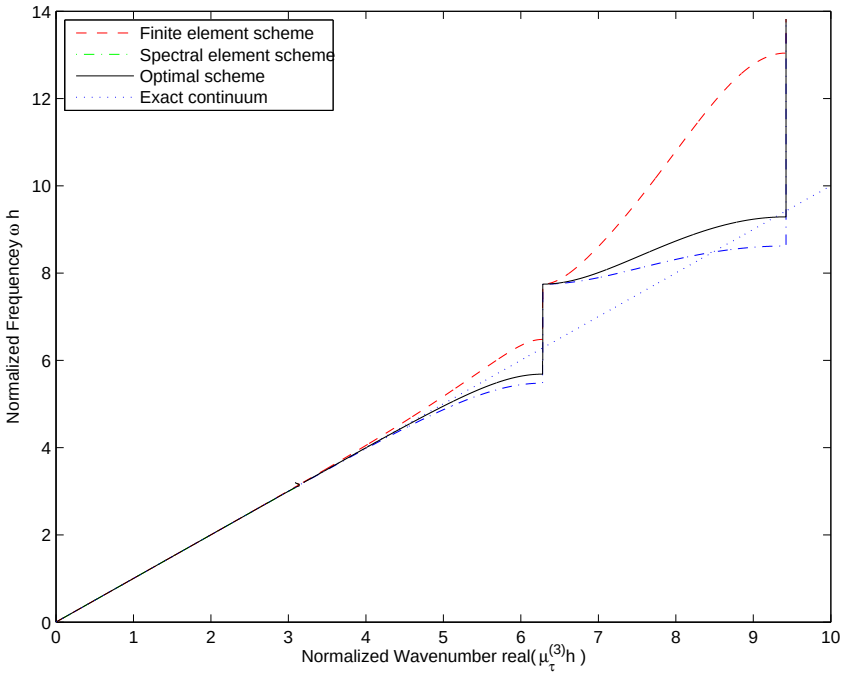

(c) p=3

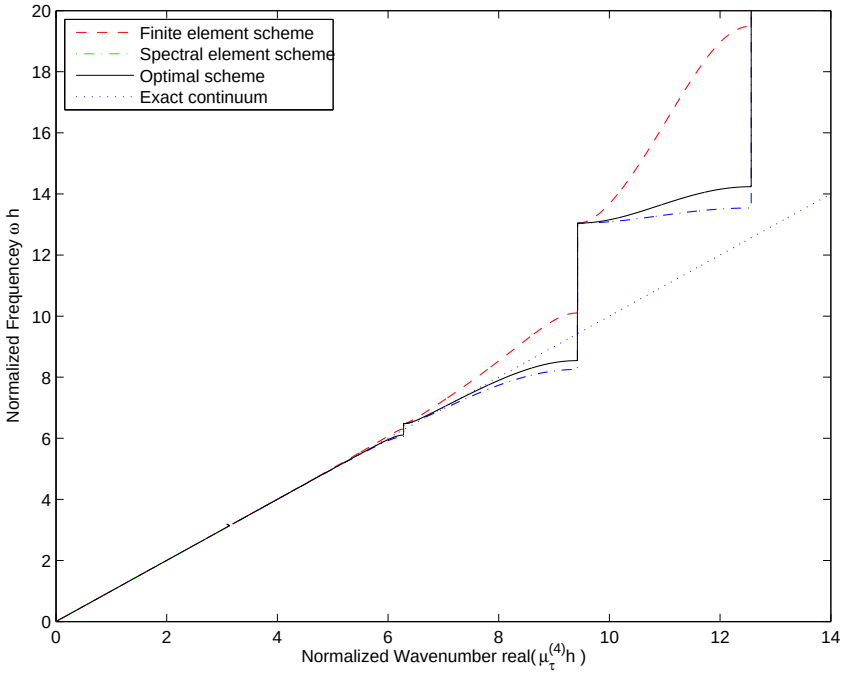

(d) p=4

Figure 3.8: Frequency spectra of the one dimensional finite element, spectral element and optimally blended schemes for elements of order $p = 1, \ldots, 4$.

this product exactly. Hence, if $v, w \in \mathbb{P}_p$ then

$$\hat{B}_\tau(v,w) = \int_{-1}^{1} v'w'dx - \kappa^2 \left\{ (1-\tau) \int_{-1}^{1} vwdx + \tau \mathcal{Q}^{(p)}(vw) \right\}. \tag{3.25}$$

We reconsider basic polynomials $\Phi^p, \Psi^p \in \mathbb{P}_p, \forall p \in \mathbb{N}$ defined in Chapter 2:

$$\Phi^p(1) = 1, \;\; \Phi^p(-1) = (-1)^{p+1} : \;\; \hat{B}_\tau(\Phi^p, w) = 0 \quad \forall w \in \mathbb{P}_p \cap H_0^1(-1,1) \tag{3.26}$$

and

$$\Psi^p(1) = 1, \;\; \Psi^p(-1) = (-1)^{p} : \quad \hat{B}_\tau(\Psi^p, w) = 0 \quad \forall w \in \mathbb{P}_p \cap H_0^1(-1,1). \tag{3.27}$$

From (3.26) and considering the parity of Φ^p, we deduce that $\Phi^p \in \mathbb{P}_{p-1}$ for all $p \in \mathbb{N}$. Moreover, $w\Phi^p$ and $w'\Phi'^p \in \mathbb{P}_{2p-1}$, for $w \in \mathbb{P}_p \cap H_0^1(-1,1)$ and it follows that the quadrature rule $\mathcal{Q}^{(p)}$ is exact in (3.24) for $w = \Phi^p$, so that

$$\hat{B}_\tau(\Phi^p, w) = \int_{-1}^{1} \left(\Phi'^p w' - \kappa^2 \Phi^p w \right) dx = 0 \;\; \forall w \in \mathbb{P}_p \cap H_0^1(-1,1).$$

Hence, for Φ^p the bilinear form (3.24) coincides with the bilinear form (**??**) considered in previous chapter and we may therefore quote results for Φ^p directly from Chapter 2. In particular, from Theorem 2.5.1 of Chapter 2, we have

$$\hat{B}_\tau(\Phi^p, \Phi^p) = \hat{B}(\Phi^p, \Phi^p) = -2\kappa \frac{a_p}{b_p}.$$

where sequences $\{a_p\}_{p=1}^{\infty}$ and $\{b_p\}_{p=1}^{\infty}$ originally appeared in Theorem 2.4.1. We shall require the corresponding expression for $\hat{B}_\tau(\Psi^p, \Psi^p)$:

Theorem 3.4.1. *Let $p = 2, 3, 4, \ldots$. Then*

$$\hat{B}_\tau(\Psi^p, \Psi^p) = -2\kappa \frac{pa_{p+1} + \tau(p+1)a_{p-1}}{pb_{p+1} + \tau(p+1)b_{p-1}}, \tag{3.28}$$

where $2\kappa = \omega h$.

Proof. For the duration of this proof the superscript on Ψ^p will be omitted since no confusion is likely to arise. Suppose $w \in \mathbb{P}_{p-1} \cap H_0^1(-1,1)$, then $\Psi w \in \mathbb{P}_{2p-1}$. Using the fact that the quadrature rule in the bilinear form (3.24) is exact for functions belonging to $\mathbb{P}_{2p-1}$, and using definition (3.27) we obtain

$$\int_{-1}^{1} (\Psi'' + \kappa^2 \Psi) w dx = 0, \qquad \forall w \in \mathbb{P}_{p-1} \cap H_0^1(-1,1). \tag{3.29}$$

Now, we can write $F(x) = \Psi''(x) + \kappa^2 \Psi(x) \in \mathbb{P}_p$ in the form

$$\Psi''(x) + \kappa^2 \Psi(x) = \sum_{j=1}^{p+1} \alpha_j L_j'(x) \tag{3.30}$$

where α_j are the scalars and L_j is the Legendre polynomial of degree j. Now inserting $w(x) = (1-x^2)L_\ell'(x)$ for $1 \leq \ell \leq p-2$ together with (3.30) into (3.29), we obtain $\alpha_1 = \alpha_2 = \cdots = \alpha_{p-2} = 0$. Also, parity considerations imply that $\alpha_p = 0$. Hence,

$$F(x) = \Psi''(x) + \kappa^2 \Psi(x) = \alpha_{p+1} L_{p+1}'(x) + \alpha_{p-1} L_{p-1}'(x). \tag{3.31}$$

Now, choosing $w(x) = (1-x^2)L_{p-1}'(x) \in \mathbb{P}_p \cap H_0^1(-1,1)$ in definition (3.27), we get

$$\int_{-1}^{1} F(x) w(x) dx - \kappa^2 \tau \left\{ \int_{-1}^{1} \Psi(x) w(x) dx - \mathcal{Q}^{(p)}(\Psi w) \right\} = 0. \tag{3.32}$$

Also, using (3.31) together with the first term of the last expression gives

$$\int_{-1}^{1} F(x) w(x) dx = \int_{-1}^{1} (1-x^2) \left[\alpha_{p+1} L_{p+1}'(x) L_{p-1}'(x) + \alpha_{p-1} [L_{p-1}'(x)]^2 \right] dx,$$

and then exploiting the orthogonality property of the Legendre polynomials, we obtain

$$\int_{-1}^{1} F(x) w(x) dx = \frac{2p(p-1)}{2p-1} \alpha_{p-1}. \tag{3.33}$$

The error in the Gauss-Lobatto quadrature rule denoted by E is given by

$$E = \int_{-1}^{1} \Psi(x) w(x) dx - \mathcal{Q}^{(p)}(\Psi w) = -\frac{(p+1)p^3 2^{2p+1} [(p-1)!]^4}{(2p+1)[(2p)!]^3} D^{2p}(\Psi w)$$

using (4.10-27) from [56], with $D^{2p}(\Psi w) = \dfrac{(2p)!}{(p!)^2}\Psi_p^{(p)}(0)w^{(p)}(0)$. Moreover, $\kappa^2\Psi_p^{(p)}(0) = \alpha_{p+1}L_{p+1}^{(p+1)}(0)$ and $w^{(p)}(0) = -p(p-1)L_{p-1}^{(p-1)}(0)$. Hence,

$$E = \int_{-1}^{1}\Psi(x)w(x)dx - \mathcal{Q}^{(p)}(\Psi w) = \frac{2}{\kappa^2}\frac{(p^2-1)}{2p-1}\alpha_{p+1}. \tag{3.34}$$

Now, substituting the values from (3.33) and (3.34) into (3.32), we obtain $\alpha_{p-1} = \dfrac{\tau(p+1)}{p}\alpha_{p+1}$. Consequently, (3.31) can be rewritten in the form

$$F(x) = \Psi''(x) + \kappa^2\Psi(x) = \alpha_{p+1}\left[\tau\left(1+\frac{1}{p}\right)L'_{p-1}(x) + L'_{p+1}(x)\right]. \tag{3.35}$$

Observe that we may write

$$\Psi(x) = \sigma\Upsilon_p(x) + \rho\Upsilon_{p-2}(x) \tag{3.36}$$

for suitable constants σ and ρ where Υ is given in (Chapter 2, eq.(2.43)) and defined as

$$\Upsilon_p(x) = \sum_{j=0}^{\lfloor p/2\rfloor}\left(-\frac{1}{\kappa^2}\right)^{j+1}L_{p+1}^{(2j+1)}(x) \tag{3.37}$$

and satisfies the property

$$\Upsilon''_p(x) + \kappa^2\Upsilon_p(x) = -L'_{p+1}(x). \tag{3.38}$$

Consequently, we have

$$F(x) = \sigma\left(\Upsilon''_p(x) + \kappa^2\Upsilon_p(x)\right) + \rho\left(\Upsilon''_{p-2}(x) + \kappa^2\Upsilon_{p-2}(x)\right)$$

using the property (3.38), we get

$$F(x) = -\sigma L'_{p+1}(x) - \rho L'_{p-1}(x).$$

Comparing the last equation with (3.35), we are led to the choices $\sigma = -\alpha_{p+1}$ and $\rho = -\tau\alpha_{p+1}(p+1)/p$, and with these values, (3.36) becomes

$$\Psi(x) = -\alpha_{p+1}\left[\tau\left(1+\frac{1}{p}\right)\Upsilon_{p-2}(x) + \Upsilon_p(x)\right]. \tag{3.39}$$

Applying the boundary condition $\Psi(1) = 1$, we obtain $\alpha_{p+1} = -p/\Gamma(1)$, provided that $\Gamma(1)$ is non-zero, with $\Gamma(1) = \tau(p+1)\Upsilon_{p-2}(1) + p\Upsilon_p(1)$. Consequently, Ψ may be written in the form

$$\Psi(x) = \frac{\Gamma(x)}{\Gamma(1)}. \tag{3.40}$$

We want to obtain a closed form expression for (3.24) and for this we define $\Psi_I(x) = (x+1)/2 + (-1)^p(1-x)/2$, so

$$\begin{aligned} \hat{B}_\tau(\Psi, \Psi) &= \hat{B}_\tau(\Psi, \Psi_I) + \hat{B}_\tau(\Psi, \Psi - \Psi_I) \\ &= [\Psi'\Psi_I]_{-1}^1 - \int_{-1}^1 (\Psi'' + \kappa^2\Psi)\Psi_I dx \end{aligned}$$

applying integration by parts together with (3.35), we get

$$\begin{aligned} \hat{B}_\tau(\Psi, \Psi) &= 2\Psi'(1) - 2\alpha_{p+1}\left[1 + \tau\left(1 + \frac{1}{p}\right)\right] \\ &= \frac{2}{\Gamma(1)}[\Gamma'(1) + (p + \tau(p+1))]. \end{aligned} \tag{3.41}$$

Now, as in [1, 5], using the values of Υ and its derivatives at the boundary $x = 1$ in terms of the series a_{p+1}, a_{p-1}, b_{p+1} and b_{p-1} which can be obtained from the recurrence relation (3.19) proved in Chapter 2, $\Gamma(1)$ and $\Gamma'(1)$ can be written as

$$\Gamma(1) = -\tfrac{1}{\kappa}\left(\tau(p+1)b_{p-1} + pb_{p+1}\right)$$

and

$$\Gamma'(1) + \tau(p+1) + p = \tau(p+1)a_{p-1} + pa_{p+1}.$$

Hence, inserting the above values into (3.41) and simplifying gives

$$\hat{B}_\tau(\Psi^p, \Psi^p) = -2\kappa\left[\frac{\tau(p+1)a_{p-1} + pa_{p+1}}{\tau(p+1)b_{p-1} + pb_{p+1}}\right] \tag{3.42}$$

which completes the proof. □

For both finite element [1] and spectral element [5] schemes it is shown that $\hat{B}_\tau(\Phi^p, \Phi^p)$ can be represented in terms of Bessel functions. Since the quadrature

rule is exact for Φ^p in the bilinear form (2.33) for spectral element scheme and in the bilinear form (3.24) for optimally blended scheme. Therefore we have:

$$\hat{B}_\tau(\Phi^p, \Phi^p) = -2\kappa \frac{J_{p+1/2}(\kappa)\sin\kappa - Y_{p+1/2}(\kappa)\cos\kappa}{J_{p+1/2}(\kappa)\cos\kappa + Y_{p+1/2}(\kappa)\sin\kappa} \quad \text{with } \kappa \neq m\pi$$

and

$$\hat{B}_\tau(\Phi^p, \Phi^p) = 2\kappa \frac{J_{p+1/2}(\kappa)\cos\kappa + Y_{p+1/2}(\kappa)\sin\kappa}{J_{p+1/2}(\kappa)\sin\kappa - Y_{p+1/2}(\kappa)\cos\kappa} \quad \text{with } \kappa \neq (m+1/2)\pi$$

where $\kappa = \omega h/2$. The following result extends these results to $\hat{B}_\tau(\Psi^p, \Psi^p)$.

Corollary 3.4.2. *Let $p = 2, 3, \ldots,$ then*

1. if p is even and $\kappa \neq (m+1/2)\pi$ for all $m \in \mathbb{Z}$, then

$$\hat{B}_\tau(\Psi^p, \Psi^p) = 2\kappa \frac{\tau(p+1)(J_{p-1/2}(\kappa)\cot\kappa + Y_{p-1/2}(\kappa)) - p(J_{p+3/2}(\kappa)\cot\kappa + Y_{p+3/2}(\kappa))}{\tau(p+1)(J_{p-1/2}(\kappa) - Y_{p-1/2}(\kappa)\cot\kappa) - p(J_{p+3/2}(\kappa) - Y_{p+3/2}(\kappa)\cot\kappa)}, \quad (3.43)$$

where J and Y are cylindrical Bessel functions of the first and second kind respectively;

2. if p is odd and $\kappa \neq m\pi$ for all $m \in \mathbb{Z}$, then

$$\hat{B}_\tau(\Psi^p, \Psi^p) = 2\kappa \frac{\tau(p+1)(Y_{p-1/2}(\kappa)\cot\kappa - J_{p-1/2}(\kappa)) - p(Y_{p+3/2}(\kappa)\cot\kappa - J_{p+3/2}(\kappa))}{\tau(p+1)(J_{p-1/2}(\kappa)\cot\kappa + Y_{p-1/2}(\kappa)) - p(J_{p+3/2}(\kappa)\cot\kappa + Y_{p+3/2}(\kappa))}. \quad (3.44)$$

Proof. This corollary is proved separately for even and odd order polynomials. Consider first the case when p is even. Inserting the values of a_{p-1}, a_{p+1} and b_{p-1}, b_{p+1} given in (Chapter 2, eq.(2.62)) into (3.28) and rearranging gives (3.43), which completes the proof in the even case. Now consider the case when p is odd and once again inserting the values of a_{p-1}, a_{p+1} and b_{p-1}, b_{p+1} given in (Chapter 2, eq.(2.63)) into (3.28) and rearranging gives (3.44), which completes the proof. □

For Φ^p we rewrite expressions (2.65) and (2.67) given in Chapter 2 with higher order terms. As the quadrature rule is exact for Φ^p in the bilinear form (3.24), the estimates (2.65) and (2.67) are exactly the same as equations (4.16) and (4.15) in [1], for $p = 2N$ and $p = 2N + 1$ respectively. Therefore, when p is an even integer and $\kappa \neq (m + 1/2)\pi, m \in \mathbb{Z}$, then

$$\mathcal{E}_{\Phi}^{(p)}(\kappa) = 2\left[\frac{p!}{(2p)!}\right]^2 \frac{(2\kappa)^{2p}}{2p+1} - 2\frac{(2p+1)^2}{2p-1}\left[\frac{(p+1)!}{(2p+2)!}\right]^2 \frac{(2\kappa)^{2p+2}}{2p+3} + \mathcal{O}(2\kappa^{2p+4})$$

and when p is an odd integer and $\kappa \neq m\pi, m \in \mathbb{Z}$, then

$$\mathcal{E}_{\Phi}^{(p)}(\kappa) = \frac{1}{2}\left[\frac{p!}{(2p)!}\right]^2 \frac{(2\kappa)^{2p+2}}{2p+1} - \frac{(2p+1)^2}{2p-1}\left[\frac{(p+1)!}{(2p+2)!}\right]^2 \frac{(2\kappa)^{2p+4}}{2p+3} + \mathcal{O}(2\kappa^{2p+6}).$$

For $\mathcal{E}_{\Psi}^{(p)}(\kappa)$, we have the following results.

Theorem 3.4.3. *Let $p \in \mathbb{N}$ satisfy $p \geq 2$. Then*

1. if p is an even integer, and $\kappa \neq (m + 1/2)\pi, m \in \mathbb{Z}$, then

$$\begin{aligned}\mathcal{E}_{\Psi}^{(p)}(\kappa) &= -\frac{\tau}{2}\left(1+\frac{1}{p}\right)\left[\frac{p!}{(2p)!}\right]^2 \frac{(2\kappa)^{2p+2}}{2p+1} - \frac{1}{2}\left[\frac{(p+1)!}{(2p+2)!}\right]^2 \frac{(2\kappa)^{2p+4}}{2p+3}\widetilde{C}_{\tau}^{(p)} \\ &\quad + \mathcal{O}(2\kappa^{2p+6}); \end{aligned} \tag{3.45}$$

2. if p is an odd integer, and $\kappa \neq m\pi, m \in \mathbb{Z}$, then

$$\begin{aligned}\mathcal{E}_{\Psi}^{(p)}(\kappa) &= -2\tau\left(1+\frac{1}{p}\right)\left[\frac{p!}{(2p)!}\right]^2 \frac{(2\kappa)^{2p}}{2p+1} - 2\left[\frac{(p+1)!}{(2p+2)!}\right]^2 \frac{(2\kappa)^{2p+2}}{2p+3}\widetilde{C}_{\tau}^{(p)} \\ &\quad + \mathcal{O}(2\kappa^{2p+4}) \end{aligned} \tag{3.46}$$

where

$$\widetilde{C}_{\tau}^{(p)} = \tau^2\left(1+\frac{1}{p}\right)^2 \frac{2p+3}{2p-1} - \tau\left(1+\frac{1}{p}\right)(2p+3) - 1.$$

Proof. First, consider the case when p is even. Adding $2\kappa\tan\kappa$ to equation (3.43) and applying straightforward manipulations give

$$\hat{B}_{\tau}(\Psi^p, \Psi^p) + 2\kappa\tan\kappa = -\frac{2\kappa}{\cos^2\kappa} Q_{\tau}^{p+3/2}(\kappa)\left(1 - Q_{\tau}^{p+3/2}(\kappa)\tan\kappa\right)^{-1} \tag{3.47}$$

where

$$Q_\tau^{p+3/2}(\kappa) = \frac{\tau\,(p+1)\,J_{p-1/2}(\kappa) - pJ_{p+3/2}(\kappa)}{\tau\,(p+1)\,Y_{p-1/2}(\kappa) - pY_{p+3/2}(\kappa)} \tag{3.48}$$

and for small κ i.e. when $\kappa \ll 1$ is given by

$$Q_\tau^{p+3/2}(\kappa) = \frac{\tau}{2}\left(1+\frac{1}{p}\right)\left[\frac{p!}{(2p)!}\right]^2 \frac{(2\kappa)^{2p+1}}{2p+1} + \frac{1}{2}\left[\frac{(p+1)!}{(2p+2)!}\right]^2 \frac{(2\kappa)^{2p+3}}{2p+3}\widetilde{C}_\tau^{(p)} + \cdots . \tag{3.49}$$

The behaviour of $Q_\tau^{p+3/2}(\kappa)$ is studied in the next section and is proved in Lemma 3.5.1. With the aid of this estimate, equation (3.47) together with trivial calculations simplifies to (3.45). The assertions concerning polynomials of odd order are proved in a similar fashion. Subtracting $2\kappa\cot\kappa$ from equation (3.44) and after simplification, we obtain

$$\hat{B}_\tau(\Psi^p,\Psi^p) - 2\kappa\cot\kappa = -\frac{2\kappa}{\sin^2\kappa} Q_\tau^{p+3/2}(\kappa)\left(1+Q_\tau^{p+3/2}(\kappa)\cot\kappa\right)^{-1} \tag{3.50}$$

Now, using (3.49) into the above expression and simplifying gives (3.46) as required. □

3.4.2 Proof of Theorem 3.3.2

We now prove Theorem 3.3.2 by using expressions (2.74) and (2.76) which were derived in Chapter 2 and are valid for small wavenumbers i.e. $\kappa = \omega h/2 \ll 1$ for even and odd order polynomials.

Proof. First consider the case when p is even. We reconsider the expression

$$\cos\mu_\tau^{(p)}h - \cos\omega h = \left(\frac{\omega h}{2}\right)^2 \mathcal{E}_\Phi^{(p)} + \mathcal{E}_\Psi^{(p)} + \cdots \tag{3.51}$$

obtained in Chapter 2 for small $\omega \ll 1$. We have,

$$\left(\frac{\omega h}{2}\right)^2 \mathcal{E}_\Phi^{(p)} = \frac{1}{2}\left[\frac{p!}{(2p)!}\right]^2 \frac{(\omega h)^{2p+2}}{2p+1} - \frac{1}{2}\frac{(2p+1)^2}{2p-1}\left[\frac{(p+1)!}{(2p+2)!}\right]^2 \frac{(\omega h)^{2p+4}}{2p+3} + \cdots$$

and

$$\mathcal{E}_{\Psi}^{(p)} = -\frac{\tau}{2}\left(1+\frac{1}{p}\right)\left[\frac{p!}{(2p)!}\right]^2\frac{(\omega h)^{2p+2}}{2p+1} - \frac{1}{2}\left[\frac{(p+1)!}{(2p+2)!}\right]^2\frac{(\omega h)^{2p+4}}{2p+3}\widetilde{C}_{\tau}^{(p)} + \cdots .$$

Inserting these values into equation (3.51) and simplifying gives

$$\begin{aligned}\cos\mu_{\tau}^{(p)}h - \cos\omega h = \frac{1}{2}\left[1-\tau\left(1+\frac{1}{p}\right)\right]\left[\frac{p!}{(2p)!}\right]^2\frac{(\omega h)^{2p+2}}{2p+1} \\ -\frac{1}{2}\left[\frac{(p+1)!}{(2p+2)!}\right]^2\frac{(\omega h)^{2p+4}}{2p+3}C_{\tau}^{(p)} + \cdots \end{aligned} \tag{3.52}$$

where $C_{\tau}^{(p)} = \tau^2\dfrac{(2p+3)}{(2p-1)}\left(1+\dfrac{1}{p}\right)^2 - \tau(2p+3)\left(1+\dfrac{1}{p}\right) + 2\dfrac{2p^2+p+1}{2p-1}$.

We now consider equation (2.76) from Chapter 2 for the case when p is odd, namely

$$\cos\mu_{\tau}^{(p)}h - \cos\omega h = \left(\frac{\omega h}{2}\right)^2\mathcal{E}_{\Psi}^{(p)} + \mathcal{E}_{\Phi}^{(p)} + \cdots \tag{3.53}$$

where

$$\left(\frac{\omega h}{2}\right)^2\mathcal{E}_{\Psi}^{(p)} = -\frac{\tau}{2}\left(1+\frac{1}{p}\right)\left[\frac{p!}{(2p)!}\right]^2\frac{(\omega h)^{2p+2}}{2p+1} - \frac{1}{2}\left[\frac{(p+1)!}{(2p+2)!}\right]^2\frac{(\omega h)^{2p+4}}{2p+3}\widetilde{C}_{\tau}^{(p)} + \cdots$$

and

$$\mathcal{E}_{\Phi}^{(p)} = \frac{1}{2}\left[\frac{p!}{(2p)!}\right]^2\frac{(\omega h)^{2p+2}}{2p+1} - \frac{1}{2}\frac{(2p+1)^2}{2p-1}\left[\frac{(p+1)!}{(2p+2)!}\right]^2\frac{(\omega h)^{2p+4}}{2p+3} + \cdots .$$

Now, substituting these values into (3.53) and simplifying gives equation (3.52), which is what was required. Finally, for small ωh, the approximation

$$\cos\mu_{\tau}^{(p)}h - \cos\omega h = -\omega h(\mu_{\tau}^{(p)}h - \omega h) + \cdots$$

gives us the required estimate (3.21). □

3.4.3 Proof of Theorem 3.2.1

Proof. Let $f \in \mathbb{P}_p$ be written in the form

$$f(x) = \sum_{j=0}^{p}\ell_j(x)f(\zeta_j^{\tau})$$

where $\ell_j \in \mathbb{P}_p$ satisfies $\ell_j(\zeta_k^\tau) = \delta_{jk}, \forall j = 0, 1, 2, \ldots, p$. Applying the quadrature rule $\mathcal{Q}_\tau^{(p)}$ gives

$$\mathcal{Q}_\tau^{(p)}(f) = \sum_{j=0}^{p} w_j^\tau f(\zeta_j^\tau)$$

where $\{\zeta_j^\tau\}_{j=0}^p$ and $\{w_j^\tau\}_{j=0}^p$ are the nodes and weights of $\mathcal{Q}_\tau^{(p)}$ respectively. Later, we show that the quadrature weights defined in (3.17) satisfy

$$w_j^\tau = \int_{-1}^{1} \ell_j(x)dx. \tag{3.54}$$

Hence, for $f \in \mathbb{P}_p$

$$\mathcal{Q}_\tau^{(p)}(f) = \sum_{j=0}^{p} f(\zeta_j^\tau) \int_{-1}^{1} \ell_j(x)dx = \int_{-1}^{1} \sum_{j=0}^{p} f(\zeta_j^\tau)\ell_j(x)dx = \int_{-1}^{1} f(x)dx$$

and so $\mathcal{Q}_\tau^{(p)}$ is exact for all $f \in \mathbb{P}_p$. Now, let $f \in \mathbb{P}_{2p-1}$ be written in the form

$$f(x) = \Pi_p f(x) + \varpi(x)q(x)$$

for $q \in \mathbb{P}_{p-2}$ where $\varpi(x) = L_{p+1}(x) - \tau L_{p-1}(x)$ and $\Pi_p f \in \mathbb{P}_p$ denotes the interpolant to f at the nodes $\{\zeta_j^\tau\}_{j=0}^p$. Integrating the above equation and using the orthogonality property of the Legendre polynomials, we get

$$\int_{-1}^{1} f(x)dx = \int_{-1}^{1} \Pi_p f(x)dx.$$

Moreover, since ϖ vanishes at the nodes of $\mathcal{Q}_\tau^{(p)}$, we can write

$$\int_{-1}^{1} \Pi_p f(x)dx = \mathcal{Q}_\tau^{(p)}(\Pi_p f) = \mathcal{Q}_\tau^{(p)}(\Pi_p f + \varpi q) = \mathcal{Q}_\tau^{(p)}(f)$$

and it follows that $\mathcal{Q}_\tau^{(p)}$ is exact for all $f \in \mathbb{P}_{2p-1}$. Since the Gauss-Legendre-Lobatto rule is also exact for $f \in \mathbb{P}_{2p-1}$, it follows that

$$\mathcal{Q}_\tau^{(p)}(f) = (1-\tau)\int_{-1}^{1} f(x)dx + \tau\mathcal{Q}^{(p)}(f) \quad \forall f \in \mathbb{P}_{2p-1} \tag{3.55}$$

and hence identity (3.18) holds for $f \in \mathbb{P}_{2p-1}$.

Now let $f \in \mathbb{P}_{2p}$ be written in the form

$$f(x) = \mu\varpi(x)L_{p-1}(x) + q(x)$$

for suitable constant $\mu \in \mathbb{R}$ and $q \in \mathbb{P}_{2p-1}$. Since ϖ vanishes at the quadrature points of $\mathcal{Q}_\tau^{(p)}$, we have

$$\mathcal{Q}_\tau^{(p)}(f) = \mathcal{Q}_\tau^{(p)}(q) = (1-\tau)\int_{-1}^{1} q(x)dx + \tau\mathcal{Q}^{(p)}(q) \tag{3.56}$$

where the second step follows from (3.18) applied to $q \in \mathbb{P}_{2p-1}$. The orthogonality property of Legendre polynomials means that

$$\begin{aligned}(1-\tau)\int_{-1}^{1} \varpi(x)L_{p-1}(x)dx &= (1-\tau)\int_{-1}^{1}(L_{p+1}(x) - \tau L_{p-1}(x))L_{p-1}(x)dx \\ &= -\tau(1-\tau)\int_{-1}^{1} L_{p-1}^2(x)dx.\end{aligned}$$

Furthermore, since L_{p+1} and L_{p-1} coincide at the nodes of the Gauss-Lobatto quadrature rule, we have

$$\tau\mathcal{Q}^{(p)}(\varpi L_{p-1}) = \tau\mathcal{Q}^{(p)}([L_{p+1} - \tau L_{p-1}]L_{p-1}) = \tau(1-\tau)\mathcal{Q}^{(p)}(L_{p-1}^2)$$

and since the Gauss-Lobatto rule has precision $2p-1$, we obtain

$$\tau\mathcal{Q}^{(p)}(\varpi L_{p-1}) = \tau(\tau-1)\int_{-1}^{1} L_{p-1}^2(x)dx.$$

Consequently, we deduce that

$$(1-\tau)\int_{-1}^{1} \varpi(x)L_{p-1}(x)dx + \tau\mathcal{Q}^{(p)}(\varpi L_{p-1}) = 0$$

and then adding μ times this identity to (3.56) shows that

$$\mathcal{Q}_\tau^{(p)}(f) = (1-\tau)\int_{-1}^{1} f(x)dx + \tau\mathcal{Q}^{(p)}(f)$$

for all $f \in \mathbb{P}_{2p}$. It is trivial to see that (3.18) now holds for all $f \in \mathbb{P}_{2p+1}$ since both sides of (3.18) vanish identically when f is the odd function $f(x) = x^{2p+1}$.

The positivity of the weights can be seen by inserting $f(x) = \ell_j^2(x) \in \mathbb{P}_{2p}$ into (3.18) to obtain for $\tau \in [0, 1)$

$$w_j^\tau = (1-\tau)\int_{-1}^{1} \ell_j^2(x)dx + \tau \mathcal{Q}^{(p)}(\ell_j^2) > 0.$$

We now show that the nodes $\{\zeta_i^\tau\}_{i=0}^p$ are real, distinct and lie within the interval $(-1, 1)$. Suppose this were not the case. Let $\{\zeta_i^\tau\}_{i=0}^m$ with $m < p$ be the points where $\varpi(x) \in \mathbb{P}_{p+1}$ changes sign in $(-1, 1)$, then the polynomial $W(x) = (x - \zeta_0^\tau)(x-\zeta_1^\tau)\cdots(x-\zeta_m^\tau)\varpi(x)$ vanishes at the nodes of $\mathcal{Q}_\tau^{(p)}$ but does not change sign in $(-1, 1)$. i.e.

$$\int_{-1}^{1} (x-\zeta_0^\tau)(x-\zeta_1^\tau)\cdots(x-\zeta_m^\tau)\varpi(x)dx \neq 0. \tag{3.57}$$

Hence, thanks to (3.18) applied to $W \in \mathbb{P}_{2p+1}$, we obtain

$$0 = \mathcal{Q}_\tau^{(p)}(W) = (1-\tau)\int_{-1}^{1} W(x)dx + \tau\mathcal{Q}^{(p)}(W),$$

but the right hand side is non-zero since W does not change sign, and we obtain a contradiction. Hence $m = p$.

Above, we have shown that (3.18) holds provided that the weights satisfy (3.54). We now show that choosing the weights according to (3.54) implies (3.17) holds. Observe that $\ell_J(x) = \varpi(x)/(x-\zeta_J^\tau)\varpi'(\zeta_J^\tau) \in \mathbb{P}_p$ so that

$$w_J^\tau = \int_{-1}^{1} \ell_J(x)dx = \frac{1}{\varpi'(\zeta_J^\tau)}\int_{-1}^{1}\frac{\varpi(x)}{x-\zeta_J^\tau}dx. \tag{3.58}$$

We recall the Christoffel-Darboux identity ([56], 4.7-3):

$$\sum_{k=0}^{p} L_k(x)L_k(y)(2k+1) = \frac{L_{p+1}(x)L_p(y) - L_p(x)L_{p+1}(y)}{x-y}(p+1), \quad x \neq y.$$

Choose $y = \zeta_J^\tau$ and integrate from -1 to 1 with respect to x to get

$$\int_{-1}^{1}\frac{L_{p+1}(x)L_p(\zeta_J^\tau) - L_p(x)L_{p+1}(\zeta_J^\tau)}{x-\zeta_J^\tau}dx = \frac{2}{p+1}, \ p \in \mathbb{N}. \tag{3.59}$$

Now, inserting $L_{p+1}(x) = \varpi(x) + \tau L_{p-1}(x)$ and $L_{p+1}(\zeta_J^\tau) = \tau L_{p-1}(\zeta_J^\tau)$, gives

$$\frac{2}{p+1} = L_p(\zeta_J^\tau)\int_{-1}^{1}\frac{\varpi(x)}{x-\zeta_J^\tau}dx + \tau\int_{-1}^{1}\frac{L_{p-1}(x)L_p(\zeta_J^\tau) - L_p(x)L_{p-1}(\zeta_J^\tau)}{x-\zeta_J^\tau}dx$$

and then using (3.59), we obtain

$$\frac{2}{p+1} = L_p(\zeta_J^\tau)\varpi'(\zeta_J^\tau)w_J^\tau - \frac{2\tau}{p}.$$

Inserting $\varpi'(\zeta_J^\tau) = L'_{p+1}(\zeta_J^\tau) - \tau L'_{p-1}(\zeta_J^\tau)$ in above equation and performing straightforward manipulations, we arrive at the conclusion

$$w_J^\tau = \frac{2[p(1+\tau)+\tau]}{p(p+1)L_p(\zeta_J^\tau)[L'_{p+1}(\zeta_J^\tau) - \tau L'_{p-1}(\zeta_J^\tau)]},\ \ \forall J = 0, 1, \ldots, p$$

as required. □

3.5 Analysis of $Q_\tau^m(\kappa)$

Now to analyse the behaviour of the quotient $Q_\tau^m(\kappa)$

$$Q_\tau^m(\kappa) = \frac{\tau\left(m-\frac{1}{2}\right)J_{m-2}(\kappa) - \left(m-\frac{3}{2}\right)J_m(\kappa)}{\tau\left(m-\frac{1}{2}\right)Y_{m-2}(\kappa) - \left(m-\frac{3}{2}\right)Y_m(\kappa)},\quad m = integer + \frac{1}{2} \tag{3.60}$$

for both limits, i.e. when $\kappa \ll 1$ and $\kappa \gg 1$, we virtually follow exactly the same arguments used in the previous chapter for the analysis of the quotient $\tilde{Q}^m(\kappa)$. The quotient defined above appeared in equation (3.48) in a form which we shall prove is equivalent to the above in the following lemma for small values of κ.

Lemma 3.5.1. *Let $m = integer + 1/2$ and let Q_τ^m be defined as above. Then, for $\kappa \ll 1$,*

$$Q_\tau^m(\kappa) = \frac{\tau}{2}\frac{(2m-1)}{(2m-3)}\left[\frac{\left(m-\frac{3}{2}\right)!}{(2m-3)!}\right]^2\frac{(2\kappa)^{2m-2}}{2m-2} + \frac{1}{2}\left[\frac{\left(m-\frac{1}{2}\right)!}{(2m-1)!}\right]^2\frac{(2\kappa)^{2m}}{2m}\widetilde{C}_\tau^{(m)}\cdots \tag{3.61}$$

where

$$\widetilde{C}_{\tau}^{(m)} = \tau^2 \left(\frac{2m-1}{2m-3}\right)^2 \frac{m}{m-2} - 2m\tau\frac{(2m-1)}{(2m-3)} - 1.$$

Proof. Write $m = n + 1/2$, where $n \in \mathbb{Z}$. For small κ, inserting identities (2.82), (2.83), (2.84) and (2.85) obtained in Chapter 2 into (3.60) and simplifying, we arrive at

$$Q_{\tau}^{m}(\kappa) = \frac{\tau}{2}\left(\frac{n}{n-1}\right)\left[\frac{(n-1)!}{(2n-2)!}\right]^2 \frac{(2\kappa)^{2n-1}}{2n-1} + \frac{1}{2}\left[\frac{(n)!}{(2n)!}\right]^2 \frac{(2\kappa)^{2n+1}}{2n+1}\widetilde{C}_{\tau}^{(n)} + \cdots$$

where

$$\widetilde{C}_{\tau}^{(n)} = \tau^2 \left(\frac{n}{n-1}\right)^2 \frac{2n+1}{2n-3} - \tau\frac{n}{n-1}(2n+1) - 1$$

which in terms of m gives the result claimed. □

Lemma 3.5.1 shows that $Q_{\tau}^{m}(\kappa)$ also decays algebraically as κ becomes small. The remainder of the section describes the behaviour of the ratio Q_{τ}^{m} for high wave numbers i.e. when $\kappa = \omega h/2 \gg 1$.

Theorem 3.5.2. *Let $Q_{\tau}^{m}(\kappa)$ be defined as above and $m = \text{integer} + \dfrac{1}{2}$. Then, as m is increased, $Q_{\tau}^{m}(\kappa)$ passes through two phases:*

1. *For $m < \kappa + 1 + o(\kappa^{1/3})$, $Q_{\tau}^{m}(\kappa)$ oscillates around unity but does not decay as m is increased.*

2. *For $m > \kappa + 1 + o(\kappa^{1/3})$, $Q_{\tau}^{m}(\kappa)$ converges to the ratio obtained with spectral element scheme $\tilde{Q}^{m}(\kappa)$ and decays super-exponentially with the same rate as $\tilde{Q}^{m}(\kappa)$ decays.*

The proof of this result is covered in the following sections.

3.5.1 Preasymptotic regime: $m < \kappa + 1$

In the preasymptotic regime inserting Langer's formulae given in Section 7.13.4 of [23] into (3.60), and performing straightforward manipulations, give

$$Q_\tau^m(\kappa) = \frac{J_{1/3}(z_{m-2})\cos(\pi/6) - Y_{1/3}(z_{m-2})\sin(\pi/6) + \mathcal{O}((m-2)^{-4/3})}{J_{1/3}(z_{m-2})\sin(\pi/6) + Y_{1/3}(z_{m-2})\cos(\pi/6) + \mathcal{O}((m-2)^{-4/3})} \times \left\{ \frac{\tau - \beta \dfrac{J_{1/3}(z_m)\cos(\pi/6) - Y_{1/3}(z_m)\sin(\pi/6) + \mathcal{O}(m^{-4/3})}{J_{1/3}(z_{m-2})\cos(\pi/6) - Y_{1/3}(z_{m-2})\sin(\pi/6) + \mathcal{O}((m-2)^{-4/3})}}{\tau - \beta \dfrac{J_{1/3}(z_m)\sin(\pi/6) + Y_{1/3}(z_m)\cos(\pi/6) + \mathcal{O}(m^{-4/3})}{J_{1/3}(z_{m-2})\sin(\pi/6) + Y_{1/3}(z_{m-2})\cos(\pi/6) + \mathcal{O}((m-2)^{-4/3})}} \right\} \tag{3.62}$$

where

$$\beta = \left[\frac{(\kappa^2 - (m-2)^2)}{(\kappa^2 - m^2)}\right]^{1/4} \frac{(2m-3)}{(2m-1)} \left(\frac{z_m}{z_{m-2}}\right)^{1/2} \tag{3.63}$$

with

$$z_m = m(w_m - \tan^{-1} w_m), \qquad w_m = \sqrt{\kappa^2/m^2 - 1},$$

$$z_{m-2} = (m-2)(w_{m-2} - \tan^{-1} w_{m-2}) \quad \textit{and} \quad w_{m-2} = \sqrt{\kappa^2/(m-2)^2 - 1}.$$

3.5.1.1 Oscillatory phase: $m < \kappa + 1 - o(\kappa^{1/3})$

In this region inserting (2.90) and (2.91) given in Chapter 2 into (3.62) and applying simplification gives

$$Q_\tau^m(\kappa) \approx \cot\left(z_{m-2} - \frac{\pi}{4}\right) \left[\frac{\tau - \beta' \cos\left(z_m - \frac{\pi}{4}\right)\sec\left(z_{m-2} - \frac{\pi}{4}\right)}{\tau - \beta' \sin\left(z_m - \frac{\pi}{4}\right)\operatorname{cosec}\left(z_{m-2} - \frac{\pi}{4}\right)}\right] \tag{3.64}$$

with

$$\beta' = \left[\frac{(\kappa^2 - (m-2)^2)}{(\kappa^2 - m^2)}\right]^{1/4} \frac{(2m-3)}{(2m-1)}.$$

3.5.1.2 Transition zone: $\kappa + 1 - o(\kappa^{1/3}) < m < \kappa + 1$

In this region, we consider the behaviour when m approaches $\kappa + 1$ from the left and the value of the expression (3.63) is approximately 1. Using the series

representations for Bessel functions given in equation (8.440) of [28], equation (3.60) becomes

$$Q_\tau^m(\kappa) \approx -\frac{1}{\sqrt{3}} + \frac{3}{\pi}\Gamma\left(\frac{2}{3}\right)^2 \left(\frac{z_m}{2}\right)^{2/3} \left[\tau \left(\frac{z_{m-2}}{2}\right)^{1/3} \left(\frac{z_m}{2}\right)^{-1/3} - 1\right] + \cdots . \quad (3.65)$$

Now, substituting the values of z_m and z_{m-2} from (2.94) and (2.95) into (3.65), we finally arrive at

$$Q_\tau^m(\kappa) \approx -\frac{1}{\sqrt{3}} + \frac{1}{\pi}\Gamma\left(\frac{2}{3}\right)^2 (\kappa - m) \left(\frac{6}{m}\right)^{1/3} \left[\tau \frac{\sqrt{\kappa - m + 2}}{\sqrt{\kappa - m}} \left(\frac{m}{m-2}\right)^{1/6} - 1\right] + \cdots$$

which is increasing algebraically at a rate of $\mathcal{O}(m^{1/3})$ as m increases in this region.

3.5.2 Asymptotic regime: $m > \kappa + 1$

In this regime the order m of the Bessel functions exceeds the argument $\kappa + 1$. Again, using Langer's formulae from Section 7.13.4 of [23] together with (3.60) gives

$$Q_\tau^m(\kappa) = -\frac{\pi^{-1} K_{1/3}(z_{m-2}) + \mathcal{O}((m-2)^{-4/3})}{I_{1/3}(z_{m-2}) + I_{-1/3}(z_{m-2}) + \mathcal{O}((m-2)^{-4/3})} \times \left\{ \frac{\tau - \gamma \dfrac{K_{1/3}(z_m) + \mathcal{O}(m^{-4/3})}{K_{1/3}(z_{m-2}) + \mathcal{O}((m-2)^{-4/3})}}{\tau - \gamma \dfrac{I_{1/3}(z_m) + I_{-1/3}(z_m) + \mathcal{O}(m^{-4/3})}{I_{1/3}(z_{m-2}) + I_{-1/3}(z_{m-2}) + \mathcal{O}((m-2)^{-4/3})}} \right\} \quad (3.66)$$

where

$$\gamma = \left[\frac{(m-2)^2 - \kappa^2}{(m^2 - \kappa^2)}\right]^{1/4} \frac{(2m-3)}{(2m-1)} \left(\frac{z_m}{z_{m-2}}\right)^{1/2} \quad (3.67)$$

with

$$z_m = m(\tanh^{-1} w_m - w_m), \qquad w_m = \sqrt{1 - \kappa^2/m^2},$$

$$z_{m-2} = (m-2)(\tanh^{-1} w_{m-2} - w_{m-2}) \quad \textit{and} \quad w_{m-2} = \sqrt{1 - \kappa^2/(m-2)^2}.$$

Now exploiting identities (2.98) and (2.99) for subscripts m and $m-2$ into (3.66) and dropping the higher order terms after simplification gives

$$Q_\tau^m(\kappa) \approx -\frac{e^{-2z_{m-2}}}{2} \left(\frac{\tau - \gamma' e^{(z_{m-2} - z_m)}}{\tau - \gamma' e^{-(z_{m-2} - z_m)}}\right) \quad (3.68)$$

with

$$\gamma' = \left[\frac{(m-2)^2-\kappa^2}{m^2-\kappa^2}\right]^{1/4} \frac{(2m-3)}{(2m-1)}. \tag{3.69}$$

3.5.2.1 Transition zone: $\kappa + 1 < m < \kappa + 1 + o(\kappa^{1/3})$

In this region, we start with the expression

$$Q_\tau^m(\kappa) \approx -\frac{\xi_{m-2}^{1/2}\mathrm{Ai}(\xi_m) - \tau\xi_m^{1/2}\mathrm{Ai}(\xi_{m-2})}{\xi_{m-2}^{1/2}\mathrm{Bi}(\xi_m) - \tau\xi_m^{1/2}\mathrm{Bi}(\xi_{m-2})}$$

which is obtained from (3.66) by using the formulae (11.1.04) and (11.1.12) from [54]. Moreover, using series representations for Airy functions, given in equations (11.1.07) and (11.1.16) of [54], the above expression gives

$$Q_\tau^m(\kappa) \approx -\frac{1}{\sqrt{3}} + \frac{3^{1/3}}{\pi}\Gamma\left(\frac{2}{3}\right)^2 \xi_m \left[1 - \tau\xi_m^{-1/2}\xi_{m-2}^{1/2}\right] \tag{3.70}$$

where

$$\xi_m \simeq \left(\frac{2}{m}\right)^{1/3}(m-\kappa) \text{ and } \xi_{m-2} \simeq \left(\frac{2}{m-2}\right)^{1/3}(m-2-\kappa).$$

Inserting these values into (3.70), we finally obtain

$$Q_\tau^m(\kappa) \approx -\frac{1}{\sqrt{3}} + \frac{1}{\pi}\Gamma\left(\frac{2}{3}\right)^2 (m-\kappa)\left(\frac{6}{m}\right)^{1/3}\left[1 - \tau\frac{\sqrt{m-2-\kappa}}{\sqrt{m-\kappa}}\left(\frac{m}{m-2}\right)^{1/6}\right] + \cdots$$

where Q_τ^m is decreasing algebraically at a rate of $\mathcal{O}(m^{-1/3})$ with increasing m. Therefore, Q_τ^m is still oscillating in the transition region.

3.5.2.2 Exponential decay phase: $m > \kappa + 1 + o(\kappa^{1/3})$

When m exceeds $\kappa + 1 + o(\kappa^{1/3})$ then it is easy to verify that γ', which is defined in (3.69), is approximately equal to 1. Moreover, the value of the blending parameter τ is also approximately equal to 1 in this region

$$\tau = \frac{2m-3}{2m-1} \approx 1 \quad \text{when } m \gg 1.$$

Hence the blending scheme overlaps with spectral element scheme and have the same superexponential expression (2.87) obtained in the previous Chapter 2.

Chapter 4

Explicit discrete dispersion relations for Helmholtz equation in d-dimensions

4.1 Introduction

In this chapter, we study the dispersive properties of finite element, spectral element and optimally blended schemes using tensor product elements defined on rectangular grid in d-dimensions. We prove and give analytical expressions for discrete dispersion relations for the above mentioned schemes by adopting the same approach used in [3] where it is shown that the discrete dispersion relation may be expressed in terms of that for the approximation of the scalar Helmholtz equation in one dimension. We show that for a rectangular grid the analytical expressions for the discrete dispersion error in higher dimensions can be obtained using one dimensional discrete dispersion error expressions.

This chapter is organised as follows. In Section 4.2, we give continuous discrete

dispersion relations and derive discrete dispersion relations using tensor product meshes valid for d-dimensions. In Section 4.3, discrete dispersion relations are derived for finite element, spectral element and optimally blended schemes. In final section the numerical results obtained with these schemes are shown.

4.2 Acoustic wave equation

Consider the acoustic wave equation in d-dimensions

$$\frac{\partial^2 u}{\partial t^2} - \triangle u = 0 \quad \text{in } \mathbb{R}^d. \tag{4.1}$$

We seek time-harmonic solutions of the form $u(\boldsymbol{x}, t) = e^{i\omega t} U(\boldsymbol{x})$ to the above equation, so that U satisfies the Helmholtz equation

$$\omega^2 U + \triangle U = 0 \quad \text{in } \mathbb{R}^d \tag{4.2}$$

where $\omega > 0$ is the given angular frequency.

4.2.1 Continuous dispersion relation

Observe that in one dimension, the function $u(\omega; x) = e^{i\omega x}$ satisfies

$$(u', v') = \omega^2 (u, v) \quad \forall v \in H^1_{loc}(\mathbb{R}) \tag{4.3}$$

where

$$H^1_{loc}(\mathbb{R}^d) = \{v : \mathbb{R}^d \to \mathbb{R}, v \in H^1(\Omega) \text{ for all } \Omega \subset\subset \mathbb{R}^d\}$$

and

$$(u, v) = \int_{\mathbb{R}} u \overline{v} dx$$

is the L_2-inner product on $\mathbb{R}$. We note that (4.3) is the variational formulation of (4.2) in one dimension. Furthermore, it is trivial to verify that the function

$u(\omega; x)$ satisfies

$$u(\omega; x + nh) = e^{i\omega hn} u(\omega; x) \quad \forall n \in \mathbb{Z}, x, h \in \mathbb{R}$$

which is the so called *Bloch wave* property. To obtain the dispersion relation in d-dimensions for the acoustic wave equation (4.2), we start with the variational formulation of equation (4.2) which is given by

$$\omega^2 \int_{\mathbb{R}^d} U v d\boldsymbol{x} - \int_{\mathbb{R}^d} \mathbf{grad} U \cdot \mathbf{grad} v d\boldsymbol{x} = 0 \quad \forall v \in H^1_{loc}(\mathbb{R}^d). \tag{4.4}$$

Now choose U and v as the product of uni-variate functions given by

$$U(x_1, x_2, \cdots, x_d) = \prod_{\ell=1}^{d} u(\omega_\ell; x_\ell) \text{ and } v(x_1, x_2, \cdots, x_d) = \prod_{\ell=1}^{d} v_\ell(x_\ell)$$

where $\{\omega_\ell\}_{\ell=1}^d \in \mathbb{R}$ are constants to be determined, $\{v_\ell\}_{\ell=1}^d \in H^1_{loc}(\mathbb{R})$ and $u(\omega; \cdot)$ is defined above. Substituting U and v into (4.4), we get

$$\omega^2 \prod_{\ell=1}^{d} (u(\omega_\ell; \cdot), v_\ell) - \sum_{r=1}^{d} \left((u'(\omega_r; \cdot), v_r') \prod_{\ell \neq r} (u(\omega_\ell; \cdot), v_\ell) \right) = 0. \tag{4.5}$$

Now, exploiting the identity (4.3), and performing straightforward manipulations, the above equation simplifies to

$$\left(\omega^2 - \sum_{r=1}^{d} \omega_r^2 \right) \prod_{\ell=1}^{d} (u(\omega_\ell; \cdot), v_\ell) = 0, \tag{4.6}$$

from which we see that non-trivial solutions of (4.6) exist only when the parameters $\{\omega_\ell\}_{\ell=1}^d$ satisfy

$$\omega^2 = \omega_1^2 + \omega_2^2 + \cdots + \omega_d^2. \tag{4.7}$$

Equation (4.7) is the well known *continuous dispersion relation* of the acoustic wave equation (4.2) which is usually derived by inserting u directly into the differential equation (4.2).

4.2.2 Framework for discrete dispersion relations

To obtain the dispersion relation for the discrete case, we partition the real line $\mathbb{R}$ into infinitely many subintervals of uniform length $h > 0$ with nodes located at $h\mathbb{Z}$. The space $V_{hp} \subset H^1_{loc}(\mathbb{R})$ is the corresponding space of continuous piecewise polynomials of degree p relative to the grid. We seek an approximation $u_{hp} \in V_{hp}$ such that

$$(u'_{hp}, v') - \omega^2 \langle u_{hp}, v \rangle = 0 \quad \forall v \in V_{hp}$$

where $\langle \cdot, \cdot \rangle$ is an appropriate discrete L_2-inner product on V_{hp}. Examples of suitable choices for $\langle \cdot, \cdot \rangle$ will be given later, but we shall require that for $v, w \in V_{hp}$, $\langle v', w' \rangle = (v', w')$. To obtain the corresponding bilinear form in d-dimensions we consider the tensor product grid where each side of the grid has length $h_\ell > 0, \ell = 1, \ldots, d$. Let $V^d_{hp} \subset H^1_{loc}(\mathbb{R}^d)$ denote the space of continuous piecewise polynomials of degree p in each variable relative to the grid in d-dimensions, then we seek an approximate $u_{hp} \in V^d_{hp}$ such that

$$\langle \nabla u_{hp}, \nabla v \rangle_d - \omega^2 \langle u_{hp}, v \rangle_d = 0 \quad \forall v \in V^d_{hp} \tag{4.8}$$

where $\langle \cdot, \cdot \rangle_d$ is the tensor product bilinear form obtained from $\langle \cdot, \cdot \rangle$. Motivated by the arguments leading to the dispersion relation in the continuous case, we have the following theorem for the discrete dispersion relation.

Theorem 4.2.1. *Suppose there exists a non-trivial function $u_{hp}(\omega; \cdot) \in V_{hp}$ such that $u_{hp}(\omega; \cdot)$ has*

1. *the discrete Bloch wave property*

$$u_{hp}(\omega; x + nh) = e^{inh\xi} u_{hp}(\omega; x), \quad \forall n \in \mathbb{Z}, x, h \in \mathbb{R} \tag{4.9}$$

with discrete frequency $\xi = \xi(\omega)$ and satisfies

2.

$$(u'_{hp}, v') = \omega^2 \langle u_{hp}, v \rangle, \quad \forall v \in V_{hp}. \tag{4.10}$$

Let

$$E_{hp}(\omega) = \xi^2(\omega) - \omega^2. \tag{4.11}$$

Then, the discrete dispersion relation for Helmholtz equation in d-dimensions is given by

$$\omega_h^2 = \omega^2 + \sum_{\ell=1}^{d} E_{hp}(\omega_\ell) \text{ with } \omega^2 = \omega_1^2 + \omega_2^2 + \cdots + \omega_d^2. \tag{4.12}$$

Proof. By analogy with the derivation of the dispersion relation in the continuous case, we seek a non-trivial solution $U_{hp} \in V_{hp}^{(d)}$ of the form:

$$U_{hp}(x_1, x_2, \cdots, x_d) = \prod_{\ell=1}^{d} u_{hp}(\omega_\ell; x_\ell) \tag{4.13}$$

where $\{\omega_\ell\}_{\ell=1}^{d} \in \mathbb{R}$ are again constants to be determined. The corresponding discrete variational formulation of (4.2) is given by (4.8). Now, substituting v of the form $v = \prod v_\ell(x_\ell)$ and U_{hp} from (4.13) into (4.8), we obtain

$$\omega^2 \prod_{\ell=1}^{d} \langle u_{hp}(\omega_\ell; \cdot), v_\ell \rangle - \sum_{r=1}^{d} \left((u'_{hp}(\omega_r; \cdot), v'_r) \prod_{\ell \neq r} \langle u_{hp}(\omega_\ell; \cdot), v_\ell \rangle \right) = 0. \tag{4.14}$$

Now, exploiting the property (4.10), we get

$$\left(\omega^2 - \left[\omega_1^2 + \omega_2^2 + \cdots + \omega_d^2\right]\right) \prod_{\ell=1}^{d} \langle u_{hp}(\omega_\ell; \cdot), v_\ell \rangle = 0$$

which has non-trivial solutions only when

$$\omega^2 = \omega_1^2 + \omega_2^2 + \cdots + \omega_d^2. \tag{4.15}$$

Now, consider

$$U_{hp}(x_1 + n_1 h_1, x_2 + n_2 h_2, \cdots, x_d + n_d h_d) = \prod_{\ell=1}^{d} u_{hp}(\omega_\ell; x_\ell + n_\ell h_\ell)$$

which, on using property (4.9), gives

$$U_{hp}(x_1 + n_1h_1, x_2 + n_2h_2, \cdots, x_d + n_dh_d) =$$
$$e^{i[h_1n_1\xi(\omega_1)+h_2n_2\xi(\omega_2)+\cdots+h_dn_d\xi(\omega_d)]}U_{hp}(x_1, x_2, \cdots, x_d). \tag{4.16}$$

This is the *discrete Bloch wave property* for U_{hp}, and hence, the frequency ω_h of the discrete solution satisfies

$$\omega_h^2 = \xi(\omega_1)^2 + \xi(\omega_2)^2 + \cdots + \xi(\omega_d)^2.$$

Finally, upon using (4.11) together with (4.15) and after applying simple manipulations, the above equation gives (4.12) which is what the claimed result. □

Theorem 4.2.1 means that we can obtain the discrete dispersion relation for a scheme on a tensor product mesh in $\mathbb{R}^d$ using results for the discrete dispersion relation for the scheme in $\mathbb{R}^1$. We use this result in the following section to analyse the finite element, spectral element and a novel, so-called optimally blended scheme that was introduced in [7].

4.3 Higher order discrete dispersion relations for finite element, spectral element and optimally blended schemes in d-dimensions

In this section we will derive the explicit expressions of the discrete dispersion relations valid in d-dimensions for finite element, spectral element and optimally blended schemes of arbitrary order.

4.3.1 Standard finite element scheme

For finite elements we evaluate the stiffness and mass matrices using the $(p+1)$-point Gaussian quadrature rule

$$\int_{-1}^{1} f(x)dx \approx \mathcal{Q}_G^{(p)}(f) = \sum_{\ell=0}^{p} w_\ell f(\zeta_\ell) \tag{4.17}$$

where $\{\zeta_\ell\}_{\ell=0}^p$ are the zeros of L_{p+1} and L_{p+1} is the Legendre polynomial of degree $(p+1)$. Moreover, weights $\{w_\ell\}_{\ell=0}^p$ are given by

$$w_\ell = \frac{2}{(1-\zeta_\ell^2)[L'_{p+1}(\zeta_\ell)]^2} \quad \forall \ell \in \{0,1,\ldots,p\}. \tag{4.18}$$

The Gaussian quadrature rule (4.17) is exact for all polynomials of degree at most $2p+1$, and as a consequence

$$\int_{-1}^{1} u'\overline{v}'dx = \mathcal{Q}_G^{(p)}(u'\overline{v}') \text{ and } \int_{-1}^{1} u\overline{v}dx = \mathcal{Q}_G^{(p)}(u\overline{v})$$

for all $u, v \in \mathbb{P}_p$. Now a composite quadrature rule $\mathcal{I}_G^{(p)}$ on $\mathbb{R}$ given by

$$\int_{\mathbb{R}} f(x)dx \approx \mathcal{I}_G^{(p)}(f) = \frac{h}{2}\sum_{j\in\mathbb{Z}}\sum_{\ell=0}^{p} w_\ell f(\zeta_\ell^{j,h}) \tag{4.19}$$

is constructed using (4.17) where $\zeta_\ell^{j,h} = (j+\frac{1}{2})h + \frac{h}{2}\zeta_\ell, \forall j \in \mathbb{Z}$ and $\ell = 0,1,\ldots,p$. The discrete L_2-inner product is taken to be

$$\langle u, \overline{v}\rangle_G = \mathcal{I}_G^{(p)}(u\overline{v})$$

and will be exact for $u, v \in V_{hp}$.

Theorem 4.3.1. *Let $\omega \in \mathbb{R}$ be given and there exists a non-trivial $u_{hp} \in V_{hp}$ which satisfies*

$$(u'_{hp}, v') = \omega^2(u_{hp}, v), \quad \forall v \in V_{hp} \tag{4.20}$$

and the Bloch wave property (4.9) *with frequency $\xi(\omega)$, where*

$$\xi(\omega)^2 = \omega^2 - \left[\frac{p!}{(2p)!}\right]^2 \frac{h^{2p}\omega^{2p+2}}{2p+1} + \mathcal{O}(h)^{2p+2}. \tag{4.21}$$

Consequently, the discrete dispersion relation for finite elements in $\mathbb{R}^d$ is given by

$$\omega_h^2 = \omega^2 - \left[\frac{p!}{(2p)!}\right]^2 \frac{1}{2p+1} \sum_{\ell=1}^{d} h_\ell^{2p} \omega_\ell^{2p+2} + \mathcal{O}(h)^{2p+2} \tag{4.22}$$

where $\omega_1^2 + \omega_2^2 + \cdots + \omega_d^2 = \omega^2$.

Proof. The existence of u_{hp} is proved in Theorem 3.1 of [1] where it is also shown that

$$\xi(\omega)^2 = \omega^2 - \left[\frac{p!}{(2p)!}\right]^2 \frac{h^{2p}\omega^{2p+2}}{2p+1} + \mathcal{O}(h)^{2p+2}.$$

Hence, applying Thorem 4.2.1, we obtain (4.22) at once. □

4.3.2 Spectral element scheme

The only difference for spectral elements compared with finite elements is the replacement of the Gaussian quadrature rule (4.17) with the Gauss-Lobatto quadrature rule $\mathcal{Q}^{(p)}$ defined by

$$\int_{-1}^{1} f(x)dx \approx \mathcal{Q}^{(p)}(f) = \sum_{\ell=0}^{p} \tilde{w}_\ell f(\tilde{\zeta}_\ell) \tag{4.23}$$

where $\{\tilde{\zeta}_\ell\}_{\ell=0}^p$ are taken to be the zeros of $L_p'(x)(1-x^2)$ with weights $\tilde{w}_\ell$ given by

$$\tilde{w}_\ell = \frac{2}{p(p+1)[L_p(\tilde{\zeta}_\ell)]^2} \quad \forall \ell \in \{0, 1, \ldots, p\}. \tag{4.24}$$

The Gauss-Lobatto quadrature rule (4.23) is exact for all polynomials of degree at most $2p-1$. Hence the stiffness matrix is integrated exactly

$$\int_{-1}^{1} u'\overline{v}'dx = \mathcal{Q}^{(p)}(u'\overline{v}')$$

whereas the mass matrix is underintegrated

$$\int_{-1}^{1} u\overline{v}dx \approx \mathcal{Q}^{(p)}(u\overline{v}).$$

We use this quadrature rule to develop a composite quadrature rule on $\mathbb{R}$, which we denote by $\mathcal{I}_{GL}^{(p)}(\cdot)$, following the same construction used in the case of finite elements. The discrete L_2-inner product is taken to be

$$\langle u, \overline{v} \rangle_L = \mathcal{I}_{GL}^{(p)}(u\overline{v}).$$

The only difference now is that the mass matrix will be under-integrated.

Theorem 4.3.2. *Let $\omega \in \mathbb{R}$ be given and there exists a non-trivial $u_{hp} \in V_{hp}$ which satisfies*

$$(u'_{hp}, v') = \omega^2 \langle u_{hp}, v \rangle_L, \quad \forall v \in V_{hp} \tag{4.25}$$

and the Bloch wave property (4.9) *with frequency $\xi(\omega)$, where*

$$\xi(\omega)^2 = \omega^2 + \frac{1}{p}\left[\frac{p!}{(2p)!}\right]^2 \frac{h^{2p}\omega^{2p+2}}{2p+1} + \mathcal{O}(h)^{2p+2}. \tag{4.26}$$

Consequently, the discrete dispersion relation for spectral elements in $\mathbb{R}^d$ is given by

$$\omega_h^2 = \omega^2 + \frac{1}{p}\left[\frac{p!}{(2p)!}\right]^2 \frac{1}{2p+1} \sum_{\ell=1}^{d} h_\ell^{2p} \omega_\ell^{2p+2} + \mathcal{O}(h)^{2p+2} \tag{4.27}$$

where $\omega_1^2 + \omega_2^2 + \cdots + \omega_d^2 = \omega^2$.

Proof. The existence of u_{hp} is established in Theorem 2.4.2 of Chapter 2 where it is also shown that

$$\xi(\omega)^2 = \omega^2 + \frac{1}{p}\left[\frac{p!}{(2p)!}\right]^2 \frac{h^{2p}\omega^{2p+2}}{2p+1} + \mathcal{O}(h)^{2p+2}.$$

Equation (4.27) then follows at once from Theorem 4.2.1. □

Interestingly, from (4.27) it is clear that for higher orders the spectral element scheme provides p-times better accuracy as compared to the discrete dispersion relation obtained with finite element scheme (4.22). The same accuracy in the case of regular tensor product meshes was conjectured in [5].

4.3.3 Optimally blended scheme

We now apply Theorem 4.2.1 to a novel scheme introduced in Chapter 3 for the wave equation, whereby the finite element and spectral element schemes are blended in such a way that the order of accuracy of the resulting discrete dispersion relation is optimised. If the blending parameter is denoted by $\tau \in [0,1]$, then we base the blended scheme on the blended quadrature rule

$$\int_{-1}^{1} f(x)dx \approx \mathcal{Q}_{\tau}^{(p)}(f) = (1-\tau)\mathcal{Q}_{G}^{(p)}(f) + \tau\mathcal{Q}^{(p)}(f)$$

where $\mathcal{Q}_{G}^{(p)}$ and $\mathcal{Q}^{(p)}$ are the $(p+1)$-point Gauss-Legendre and Gauss-Legendre-Lobatto quadrature rules defined in the previous sections and give us the standard finite element and spectral element schemes for $\tau = 0$ and $\tau = 1$ respectively. Furthermore, $\mathcal{Q}_{\tau}^{(p)}$ is the $(p+1)$-point non-standard quadrature rule given in Chapter 3 valid for elements of arbitrary order with nodes $\{\zeta_{\ell}^{\tau}\}_{\ell=0}^{p}$ chosen as the zeros of $L_{p+1} - \tau L_{p-1}$, where L_{p+1} and L_{p-1} are the Legendre polynomials of degrees $p+1$ and $p-1$ respectively, with weights given by

$$w_{\ell}^{\tau} = \frac{2[p(1+\tau)+\tau]}{p(p+1)L_p(\zeta_{\ell}^{\tau})[L'_{p+1}(\zeta_{\ell}^{\tau}) - \tau L'_{p-1}(\zeta_{\ell}^{\tau})]}, \ \ \forall \ell = 0, 1, \ldots, p. \tag{4.28}$$

Furthermore, $\mathcal{Q}_{\tau}^{(p)}$ satisfies the following identity given in Chapter 3

$$\mathcal{Q}_{\tau}^{(p)}(f) = (1-\tau)\mathcal{Q}_{G}^{(p)}(f) + \tau\mathcal{Q}^{(p)}(f) \quad \forall f \in \mathbb{P}_{2p+1} \tag{4.29}$$

and is exact for all polynomials of degrees at the most $2p-1$. We use this quadrature rule to develop a composite quadrature rule on $\mathbb{R}$, which we denote by $\mathcal{I}_{\tau}^{(p)}(\cdot)$, and follow the same construction used in the previous sections for finite element and spectral element schemes. The discrete L_2-inner product is taken to be

$$\langle u, \overline{v} \rangle_{\tau} = \mathcal{I}_{\tau}^{(p)}(u\overline{v}).$$

Once again the mass matrix is under-integrated.

Theorem 4.3.3. *Let $\omega \in \mathbb{R}$ be given and there exists a non-trivial $u_{hp} \in V_{hp}$ which satisfies*

$$(u'_{hp}, v') = \omega^2 \langle u_{hp}, v \rangle_\tau, \quad \forall v \in V_{hp} \tag{4.30}$$

and the Bloch wave property (4.9) *with frequency $\xi(\omega)$, where*

$$\xi(\omega)^2 = \omega^2 + \left[\tau\left(1 + \frac{1}{p}\right) - 1\right] \left[\frac{p!}{(2p)!}\right]^2 \frac{h^{2p}\omega^{2p+2}}{2p+1} + \mathcal{O}(h^{2p+2}). \tag{4.31}$$

Consequently, the discrete dispersion relation for optimally blended scheme in $\mathbb{R}^d$ is given by

$$\omega_h^2 = \omega^2 + \left[\tau\left(1 + \frac{1}{p}\right) - 1\right] \left[\frac{p!}{(2p)!}\right]^2 \frac{1}{2p+1} \sum_{\ell=1}^{d} h_\ell^{2p} \omega_\ell^{2p+2} \tag{4.32}$$

where $\omega_1^2 + \omega_2^2 + \cdots + \omega_d^2 = \omega^2$.

Proof. The existence of u_{hp} is proved in Theorem 3.3.2 of Chapter 3 where it is also shown that

$$\xi(\omega)^2 = \omega^2 + \left[\tau\left(1 + \frac{1}{p}\right) - 1\right] \left[\frac{p!}{(2p)!}\right]^2 \frac{h^{2p}\omega^{2p+2}}{2p+1} + \mathcal{O}(h^{2p+2}). \tag{4.33}$$

Now applying Theorem 4.2.1, we obtain (4.32) at once. □

It is not difficult to check that the above expressions leads to expression (4.22) for $\tau = 0$ and (4.27) for $\tau = 1$ which are the discrete dispersion relations corresponding to finite element and element spectral element schemes respectively. More importantly, the first term in expression (4.32) vanishes if we choose blending parameter $\tau = p/(p+1)$ which shows that the optimal blending parameter is independent of the number of spatial dimensions. Theorem 4.3.3 gives rise to the following corollary.

Corollary 4.3.4. *Let $p \geq 2$. Then for the optimal choice of the blending parameter $\tau = p/(p+1)$, the error in the discrete dispersion relation* (4.32) *is given by*

$$\omega_h^2 = \omega^2 + \frac{8}{(2p-1)} \left[\frac{(p+1)!}{(2p+2)!}\right]^2 \frac{1}{2p+3} \sum_{\ell=1}^{d} h_\ell^{2p+2} \omega_\ell^{2p+4} + \mathcal{O}(h^{2p+4}).$$

Proof. Substituting $\tau = p/(p+1)$ in (4.32) and applying trivial manipulations gives us the required result. □

Whilst the cost of all of the schemes is virtually identical, remarkably the leading error term for the optimal scheme is two orders more accurate compared with the standard spectral element and finite element schemes given in the previous sections. Moreover, the coefficient of the leading term in the error obtained with the blended scheme for the optimum value of τ is $-2/(4p^2-1)(2p+3)$ and $2p/(4p^2-1)(2p+3)$ times better compared with the coefficients of leading terms in the error obtained with finite element and spectral element schemes respectively.

4.4 Numerical examples

In order to study the behaviour of finite element, spectral element and optimally blended schemes in practical computations, we consider a simple one dimensional scattering problem on the interval $(0,3)$ with fixed $\omega > 0$, and $\omega_s > 0$ with relative density $\rho = \omega_s^2/\omega^2$ given by

$$-u'' - \omega^2(x)u = f(x) \tag{4.34}$$

where

$$\omega(x) = \begin{cases} \omega, & \text{for } x \notin (1,2), \\ \omega_s, & \text{for } x \in (1,2) \end{cases} \quad \text{and } f(x) = \begin{cases} 0, & \text{for } x \notin (1,2), \\ (\omega^2 - \omega_s^2)e^{i\omega x}, & \text{for } x \in (1,2) \end{cases}$$

with the following non-reflecting boundary conditions applied at both ends of the domain

$$u'(0) + i\omega u(0) = 0 \text{ and } u'(3) - i\omega u(3) = 0.$$

Evidently, the model problem corresponds to scattering of an incoming plane wave by a slab of relative density ω_s^2/ω^2 located on $(1,2)$. In Figure 4.1 (a), we approximate scattered wave using 35 and 300 linear elements outside and inside the slab

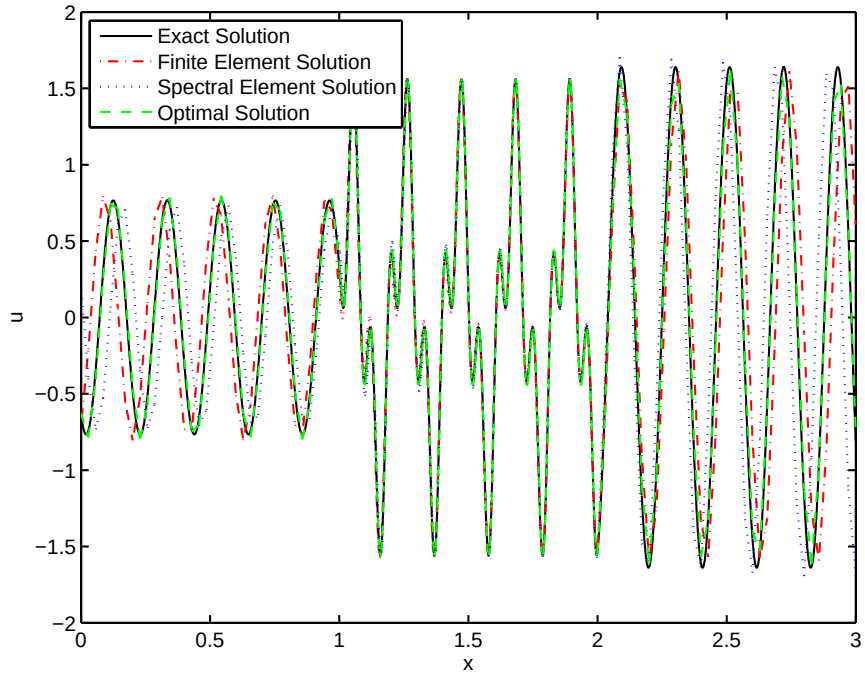
Exact Solution
Finite Element Solution
Spectral Element Solution
Optimal Solution
u
x
2
1.5
1
0.5
0
−0.5
−1
−1.5
−2
0
0.5
1
1.5
2
2.5
3

(a)

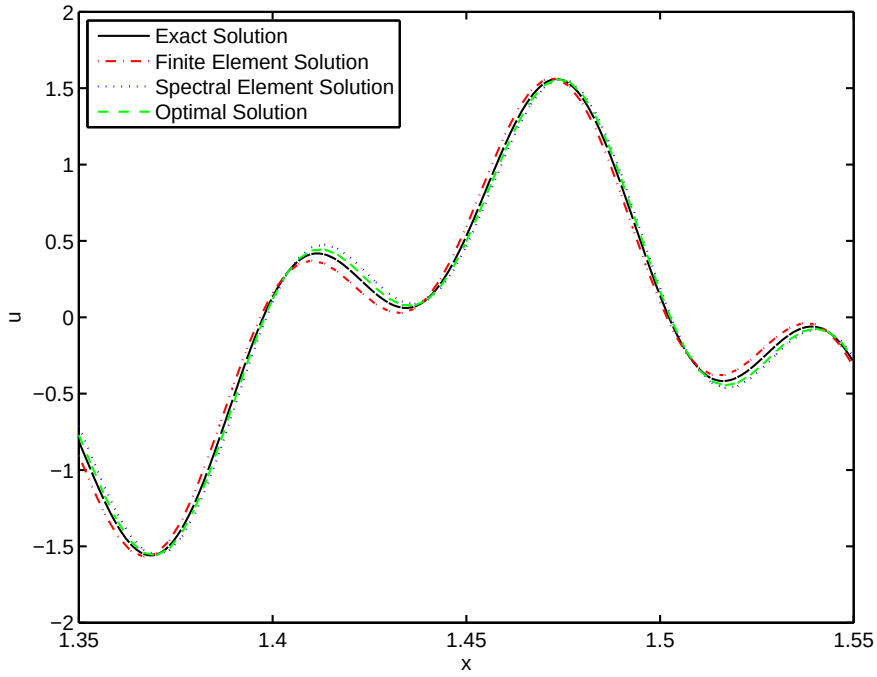
Exact Solution
Finite Element Solution
Spectral Element Solution
Optimal Solution
u
x
2
1.5
1
0.5
0
−0.5
−1
−1.5
−2
1.35
1.4
1.45
1.5
1.55

(b)

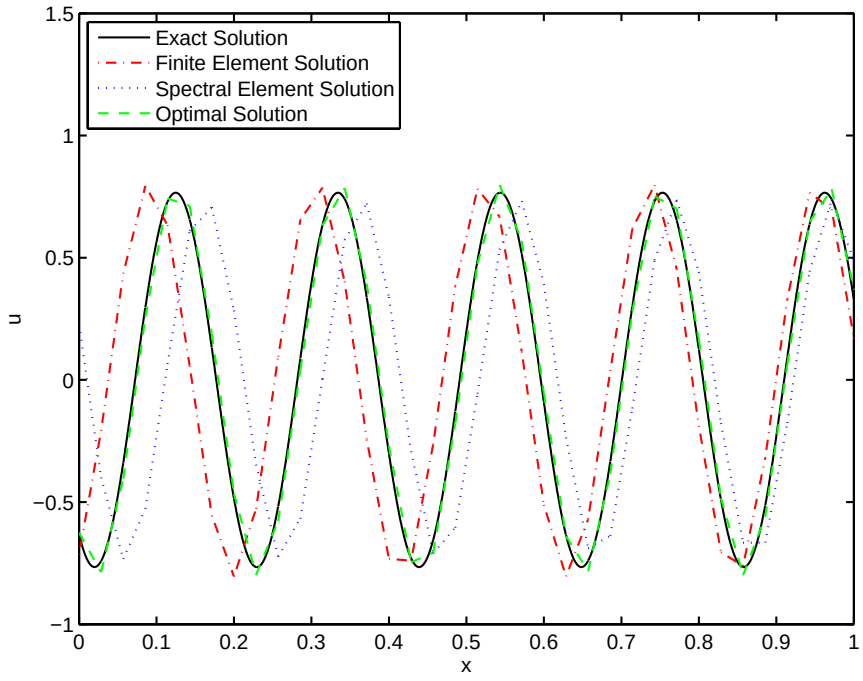

(c)

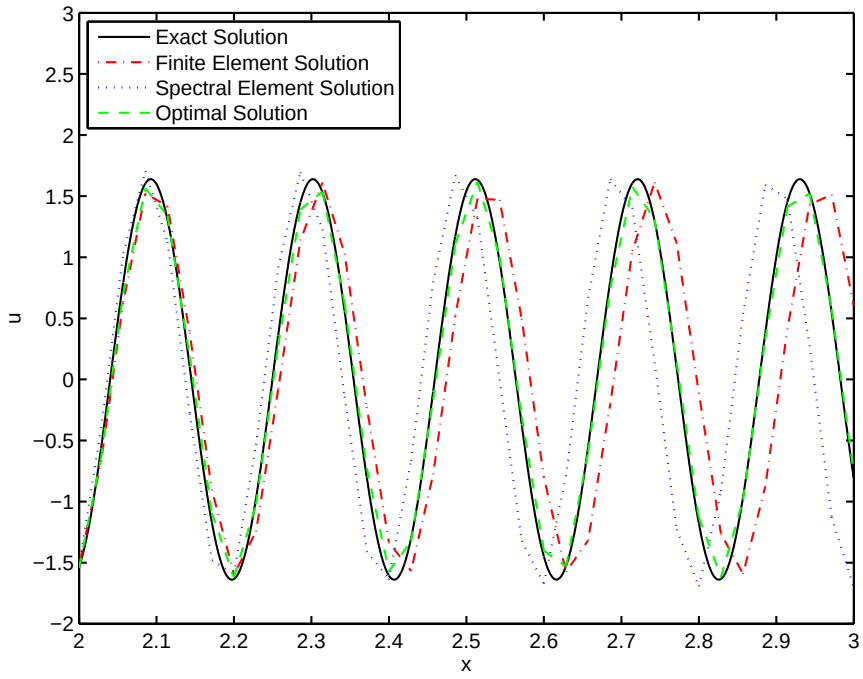

(d)

Figure 4.1: Numerical approximations of the solution to equation (4.34) obtained for $p = 1$ with $\omega = 30$ and $\rho = 9$. Furthermore 35 and 300 elements are used outside and inside the slab respectively.

respectively for finite element, spectral element and optimally blended schemes with given frequency $\omega = 30$ and relative density $\rho = 9$. Scattered waves on the left and right side of the slab are shown in Figure 4.1 $(c) - (d)$ to analyse better the numerical approximations obtained with all the schemes. The phase lead and lag of equal magnitudes are clearly visible and correspond to finite element and spectral element schemes which is consistent with error expressions given in (4.22) and (4.27). The same observation was made in [5–7, 60] in the case of linear elements. Furthermore the numerical approximation corresponding to the optimal scheme is noticeably better than that of finite element and spectral element schemes which was also observed in [7]. Figure 4.1 (b), represents the scattered wave inside the slab and once again optimal scheme performs better than that of finite element and spectral element schemes nonetheless phase lead and lag of equal magnitudes with linear elements are still prominent even inside the slab.
In Figures 4.2 and 4.3, we show numerical approximations obtained for all the schemes using quadratic and cubic elements. It is clear from Figures 4.2(a) and 4.3(a) that with piecewise quadratic and cubic elements both spectral element and optimally blended schemes are performing much better than that of finite element scheme. This conjecture is consistent with analytical results (4.27) and (4.32) of dispersion error obtained for spectral element and optimally blended schemes. The magnitude of the leading order error term for spectral element and optimally blended schemes are $\mathcal{O}(p^{-1})$ and $\mathcal{O}(p^{-3})$ times better than that of the pure finite element scheme. Moreover, the numerical approximation obtained with finite element scheme is unresolved both for quadratic and cubic elements in each region. The same conjecture is observed even inside the slab which is presented in Figures 4.2(b) and 4.3(b) for quadratic and cubic elements respectively. In Figure 4.4, we show the effect of using polynomials of different orders in different regions. In

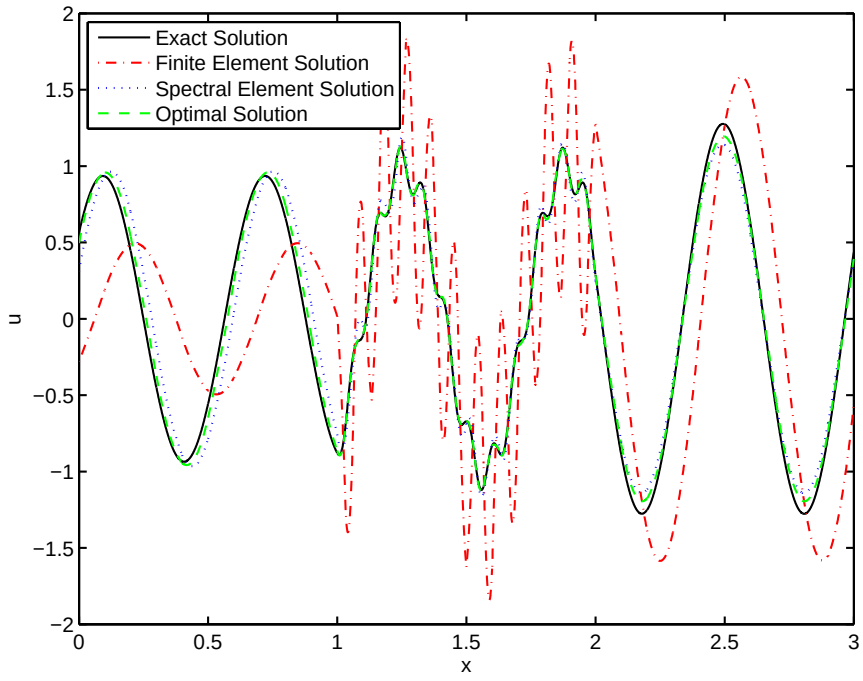

(a)

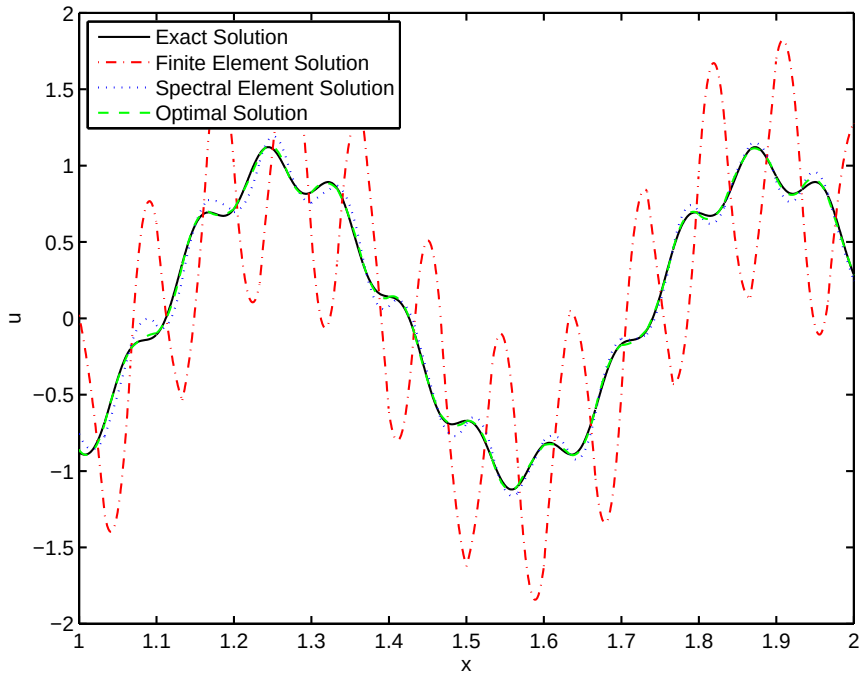

(b)

Figure 4.2: Numerical approximations of the solution to equation (4.34) obtained for $p = 2$ with $\omega = 10$ and $\rho = 49$. Furthermore 10 and 30 elements are used outside and inside the slab respectively.

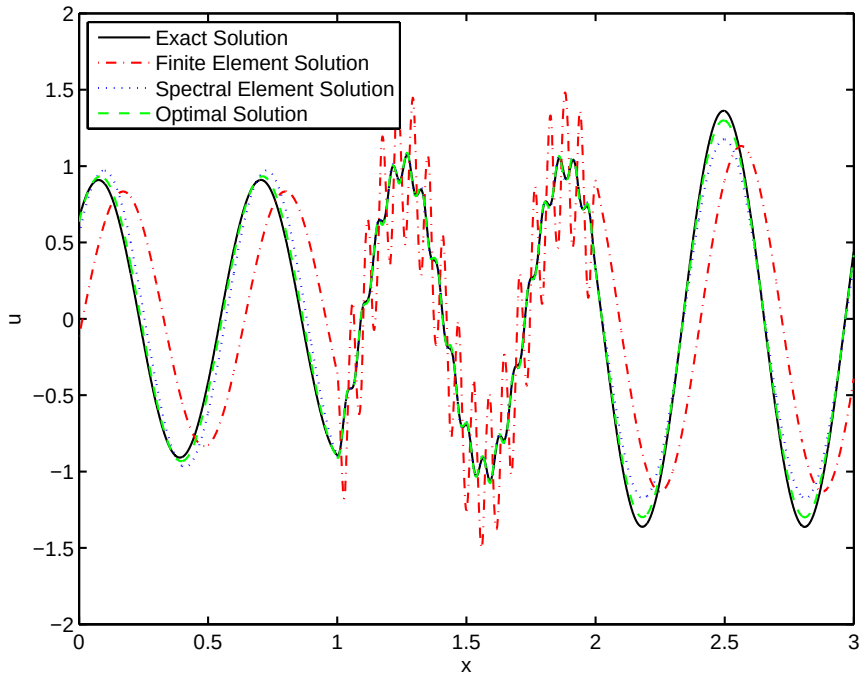

(a)

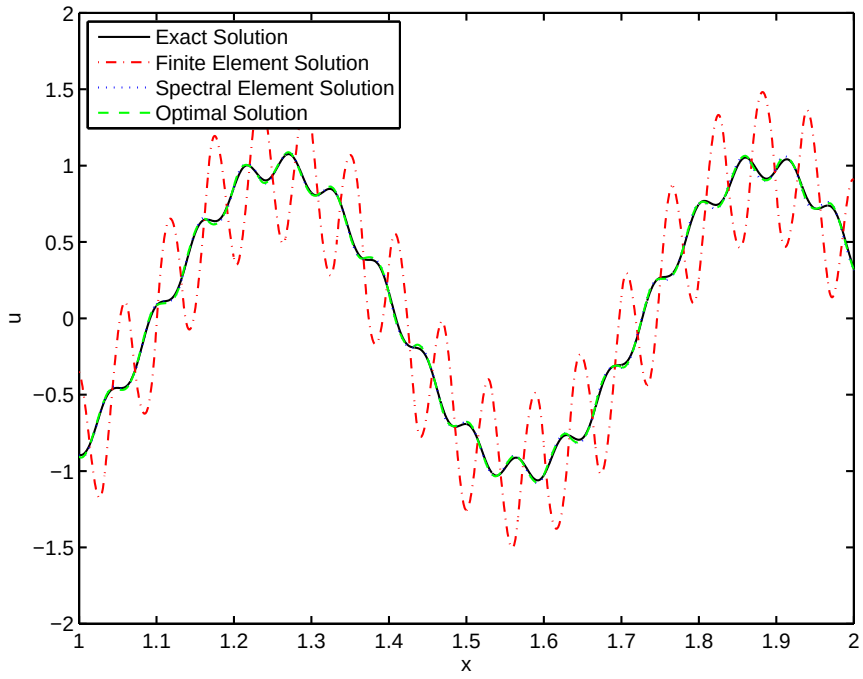

(b)

Figure 4.3: Numerical approximations of the solution to equation (4.34) obtained for $p = 3$ with $\omega = 10$ and $\rho = 115$. Furthermore 10 and 30 elements are used outside and inside the slab respectively.

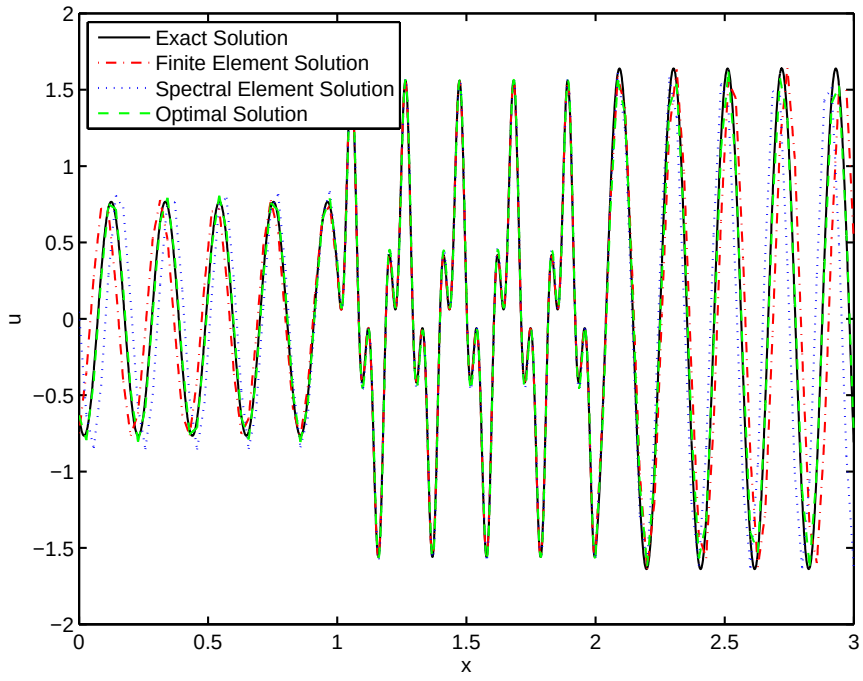

(a)

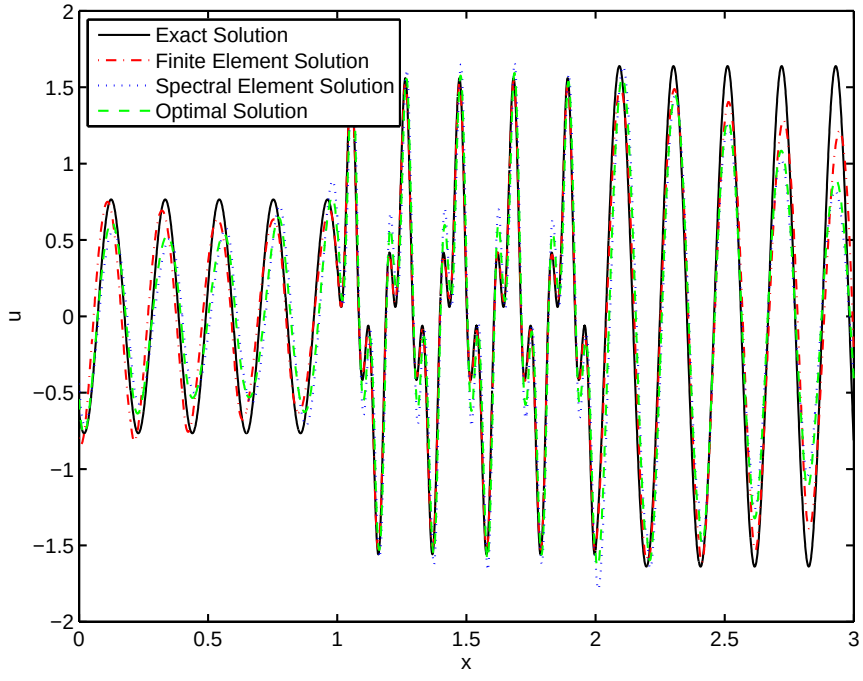

(b)

Figure 4.4: Numerical approximations of the solution to equation (4.34) obtained with $\omega = 30$ and $\rho = 9$ for (a) 35 linear and 50 cubic elements (b) 5 quartic and 15 fifth order elements used outside and inside the slab respectively.

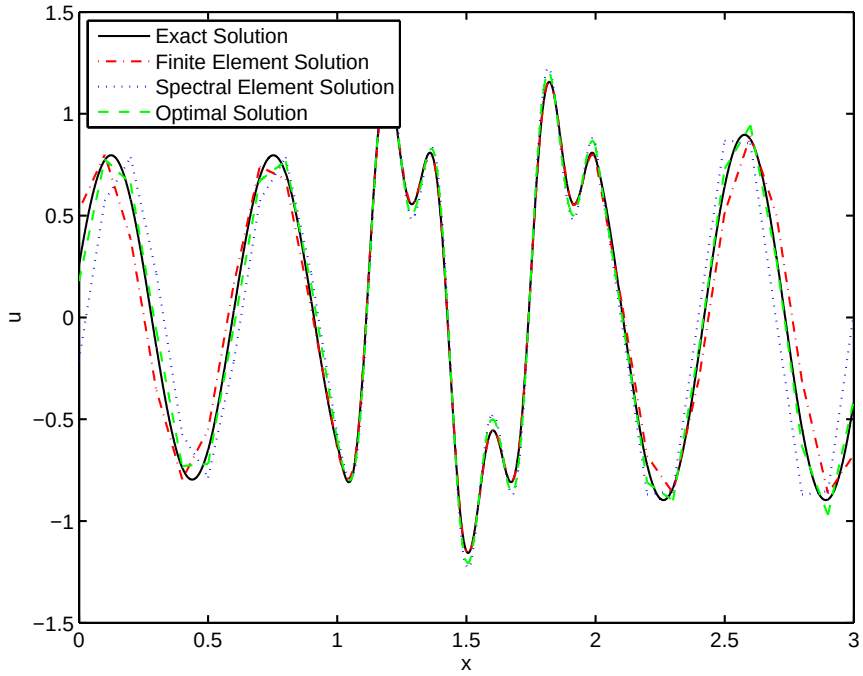
Exact Solution
Finite Element Solution
Spectral Element Solution
Optimal Solution
u
x
1.5
1
0.5
0
−0.5
−1
−1.5
0
0.5
1
1.5
2
2.5
3

(a)

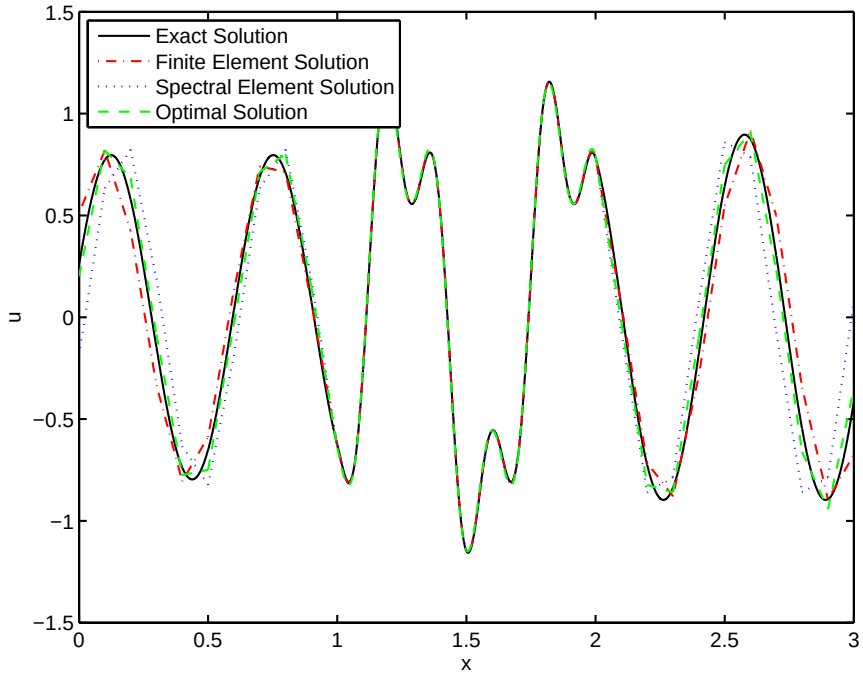
Exact Solution
Finite Element Solution
Spectral Element Solution
Optimal Solution
u
x
1.5
1
0.5
0
−0.5
−1
−1.5
0
0.5
1
1.5
2
2.5
3

(b)

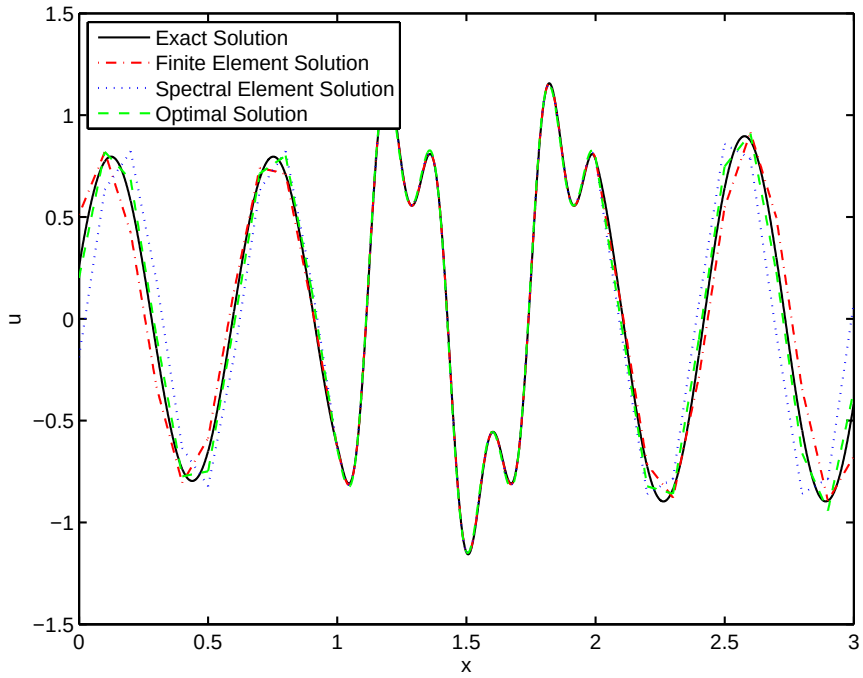

(c)

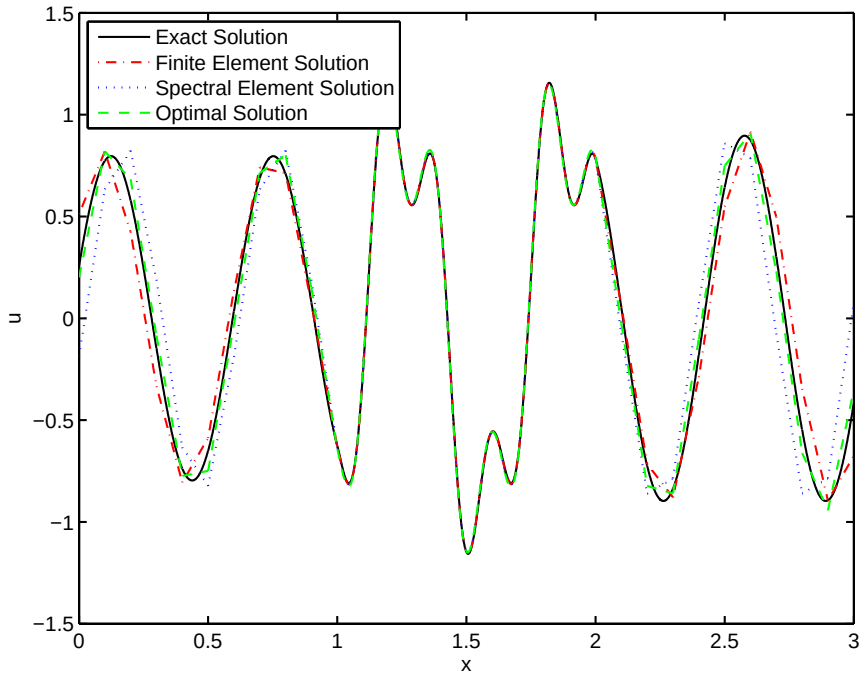

(d)

Figure 4.5: Numerical approximations of the solution to equation (4.34) obtained with $\omega = 10$ and $\rho = 9$ using 10 linear elements outside the slab and using (a) ten cubic (b) 10 fifth order (c) 20 cubic (d) 20 fifth order elements inside the slab.

Figure 4.4(a), we show numerical results approximated outside the slab with first order ($p = 1$) elements whereas cubic elements are used inside the slab. We use the same number of elements i.e. $n1 = n3 = 35$ outside the slab as we used in Figure 4.1 but inside the slab using $n2 = 50$ cubic elements instead of 300 linear elements gives us much better results but phase leads and lags of equal magnitude are visible outside the slab as we are using linear elements there. Now using $n1 = n3 = 5$ quartic elements outside the slab and $n2 = 15$ elements of fifth order provides very accurate results as shown in Figure 4.4 (b). In Figure 4.5, we show that when the waves are fully resolved inside the slab then increasing the order or the number of elements or both the order and the number of elements inside the slab do not help the waves outside the slab to converge. Hence, when the waves are almost resolved inside the slab then the waves outside the slab can be resolved by either increasing the number of elements or using higher order elements. In the case where the wave is not resolved inside the slab then increasing the number of elements or using higher order elements or increasing the number of elements and using the higher order elements simultaneously outside the slab do not give us a completely resolved wave and this behaviour is shown in Figure 4.6.

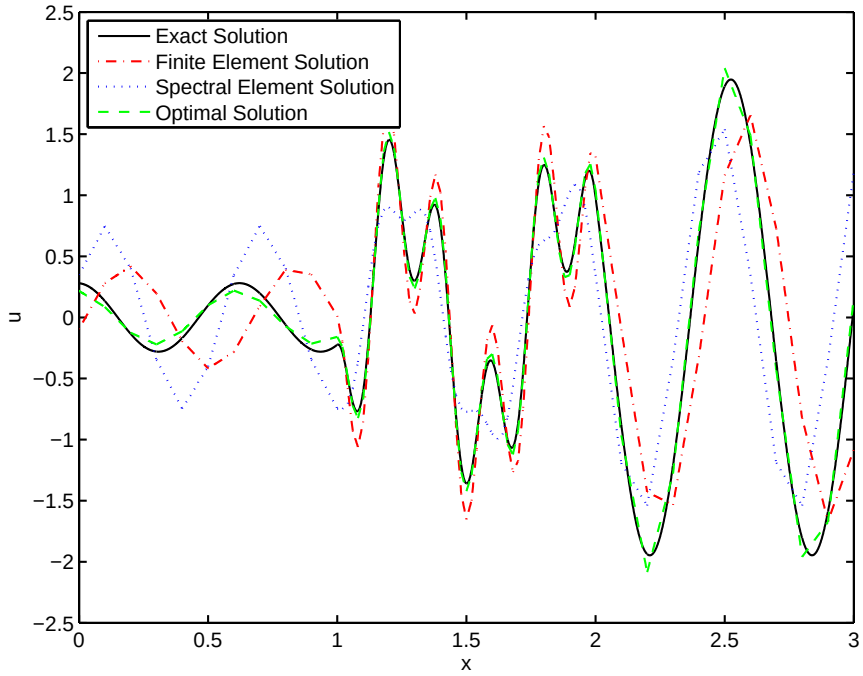
Exact Solution
Finite Element Solution
Spectral Element Solution
Optimal Solution
u
x
2.5
2
1.5
1
0.5
0
−0.5
−1
−1.5
−2
−2.5
0
0.5
1
1.5
2
2.5
3

(a)

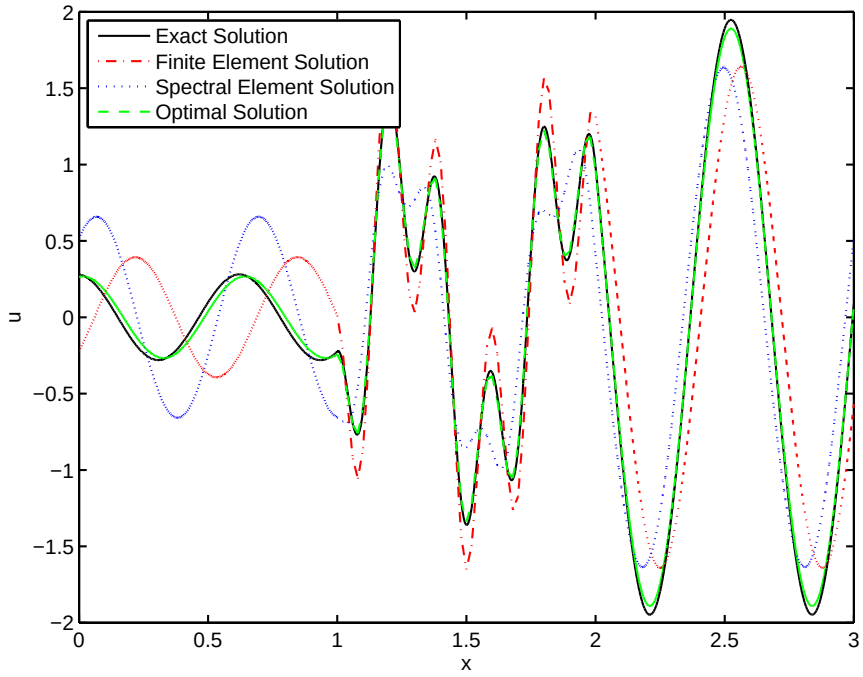
Exact Solution
Finite Element Solution
Spectral Element Solution
Optimal Solution
u
x
2
1.5
1
0.5
0
−0.5
−1
−1.5
−2
0
0.5
1
1.5
2
2.5
3

(b)

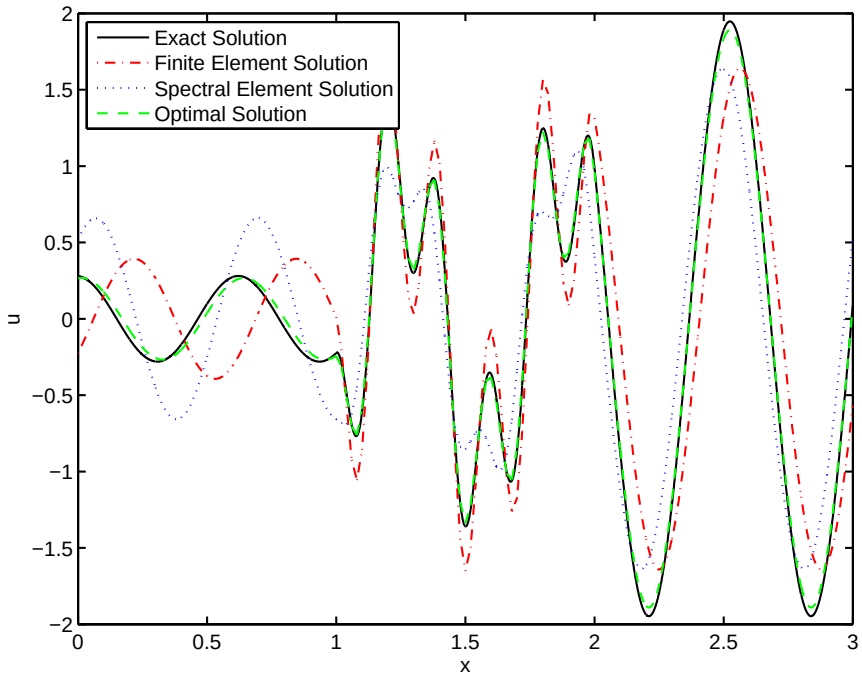

(c)

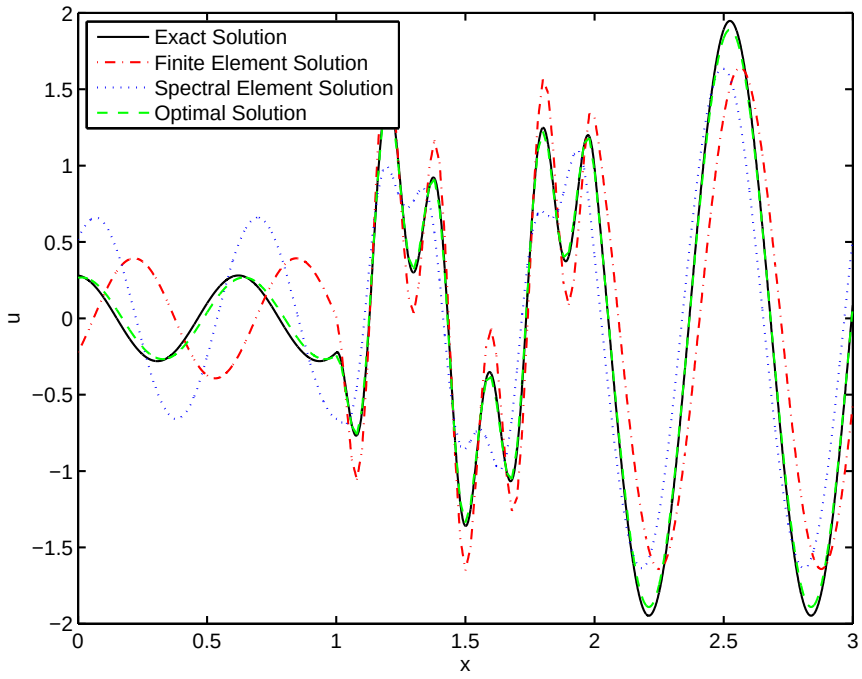

(d)

Figure 4.6: Numerical approximations of the solution to equation (4.34) obtained with $\omega = 10$ and $\rho = 10$ for (a) 10 linear (b) 200 linear (c) 10 fifth order (d) 20 fifth order elements inside the slab and 50 linear elements are used outside the slab in all cases.

Chapter 5

Conclusions

In this work high-order accurate numerical methods for computational wave propagation are developed for the reduced wave equation (Helmholtz equation). We started with the mass-lumped finite element scheme in which the mass matrix becomes diagonal if the nodes for the spectral element scheme are chosen to be the Gauss-Legendre-Lobattto points in conjunction with a Lagrange basis. This is sometimes described as the Gauss-point mass lumped finite element scheme. We then appropriately blended the standard finite element and spectral element schemes following the suggestion of Marfurt (1984). Finally, we extended the one dimensional discrete dispersion relations of finite element, spectral element and optimally blended schemes to higher dimensions using tensor product meshes on a rectangular grid.

5.1 Spectral element scheme

The main conclusions and comparisons of the spectral element scheme with the finite element scheme for approximation of a wave of frequency ω are as follows:

1. for fixed order of approximation p, as ωh tends to zero:

   (a) *both* the finite element and spectral element schemes give the same $\mathcal{O}(\omega h)^{2p+1}$ accuracy for the phase error [1, 35, 37, 38, 60];

   (b) the multiplicative constant appearing in front of the leading order term for the error in the spectral element case is $-1/p$ times that for the finite element case.

   The first conclusion agrees with the practical observation that the Gauss-point mass lumped scheme (i.e. spectral element method) tends to exhibit *phase lag* whereas the (consistent) finite element scheme tends to exhibit *phase lead*. More interestingly, the conclusion shows that the absolute accuracy of the spectral element scheme is $1/p$ times better than that of the finite element scheme despite the use of numerical integration;

2. for a fixed mesh of size h with $\omega h \gg 1$, as the order of the scheme p is increased:

   (a) for $p = \mathcal{O}(1)$, the phase error of the finite element scheme is $\mathcal{O}(1)$ whereas the spectral element scheme is of order $\frac{1}{2}(\omega h)^2$;

   (b) for $\omega h - o(\omega h)^{1/3} \leq 2p + 1 \leq \omega h + o(\omega h)^{1/3}$, the phase accuracy of both schemes undergoes a sharp transition between an error of order $\mathcal{O}(1)$ and a situation in which both schemes provide an essentially fully resolved numerical wave;

   (c) for $2p + 1 \gg \omega h$, the error obtained with the spectral element scheme performs $(\omega h/4p)^2$ times better than that of the finite element scheme.

$$\mathcal{E}_{SE}^{(p)} \approx \left(\frac{\omega h}{4p}\right)^2 \mathcal{E}_{FE}^{(p)}$$

The second conclusion means that in the unresolved regime, the spectral element method behaves rather erratically (in numerical examples one sees drastic over-shooting and under-shooting of the true wave) in contrast with the less erratic (but still very poor) behaviour of the finite element scheme. Both schemes exhibit a sharp transition whereby the true wave is essentially fully resolved by increasing the order from p to roughly order $p+1$ or $p+2$.

The transition corresponding to the stage where the spectral element scheme essentially provides full resolution occurs when the order p, the mesh-size h and the frequency ω are related by $2p+1 \approx \omega h$. A mesh of size h corresponds to there being $2\pi/\omega h$ elements per wavelength. Each element in a p-th order scheme involves $p+1$ Gauss-Legendre-Lobatto points in each direction, or on average $p+1/2$ degrees of freedom per element in each direction. Consequently, at the point when full resolution occurs, the scheme requires roughly $(p+1/2) \times 2\pi/\omega h = \pi$ degrees of freedom per wavelength. This agrees with the general rule of thumb sometimes quoted in the context of spectral element methods: *π modes per wavelength are needed to resolve a wave*, and the arguments presented here can be regarded as a rigorous proof of that fact.

Finally, it is worth recalling the fundamental fact that at least two degrees of freedom per wavelength are needed for *any* scheme to resolve a wave. Consequently, the ability of the spectral element (and finite element) method to resolve a wave with π degrees of freedom per wavelength is close to optimal and perhaps helps to explain the popularity of such methods for computational wave propagation.

5.2 Optimally blended scheme

The main conclusions and comparisons of the optimally blended scheme with the standard finite element and spectral element schemes for approximation of a wave of frequency ω are as follows:

1. for fixed order of approximation p, as ωh tends to zero:

   (a) For p-th order scheme both the finite element and spectral element schemes are $\mathcal{O}(\omega h)^{2p+1}$ order accurate whereas the optimally blended scheme is $\mathcal{O}(\omega h)^{2p+3}$ order accurate;

   (b) the multiplicative constant appearing in front of the leading order term for the error for optimally blended scheme is $\mathcal{O}(p^{-3})$ and $\mathcal{O}(p^{-2})$ times better than that of the standard finite element and spectral element schemes respectively;

   The first conclusion means that the optimally blended scheme is two orders more accurate compared with the standard finite element and spectral element schemes and tends to exhibit *phase lag*. Furthermore, for the optimum value of the blending parameter $\tau = p/(p+1)$, the absolute phase accuracy of the optimally blended scheme is $-2/(4p^2-1)(2p+3)$ and $2p/(4p^2-1)(2p+3)$ times better than that of the finite element and spectral element schemes respectively;

2. the optimally blended scheme can be efficiently implemented by using non-standard quadrature rule. More specifically it means that an existing, standard finite element code can be adapted to implement the optimally blended scheme merely by replacing the usual Gaussian quadrature rule by the non-standard rules;

3. the blending parameter τ is independent of the frequency ω and the number of spatial dimensions. It means that the optimally blended scheme can be used directly for transient wave propagation problems in contrast to the GFEM [8] and GLS [32, 53, 61] schemes where the coefficient matrix depends upon the frequency ω or the wavenumber k.

5.3 Explicit discrete dispersion relations in d-dimensions

We conclude that analytical expressions for the discrete dispersion relations for finite element, spectral element and optimally blended schemes in higher dimensions can be obtained using their corresponding one dimensional discrete dispersion relations. More interestingly, the optimum value of the blending parameter for optimally blended scheme is same even for rectangular grids i.e. $\tau = p/(p+1)$ for all $p \in \mathbb{N}$.

Bibliography

[1] M. Ainsworth. Discrete dispersion relation for *hp*-version finite element approximation at high wave number. *SIAM J. Numer. Anal.*, 42(2):553–575 (electronic), 2004.

[2] M. Ainsworth. Dispersive and dissipative behaviour of high order discontinuous Galerkin finite element methods. *J. Comput. Phys.*, 198(1):106–130, 2004.

[3] M. Ainsworth. Dispersive properties of high-order Nédélec/edge element approximation of the time-harmonic Maxwell equations. *Philos. Trans. R. Soc. Lond. Ser. A Math. Phys. Eng. Sci.*, 362(1816):471–491, 2004.

[4] M. Ainsworth, P. Monk, and W. Muniz. Dispersive and dissipative properties of discontinuous Galerkin finite element methods for the second-order wave equation. *J. Sci. Comput.*, 27(1-3):5–40, 2006.

[5] M. Ainsworth and H. A. Wajid. Dispersive and dissipative behaviour of the spectral element method. *Technical Report 8*, University of Strathclyde, 2008 (submitted to *SIAM J. Numer. Anal.*, 2008).

[6] M. Ainsworth and H. A. Wajid. Explicit discrete dispersion relations for the acoustic wave equation in *d*-dimensions using finite element, spectral element

and optimally blended schemes. *Computer Methods in Mechanics-Lectures on the CMM 2009*, 2009.

[7] M. Ainsworth and H. A. Wajid. Optimally blended spectral-finite element scheme for wave propagation, and non-standard reduced integration. *Technical Report 12*, University of Strathclyde, 2009 (submitted to *SIAM J. Numer. Anal.*, 2009).

[8] I. Babuška, F. Ihlenburg, E. T. Paik, and S. A. Sauter. A generalized finite element method for solving the Helmholtz equation in two dimensions with minimal pollution. *Comput. Methods Appl. Mech. Engrg.*, 128(3-4):325–359, 1995.

[9] I. Babuška and J. M. Melenk. The partition of unity method. *Internat. J. Numer. Methods Engrg.*, 40(4):727–758, 1997.

[10] I. Babuška and S. A. Sauter. Is the pollution effect of the FEM avoidable for the Helmholtz equation considering high wave numbers? *SIAM J. Numer. Anal.*, 34(6):2392–2423, 1997.

[11] S. C. Brenner and L. R. Scott. *The mathematical theory of finite element methods*, volume 15 of *Texts in Applied Mathematics*. Springer, New York, third edition, 2008.

[12] J. Callerame. X-ray backscatter imaging: photography through barriers. *American Science and Engineering, Inc.*, 2006.

[13] C. Canuto, M. Y. Hussaini, A. Quarteroni, and T. A. Zang. *Spectral methods*. Scientific Computation. Springer, Berlin, 2007. Evolution to complex geometries and applications to fluid dynamics.

[14] S. Challa. *High-order Accurate spectral elements for wave propagation.* Masters thesis in mechanical engineering, Clemson University, 1998.

[15] J. L. Cipolla. Subgrid modeling in a Galerkin method for the Helmholtz equation. *Comput. Methods Appl. Mech. Engrg.*, 177(1-2):35–49, 1999.

[16] R. D. Ciskowski and C. A. Brebbia, editors. *Boundary element methods in acoustics.* International Series on Computational Engineering. Computational Mechanics Publications, Southampton, 1991.

[17] G. C. Cohen. *Higher-order numerical methods for transient wave equations.* Scientific Computation. Springer-Verlag, Berlin, 2002. With a foreword by R. Glowinski.

[18] G. C. Cohen and M. Duruflé. Non spurious spectral-like element methods for Maxwell's equations. *J. Comput. Math.*, 25(3):282–304, 2007.

[19] G. C. Cohen and P. Monk. Gauss point mass lumping schemes for Maxwell's equations. *Numer. Methods Partial Differential Equations*, 14(1):63–88, 1998.

[20] L. Conyers and D. Goodman. *Ground Penetrating Radar: An Introduction for Archaeologists.* AltaMira Press,U.S., 1997.

[21] D. Daniels. *Ground Penetrating Radar (Iee Radar, Sonar, Navigation and Avionics Series).* Institution of Engineering and Technology, 2004.

[22] J. D. De Basabe and M. K. Sen. Grid dispersion and stability criteria of some common finite-element methods for acoustic and elastic wave equation. *Geophysics*, 72(6):T81–T95, 2007.

[23] A. Erdélyi, W. Magnus, F. Oberhettinger, and F. G. Tricomi. *Higher transcendental functions. Vols. I, II.* McGraw-Hill Book Company, Inc., New York-Toronto-London, 1953. Based, in part, on notes left by Harry Bateman.

[24] B. Fornberg. *A practical guide to pseudospectral methods*, volume 1 of *Cambridge Monographs on Applied and Computational Mathematics*. Cambridge University Press, Cambridge, 1996.

[25] L. P. Franca, C. Farhat, A. P. Macedo, and M. Lesoinne. Residual-free bubbles for the Helmholtz equation. *Internat. J. Numer. Methods Engrg.*, 40(21):4003–4009, 1997.

[26] I. Fried and M. Chavez. Superaccurate finite element eigenvalue computation. *Journal of sound and vibration*, 275:415–422, 2004.

[27] I. Fried and K. Leong. Superaccurate finite element eigenvalues via a raleigh quotient correction. *Journal of sound and vibration*, 288:375–386, 2005.

[28] I. S. Gradshteyn and I. M. Ryzhik. *Table of integrals, series, and products*. Fourth edition prepared by Ju. V. Geronimus and M. Ju. Ceĭtlin. Translated from the Russian by Scripta Technica, Inc. Translation edited by Alan Jeffrey. Academic Press, New York, 1965.

[29] M. N. Guddati and B. Yue. Modified integration rules for reducing dispersion error in finite element methods. *Comput. Methods Appl. Mech. Engrg.*, 193:275–287, 2004.

[30] M. N. Guddati and B. Yue. Dispersion-reducing finite elements for transient acoustics. *J. Acoust. Soc. Am.*, 118(4):2132–2141, 2005.

[31] I. Harari. A survey of finite element methods for time-harmonic acoustics. *Comput. Methods Appl. Mech. Engrg.*, 195(13-16):1594–1607, 2006.

[32] I. Harari and T. J. R. Hughes. Galerkin/least-squares finite element methods for the reduced wave equation with nonreflecting boundary conditions in unbounded domains. *Comput. Methods Appl. Mech. Engrg.*, 98(3):411–454, 1992.

[33] I. Harari and E. Turkel. Accurate finite difference methods for time-harmonic wave propagation. *J. Comput. Phys.*, 119(2):252–270, 1995.

[34] M. H. Holmes. *Introduction to numerical methods in differential equations*, volume 52 of *Texts in Applied Mathematics*. Springer, New York, 2007.

[35] F. Ihlenburg. *Finite element analysis of acoustic scattering*, volume 132 of *Applied Mathematical Sciences*. Springer-Verlag, New York, 1998.

[36] F. Ihlenburg and I. Babuška. Dispersion analysis and error estimation of Galerkin finite element methods for the Helmholtz equation. *Internat. J. Numer. Methods Engrg.*, 38(22):3745–3774, 1995.

[37] F. Ihlenburg and I. Babuška. Finite element solution of the Helmholtz equation with high wave number. I. The *h*-version of the FEM. *Comput. Math. Appl.*, 30(9):9–37, 1995.

[38] F. Ihlenburg and I. Babuška. Finite element solution of the Helmholtz equation with high wave number. II. The *h-p* version of the FEM. *SIAM J. Numer. Anal.*, 34(1):315–358, 1997.

[39] M. Iskandarani, D. B. Haidvogel, and J. C. Levin. A three-dimensional spectral element model for the solution of the hydrostatic primitive equations. *J. Comput. Phys.*, 186(2):397–425, 2003.

[40] M. S. Jensen. High convergence order finite elements with lumped mass matrix. *International Journal for Numerical Methods in Engineering*, 39:1879–1888, 1996.

[41] R. Knobel. *An introduction to the mathematical theory of waves*, volume 3 of *Student Mathematical Library*. American Mathematical Society, Providence, RI, 2000. IAS/Park City Mathematical Subseries.

[42] D. Komatitsch and J. Tromp. Spectral-element simulations of global seismic wave propagation-I. Validation. *Geophys. J. Int.*, 149(2):390–412, 2002.

[43] D. Komatitsch and J. Tromp. Spectral-element simulations of global seismic wave propagation-II. 3-D models, oceans, rotation, and self-gravitation. *Geophys. J. Int.*, 150(1):303–318, 2002.

[44] D. Komatitsch and J. P. Vilotte. The spectral-element method: an efficient tool to simulate the seismic response of 2D and 3D geological structures. *Bull. Seismol. Soc. Am.*, 88(2):368–392, 1998.

[45] R. J. LeVeque. *Finite volume methods for hyperbolic problems*. Cambridge Texts in Applied Mathematics. Cambridge University Press, Cambridge, 2002.

[46] F. Maggio and A. Quarteroni. Acoustic wave simulation by spectral methods. *East-West J. Numer. Math.*, 2(2):129–150, 1994.

[47] K. J. Marfurt. Accuracy of finite-difference and finite-element modeling of the scalar and elastic wave equations. *Geophysics*, 49(5):533–549, 1984.

[48] J. M. Melenk and C. Schwab. *HP* FEM for reaction-diffusion equations. I. Robust exponential convergence. *SIAM J. Numer. Anal.*, 35(4):1520–1557 (electronic), 1998.

[49] A. R. Mitchell and D. F. Griffiths. *The finite difference method in partial differential equations*. John Wiley & Sons Ltd., Chichester, 1980. A Wiley-Interscience Publication.

[50] W. A. Mulder. Spurious modes in finite-element discretizations of the wave equation may not be all that bad. *Appl. Numer. Math.*, 30(4):425–445, 1999.

[51] W. Niemann, S. Olesinski, and T. Thiele. Detection of buried landmines with x-ray backscatter technology. *8th European Conference on Nondestructive Testing Barcelona (Spain)*, 7(10), 2002.

[52] A. A. Oberai and P. M. Pinsky. A multiscale finite element method for the Helmholtz equation. *Comput. Methods Appl. Mech. Engrg.*, 154(3-4):281–297, 1998.

[53] A. A. Oberai and P. M. Pinsky. A residual-based finite element method for the Helmholtz equation. *Internat. J. Numer. Methods Engrg.*, 49(3):399–419, 2000.

[54] F. W. J. Olver. *Asymptotics and special functions*. Academic Press [A subsidiary of Harcourt Brace Jovanovich, Publishers], New York-London, 1974. Computer Science and Applied Mathematics.

[55] K. C. Patidar. Dispersion induced by the pollution for the wave equation. *Appl. Math. Comput.*, 160(2):329–341, 2005.

[56] A. Ralston. *A first course in numerical analysis*. McGraw-Hill Book Co., New York, 1965.

[57] G. Seriani and S. P. Oliveira. Optimal blended spectral-element operators for acoustic wave modeling. *Geophysics*, 72(5):SM95–SM106, 2007.

[58] S. Suleau, A. Deraemaeker, and P. Bouillard. Dispersion and pollution of meshless solutions for the Helmholtz equation. *Comput. Methods Appl. Mech. Engrg.*, 190(5-7):639–657, 2000.

[59] L. L. Thompson. A review of finite element methods for time-harmonic acoustics. *Journal of the Acoustical Society of America*, 119(3):1315–1330, 2006.

[60] L. L. Thompson and P. M. Pinsky. Complex wavenumber Fourier analysis of the p-version finite element method. *Comput. Mech.*, 13(4):255–275, 1994.

[61] L. L. Thompson and P. M. Pinsky. A Galerkin least-squares finite element method for the two-dimensional Helmholtz equation. *Internat. J. Numer. Methods Engrg.*, 38(3):371–397, 1995.

[62] J. Valenciano and M. A. J. Chaplain. An explicit subparametric spectral element method of lines applied to a tumour angiogenesis system of partial differential equations. *Math. Models Methods Appl. Sci.*, 14(2):165–187, 2004.

[63] F. I. Zyserman and P. M. Gauzellino. Dispersion analysis of a nonconforming finite element method for the three-dimensional scalar and elastic wave equations. *Finite Elem. Anal. Des.*, 41(13):1309–1326, 2005.